ABSTRACT

EXPERIMENTAL AND NUMERICAL STUDY OF FLOW CHARACTERISTICS AND SEGREGATION IN FLOW ENHANCED SYSTEMS

BY
Gregory James

In the study of granular materials, two major topics of importance are powder flow enhancement mechanisms and the flow characterization. This dissertation is involved with both of these topics. With respect to the powder flow enhancement, this study involves investigation of two types of flow enhancement methods. The first flow enhancement method examined is a novel method called the Magnetically Assisted Powder Flow (MAPF) method. In the MAPF, small magnetic particles and powders are placed in a test hopper. A mesh is placed at the bottom of the hopper to hold the magnetic particles while the powder is discharged through the mesh. It is shown that this method may be used for controlled discharge of cohesive powders and hence may be used also for cohesive powder flow characterization. Therefore this technique is utilized for the angle of repose (AOR) measurements, which is the most convenient and popular method used in industry for powder characterization. It is found that many factors affect the results obtained for AOR, including the technique of measurement. The AOR measurement through MAPF method is developed and the effects of various variables including the dropping height, mass of the powder used in the hopper, magnetic field strength, hopper position in the magnetic field, mass of magnetic particles hopper outlet area and mesh size are evaluated. This novel AOR measurement method is found to be more reliable and easier to use.

The second flow enhancement method examined is the use of vibration, which is currently a commonly applied industrial method to enhance powder flow. However, it is well known that vibration causes segregation due to the difference in particle size or density and thus causes certain adverse effects on products. In order to understand the mechanisms of segregation in vibrating systems, a systematic study of vibrated hoppers with mono-disperse as well as binary system of particles is carried out. This includes physical experiments as well a computer model using the Discrete Element Method (DEM) to simulate the model system. The first part of the study involves hoppers with the outlet closed, and includes experiments and simulations. The effects of various system parameters are investigated and several important regimes of behavior are identified based on the state diagram of dimensionless amplitude and frequency of applied vibrations. A plausible explanation through the experimental and simulation results is given for one of the most interesting regimes, where the hopper surface is inclined (i.e. forms a heap). It is shown that this occurs due to the existence of lateral (i.e. horizontal) vibration mode.

For the binary system, mixtures of equal-density glass at different size ratios are vibrated and behavior is characterized as a function of the vibration amplitude. Experiments are also conducted on funnel and mass flow hoppers with outlet open, and the segregation upon discharge is measured for various operating conditions as well as hopper geometries. It is found that the segregation upon discharge varies depending on the operating conditions and flow pattern in the bed.

EXPERIMENTAL AND NUMERICAL STUDY OF FLOW CHARACTERISTICS AND SEGREGATION IN FLOW ENHANCED SYSTEMS

by
Gregory James

A Dissertation
Submitted to the Faculty of
New Jersey Institute of Technology
in Partial Fulfillment of the Requirements for the Degree of
Doctor of Philosophy in Mechanical Engineering

Department of Mechanical Engineering

January 2002

APPROVAL PAGE

EXPERIMENTAL AND NUMERICAL STUDY OF FLOW CHARACTERISTICS AND SEGREGATION IN FLOW ENHANCED SYSTEMS

Gregory Anthony James

Dr. Rajesh N. Dave, Dissertation Advisor
Professor of Mechanical Engineering, NJIT — Date

Dr. Ian S. Fisher, Committee Member
Professor of Mechanical Engineering, NJIT — Date

Dr. Jay N. Meegoda, Committee Member
Professor of Civil Engineering, NJIT — Date

Dr. Chao Zhu, Committee Member
Professor of Mechanical Engineering, NJIT — Date

Dr. Moinuddin Malik, Committee Member
Senior Scientist, Highly Filled Materials,
Stevens Institute of Technology — Date

BIOGRAPHICAL SKETCH

Author: Gregory Anthony James

Degree: Doctor of Philosophy in Mechanical Engineering

Date: January, 2002

Undergraduate and Graduate Education:

- Doctor of Philosophy in Mechanical Engineering,
  New Jersey Institute of Technology, Newark, NJ, 2002
- Master of Science in Agricultural Engineering,
  University of Illinois, Urbana/Champaign, IL, 1991
- Bachelor of Science in Mechanical Engineering
  University of Guyana, Turkeyen, Guyana, 1988

Major: Mechanical Engineering

Presentations and Publications:

Gregory James, M. Malik, and R. N. Dave,
"Experimentally –Observed and Numerically Simulated Characteristics of Granular Flow in Vibrated Wedge-Shaped Containers", AICHE Meeting, Los Angeles, CA Nov 12 – Nov 17, 2000.

Gregory James, Rajesh N. Dave, M. Malik,
"Particle Behavior in a Vertically Vibrated Hopper",
9th Annual Uni-Tech Conference, NJIT, May 2000.

Gregory James, B. Chaudhari, C. Y. Wu, S. Wantano, R. N. Dave,
"Experiments and Simulations of a Magnetically Enhanced Powder Discharge System", 9th Annual Uni-Tech Conference, NJIT, May 2000.

T. P. Ravichandran, A. Mujumdar, Gregory James, R. N. Dave, C. Y. Wu, S. Wantano,
"Study of Powder Discharge from a Vibrated Hopper", Mini-symposium on Particle Technology, Particle Processing Research Center, New Jersey Institute of Technology, March 25-26, 1999.

Gregory James, C. Y. Wu, Rajesh N. Dave,
"Controlling Powder Discharge from Storage by Magnetically Enhanced Powder Discharge System", Mini-symposium on Particle Technology, Particle Processing Research Center, New Jersey Institute of Technology, March 25-26, 1999.

Gregory James, C. Y. Wu, R. N. Dave " Measuring the Angle of Repose by Magnetically Assisted Powder Flow System", Advanced Technologies of Particle Processing: 1998 AICHE Conference, Vol. I, pp. 488-494, November 1998.

To my family: for their love, support and encouragement

ACKNOWLEDGMENT

I would like to express my sincere gratitude to my advisor Dr. Rajesh N. Dave, for his guidance, advice, suggestions, compassion, patience and support in all matters related to my research work, including the writing of this dissertation.

Special thanks, to Dr. Ian S. Fisher, Dr. Jay N. Meegoda, Dr. Chao Zhu, and Dr. Moinuddin Malik for serving as members of the committee.

Special thanks, to the New Jersey Commission on Science and Technology for financial support in enabling the completion of this dissertation.

I would like to thank my friend, Bernard Rollins for his moral support. To the people in my research group who I have worked with: Prof. C. Y. Wu, Ajit Mujumdar, Thottiam Ravichandran, Wenliang Chen, and Manoj Agnihotri, I would like to express my sincere gratitude for their help and support. Special thanks to Dr. Moinuddin Malik for his work on the simulation code used in this dissertation.

I would like to thank my wife and son, Vanessa and Gregory James Jr. for their understanding; words cannot express the support, love and encouragement they have given me throughout the past five years. To my Mum, I wish to extend thanks for her love, support and encouragement throughout my school career.

TABLE OF CONTENTS

TABLE OF CONTENTS
(Continued)

Chapter **Page**

TABLE OF CONTENTS
(Continued)

Chapter **Page**

TABLE OF CONTENTS
(Continued)

Chapter **Page**

LIST OF TABLES

Table **Page**

LIST OF FIGURES

LIST OF FIGURES
(Continued)

Figure **Page**

LIST OF FIGURES
(Continued)

Figure **Page**

LIST OF FIGURES
(Continued)

Figure **Page**

NOMENCLATURE

g	acceleration due to gravity g = 9.81 m/s^2
a	oscillation amplitude [m]
f	oscillation cyclic frequency [Hz]
ω	oscillation radian frequency [rad/s] (w=2π f)
T	oscillation period [s]
Γ	normalized oscillation acceleration amplitude [aω^2/g]
d	particle diameter [m]
r	particle radius [m]
ρ	particle-density [kg/m^3]
m	particle mass [kg]
I	particle moment of inertia [N-m^2]
N	number of particles
$k_{n,pp}$	normal spring constant for a particle/particle contact [N/m]
$k_{n,pw}$	normal spring constant for a particle/wall contact [N/m]
$\nu_{n,pw}$	normal dashpot coefficient for a particle/particle contact
$\nu_{n.pw}$	normal dashpot coefficient for a particle/wall contact [N/(m/s)]
$k_{s,pp}$	tangential spring constant for a, particle/particle contact [N/m]
$k_{s,pp}$	tangential spring constant for a, particle/wall contact [N/m]
μ_{pp}	particle/particle sliding friction coefficient
μ_{pw}	particle/wall sliding friction coefficient
ε_{pp}	particle/particle coefficient of restitution

ε_{pw} particle/wall coefficient of restitution

t time [s]

ϕ oscillation phase angle [rad]

Δt simulation time step [s]

Δ_{ij} overlap between particles i and j [m]

$\hat{n}_{ij}$ normal unit vector pointing from the center of particle i to the center of particle j

$\hat{s}_{ij}$ tangential unit vector for the contact between particles i and j

$\vec{r}_i$ particle i position vector [m]

θ_i particle i rotational position [rad]

$\delta \dot{\vec{r}}_{ij}$ relative velocity of particle j with respect to particle i at the point of contact [m/s]

δs_{ij} the tangential displacement of particle j relative to particle i from the initial point of contact [m]

$\vec{F}_{gi}$ force acting on particle i due to gravity [N]

$\vec{F}_{ij}$ force acting on particle i due to contact with particle *j* [N]

$\vec{F}_{nij}$ contact normal force acting on particle i due to particle *j [N]*

$\vec{F}_{s,s}$ contact spring force in the tangential direction acting on particle i due to particle *j [N]*

$F_{s,f}$ contact sliding friction force acting on particle i due to particle j in the tangential direction [N]

Δ_{max} the maximum amount of overlap for a two particle collision [m]

m_{eff} the effective mass for a two particle collision ($m_{eff} = (m_i m_j)/(m_i+m_j)$) [kg]

$\dot{\delta r}_{\max,ij}$ the maximum relative velocity of particle j with respect to particle i at the point of contact [m/s]

τ collision duration time for a two particle collision [s]

τ_{trans} translational period of oscillation [s]

τ_{rot} rotational period of oscillation [s]

Γ_v normalized vertical oscillation acceleration amplitude

Γ_h normalized horizontal oscillation acceleration amplitude

CHAPTER 1

INTRODUCTION

1.1 Material Handling

Bins, hoppers, feeders, and conveyor handle bulk solids in the form of granular materials in wide ranging industries from chemical and pharmaceuticals to power generation and mining. In plants and processes involving solids, ineffective and unreliable handling systems are often the primary reasons for startup delays, process inefficiencies, and equipment downtime [1]. On the basis of extensive studies of 40 solid processing plants and companies in the US and Canada, the Rand Corporation concluded that eighty percent of all the plants studied, experienced solid handling problems [2]. The design of solid handling systems based on the flow properties of the materials being handled can avoid many of these problems. However, the design practices of bulk solid handling systems are usually based on the information gathered on prior experience which often points to what does not work, instead of what works best. In the past few decades, the theory of geometric hopper design has been well established; however, much remains to be done for high value-added specialty applications, such as pharmaceuticals, cosmetics, and ceramics, which deal with small batch processes involving a wide variety of raw materials. These industries require devices that produce predictable and controllable amount of flows, and avoid segregation upon delivery.

Many of these industrial processes involve vibration of granular materials for flow enhancement. However, there can be many situations in which vibration may negate its very purpose; a common example is of segregation in a mixing process. Also, granular

materials may be subjected to vibration unintentionally, as during their transportation from one place to another, and in such situations effects of vibration may not be desirable. Consequently, the behavior of granular assemblies in response to vibration is an important area of research, which has received wide attention, particularly during the past two decades.

Unfortunately, although many studies have been carried out in relation to the effects of vibrations on granular materials in hoppers, the effects of vibration on granular flow is still not understood. Currently, there are still many areas where the behavior of granular materials continues to elude researchers. Many variables exist, including the material being shaken, the strength of shaking, and the container in which the shaking occurs. Various researchers have carried out studies to examine the effects of these variables on the material. These experiments have demonstrated that shaken granular systems can exhibit a wide range of behavior including fluidization, surface waves, heap formation, convection and compaction. Although the convective motion of vibrated granular materials was observed by Faraday as early as 1831 [3], a full understanding of this mechanism and its relationship to heaping is still lacking, and many differences in opinions that existed earlier among researchers still exist.

While it is well known that vibration can facilitate granular flows, it invariably induces size segregation, and on the other hand, certain vibration levels can lead to material compaction and hence reduced flowability. Granular flow in vibrating hoppers is a complex phenomenon, which, despite continued research efforts remain obscure. In fact, the effects of vibration on granular flow are not characterized and methods for selecting optimal values of frequency and amplitude of vibration have not been

developed. The present research aims at investigating, both experimentally, and theoretically by numerical simulations, the granular flow characteristics in vertically vibrated hoppers.

1.2 Granular Materials at Rest

The fact that there are so many areas where we lack knowledge on the behavior of granular materials, although they are so important to our daily lives, indicates that a

Particle Size range (μm)	Classified as		
<1	Ultra-fine powder	POWDERS	Granular Materials
1 – 10	Superfine powder		
10 – 100	Granular powder		
100 – 3000	Granular solid		
> 3000	Broken solid		

Table 1.1 Classification of particulate solids based on particle size (Richards and Browne, [4] and Neddeman, [5])

theoretical description is far from simple or straightforward. Richards and Brown [4], and Nedderman [5] classified particulate materials as shown in table 1.1. From this classification it is seen that granular materials containing particles between 100 - 3000 μm may be granular solids. The main complication in the study of granular materials arises from the dissipative nature of the particle contacts. This is further complicated by the fact the that behavior of the material characteristics, lies between that of liquids on

one hand and that of solid materials on the other. Bagnold [6] using sand dunes vividly described this range of behavior by illustrating the changes depending on the existing external conditions. The behavior of granular materials at rest depends strongly on the density of packing, which is related to the concept of dilatancy, a concept introduced by Reynolds [7].

1.2.1 Dilatancy

The concept of dilatancy can be understood by considering a granular packed material being sheared, which results in expansion since particles have to make room for others to move. If there is no room for the particles to move, no motion will take place and in general there will be no deformation. As a result of the expansion of the granular system, there is an accompanying increase in pore volume, or a decrease in the volume fraction of the particles.

1.3 Solid -Fluid Transition

Due to the fact that granular materials consist of many individual particles, when a granular material moves, the density has to be below the bulk density of the material at rest. Thus, granular materials may flow if enough energy is supplied to them. In granular materials the energy required to achieve motion is much higher than for molecules. Due to the inelasticity of grain–grain interactions, the flow will cease if the supply of energy is stopped or diminished too much. This energy loss can be attributed mainly to two mechanisms: friction; and loss of relative velocity in head-on collisions.

Granular materials yield when the shear stress exceeds a certain limit. A typical example of this is an avalanche on a pile of sand. This is illustrated when a sand pile is built by dropping particles onto the pile. These particles will come to rest on the surface of the incline pile due to dissipation in collision and friction. However, when a certain limiting angle is exceeded, the surface becomes unstable (the shear stress imposed on the upper layer by gravity exceeds the yield criterion) and a small layer of grain flows down the surface. The surface is thus eroded until a smaller angle is reached which is stable. Grains added to the pile at this angle of inclination will again stop on the pile.

Another important point that has to be mentioned in describing the "liquid-solid transition" is the strong localization of the flow. When granular material yields and starts to flow, this flow is often localized in a small shear zone just like avalanche on the granular pile. Shear zones in granular materials are often only 5 to 10 particles diameter wide [8-11]. Thus, in flowing granular materials, liquid and solids parts often coexists [12]. This fact complicates their description even more.

1.4 Concept of Material Flow

Energy when supplied to a granular fluid material, e.g. via sharing, shaking, or simply by the action of gravity, may result in the initiation of flow. If there is a strong enough energy input, the material can reach a dilute state that resembles a gas. Due to the dissipation in general, energy must continually be supplied to keep the material in the agitated state. Generally, one can distinguish three types of granular flows, although the

boundaries between them are diffuse. According to Savage [12], they can be classified in the following way:

- Quasi-static regime. In this regime, shear rates are very low, the density is very high and the particles are in mutual contact. The behavior is quite insensitive to shear rate, and rather determined by the shear stress. This is a characteristic of a system that is dominated by friction.

- Grain-inertia regime. Here, due to high shear rates and low intermediate density, the shear rate dominates the behavior, since particle collisions dominate the motion. Transmission of stresses and momentum transport takes place either by collision (at intermediate density), or by particle transport (at low density). Most kinetic theories apply to this regime at intermediate densities.

- Transition regime. In situations where regions of high and low density coexist, parts of the system may be classified as quasi-static, others as in the grain-inertia regime. Both friction and collisions contribute to the dissipation. This has been described as probably both the most common regime and the most difficult to describe theoretically.

1.4.1 Theoretical Description of Granular Flows

Currently, there is no complete theory for which both collisions and continuous contact coexist that describes the theoretical description of the transitional regime. Current theories for granular flow description apply mostly to quasi-static and the grain inertia

regimes. Although the quasi-static flow models seem to work well, they are inadequate since they lack the ability to describe fluctuations.

Bagnold [13] outlined a theoretical description of the grain-inertia regime. His theoretical modeling was motivated by the observation that in shear flow, particles move in layers over each other, colliding with particles from other layers as they move along. However, in his model there is no consideration for velocity fluctuations. Although velocity fluctuations are taken into consideration in kinetic theories, these theories usually apply to nearly elastic spheres since they follow the kinetic theory of gases. Kinetic theory use is also limited and this is due to the fact that it deviates for granular materials from that of gases, in that an energy balance is utilized in the equations rather than energy conservation.

1.4.2 Flow Indices

Carr [14] carried out extensive research to define the properties of solid particles that affect their flow through bins, hoppers and feeders. He outlined simple tests and a classification system aid in design and selection of equipment. The American System for Testing and Materials [15] adopted tests for the apparatus and procedures for measuring the test properties referred to as Carr Indices. These test indices are: Angle of repose, angle of fall, angle of difference, loose bulk density, packed bulk density, compressibility, cohesion, uniformity, angle of spatula, and dispersibility.

1.5 Vibrated Granular Materials

Besides using the influence of gravity for shearing of granular materials to set it in motion, the simplest way to supply energy to the system is to vibrate the hopper. Vibration as a means of agitating bulk of particulate solids is employed in many industries. Although numerous research has been done relating to vertical vibration of hoppers, it is only recently that the study of horizontal shaking has been taken up as well [16, 17]. As a result of this, information on the material behavior observed from vertical shaking of hoppers are more advanced that that observed for purely horizontal shaking.

1.5.1 Vertical Shaking

Unfortunately, although many studies have been carried out in relation to the effects of vibrations on granular materials in hoppers, the effects of vibration on granular flow is still not understood. Currently, there are still many areas where the behavior of granular materials continues to elude researchers. Many variables exist, including the material being shaken, the strength of shaking, and the container in which the shaking occurs. Various researchers have carried out studies to examine the effects of these variables on the material. These experiments have demonstrated that shaken granular systems can exhibit a wide range of behavior including compaction, convection, heap formation, fluidization, and surface waves.

Various explanations have been given for different behavior of vibrated granular systems. Small vibrations when applied to a granular system often result in small relative motion of particles, allowing the material to compact. The maximum density, which can be reached in the end, depends on the vibration amplitude and frequency [18]. If a system

of granular particles is shaken above a certain critical amplitude, and the walls and the particles are sufficiently rough, the material may self-reorganize to form heaps [19, 20] which are sustained by convective flows, transporting the material to the top of the heap. Although the convective motion of vibrated granular materials was observed by Faraday as early as 1831 [3], a full understanding of this mechanism and its relationship to heaping is still lacking, and many differences in opinions that existed earlier among researchers still exist.

Heaping is one of the most frequently researched phenomena. Faraday [3] showed that for fine powders heaping might be due to air flow. However, heaping also persists for heavier and larger particles, where the effects of air flow effects should be negligible [19, 20]. Clement et al. [19], carried out experimental studies of heaping in a two–dimensional pile and observed spontaneous heaping and associated convection for the system studied and showed that wall friction can generate convective flows. Knight et al [21] discussed the heaping phenomenon and indicated in their review that the free surface of an initially flat horizontal surface undergoes a convective instability, with the material surface becoming inclined at a slope approaching the angle of repose of the material. Evesque and Rajchenbach [19] observed similar instability to that described by Faraday [3] in a cohesive granular material submitted to vertical vibration, and indicated that a control parameter is the vibration acceleration. The instability occurred beyond a certain threshold, where the horizontal surface became unstable, exhibiting a slope with an angle with the horizontal which was present with glass spheres of 0.2, 0.4, 1 mm diameter but was not present with 2 mm diameter particles. In an effort to explain heaping instability, Pak et al. [22, 23] carried experimental studies focusing on the effects of ambient gases

on granular materials under vertical vibrations. They considered layers of non-cohesive granular materials and found that for particles of diameter d < 1 mm the pressure P of the surrounding gas plays a significant role. In their work, they indicated that there is evidence that the presence of air is involved in the formation of slopes. There are conflicting observations concerning the role of gas in heap formation. Larouch, Douady, and Fauve [24] observed no heaping when the surrounding gas was evacuated to a pressure $P = 10^{-5}$ Torr, whereas Evesque [25] noted heaping for P down to 4 Torr. They concluded that gas plays a part but noted that convection and heaping may still be driven by mechanisms such as friction or inhomogeneous heaping.

Other possible reasons for heaping have been identified as friction between walls and particles, acoustic streaming, and gas pressure. Gallas et al. [26] presented a numerical study of granular material subjected to vibrations in a two dimensional system. They found various types of convection cells, due to the existence of walls or to spatial modulation in the amplitude vibration, and that the direction of motion relative to the walls depends on shear. They also measured the strength of convection velocity. However, they only studied rectangular system and did not offer a direct comparison with experiments. Knight et al. [21] indicated that convection is responsible for all particle motion, and state that the upward velocity is dependent on the distance of the beads from the bed surface. They also found that boundaries play a very important role, with convection being tremendously reduced for smooth or slippery walls. During the application of vibration to particles, depending on the depth of the bed, different flow patterns are often observed. These convective patterns have been observed in both two-dimensional [20] and three-dimensional [27, 28] geometries. In two-dimensions the

convective patterns were simply observed with the help of high-speed cameras [20], while in three-dimensions NMR (Nuclear Magnetic Resonance) was used to visualize the flow patterns [27, 29, 30]. Whereas in two-dimensional systems surface waves are observed, in three-dimensional systems even more complicated patterns like stripes, squares and hexagons are observed. De Gennes [31] proposed a theoretical approach to this instability based on a series of alternative active and passive regimes.

The shape of the system also significantly influences the convection patterns [27, 32], the motion of the boundary particles moving up along the sides of the container down the middle or reversed, depending on if the container is wedge shaped or vertical. Generally, in wedge shaped containers the particles move up the sides of the containers and down the center, while in containers with vertical sides the particles move up the center and down the sides. The wall angle for which the direction of the rolls is reversed depends on the roughness of the walls [32], but even for relatively smooth walls, this reversal is observed [33].

1.5.2 Horizontal Shaking

Although applying vertical vibrations to containers have been studied for some time, and in the more recent past horizontal vibrations have been studied [16, 17], it was only very recently that both horizontal and vibrations simultaneous have been studied [34, 35]. Tennakoon and Beheringer [35] have studied the stability of granular surfaces to both vertical and horizontal vibrations by observing "self piling". Under certain conditions of applied vertical and horizontal vibrations a granular system will spontaneously develop a

slope, the angle that increases with time until equilibrium is reached. Tennakoon and Behringer [35] measured this slope as a function of the horizontal acceleration.

It is well established that in the case of vertical-vibrations experiments, one has to overcome gravity in order to get global particle motion. Using numerical simulations, Liffman et al. [16] investigated convection patterns close to fluidization threshold under horizontal forcing. They detected bulk particle motion by plotting the average particle displacement versus the relative acceleration. Although in their early work they did not find any bulk motion below $\Gamma = 1$, in later work the authors distinguished between two different convection patterns depending on the relative accelerations. No bulk motion was found for $\Gamma < 0.5$. In the range $1.2 < \Gamma < 2.2$, which is marked by a four roll-state with a large amount of surface agitation was found.

1.6 Segregation

Another important aspect of the dynamics of granular materials is the phenomenon of segregation. That is, granular materials of different properties tend to collect together in some region of a specific apparatus. In many industrial applications it is necessary to mix different types of particles before processing, for example, to produce pills. This property is thus counterproductive in industrial applications where uniform mixing of granular particles are necessary. Although recently some progress has been made in understanding the mechanisms behind certain forms of segregation, this has been mainly on a qualitative basis.

Besides using the influence of gravity for shearing of granular materials to set it in motion, the simplest way to supply energy to the system is to vibrate the hopper. Vibration as a means of agitating bulk of particulate solids is employed in many industries. However, size segregation of granular material during vibration is one of the major problems that plague all processing industries handling bulk solids [1, 2, 47]. Considerable literature exists on the mechanisms for particle segregation [36-54]. Arnold [36] listed the primary mechanisms that account for particle segregation as sifting, air entrainment, particle entrainment, trajectory effect, particle size and shape, cohesiveness, and bin flow pattern. Often segregation occurs during loading of hoppers and also upon discharge. One of the problems encountered in trying to understand size segregation is the fact that this phenomenon seems to contradict equilibrium statistical mechanics since the density of the overall packing increases with polydispersivity [37]. The resulting gravity makes the situation with larger particles on the bottom more favorable. Numerous researchers have studied the effects of vibration [36-54] and different theories governing segregation due to vibration has been proposed. Although extensive research literature on the vibration behavior of particulate solids and segregation exists, theories that could predict quantitatively the amount of segregation even in ideal systems, let alone those of industrial complexity have been elusive. Of the different explanations offered by researchers for the segregation phenomenon, two dominant theories have evolved. Namely geometric segregation and segregation due to convection:

- Geometric methods are based on the assumption that when the material is shaken, the pore volume of the system expands and the material lifts off from the bottom plate. Small particles may percolate through these small holes while the material is falling

down. When the material is compressed again by making contact with the boundary, the small holes are most likely filled by smaller particles. The segregation velocity obtained with this mechanism depends strongly on the relative size of the particles [41-43]. Geometric segregation mechanisms are observed to be dominant at low accelerations.

- While the convection theory focuses on the formation of convection rolls that rise in the vessel, the direction of motion of the convection cells changes in direction in rectangular sections or wedge shaped hoppers. A large particle would rise with the convection flow in the container center, and depending on the size ratio of the particles, may not be able to follow the downward stream and thus gets trapped at the surface. In this manner, segregation is an outcome of the convective motion [6, 43, 46, 49].

Among the various parameters that may come into effect during segregation is the form of shaking or the manner in which vibration is applied to the hopper or the container. Julian et al. [40], Duran et al. [41], and Rosato et al. [38, 39] have all given the bed an upward motion and then allowed it to relax. This vibrating technique is not continuous and only geometric segregation was observed. Knight et al. [21] sinusoidally vibrated the bed, but have also allowed periods of relaxation after each cycle. They observed segregation due to convection to occur only above a critical acceleration. No motion of the large particle was observed at lower accelerations. On the other hand, Poschel and Herrmann [45] continuously vibrated the bed using a sine wave and have found that convection could lead to segregation even at low accelerations. Brone and

Muzzio [48] vibrated their binary system of particles using a continuous sine wave and observed segregation and mixing to occur under different vibrating parameters. The rising of a large sphere in the absence of convection was also observed [43].

Applying vibrations to a hopper will also affect the particle-to-particle friction. Half and Warner [50] found that segregation, in a 2D system, was highly dependent on the particle-to-particle friction and that the large particle rose to higher levels as the friction was increased. Knight et al. [21] found that changing the angles of the wall from parallel to slanted cause the convection rolls to reverse in direction. This change in direction was attributed to the particle wall friction.

Various researchers have also examined the effect of particle-wall friction during vibration. Knight et al. [21] found that convection was reduced, as the walls were made smooth. Stronger and more symmetric rolls were formed as the walls were roughened. Lan and Rosato [47] found that the long-term velocity fields reverse direction when the particle-wall friction is set to zero. They also found that the overall convection velocity increased as the wall friction was increased.

Although many factors under different circumstances produce segregation, all the evidence seems to show that the difference in particle size is by far the most important. Jullien et al. [40] and Duran et al. [41] found critical diameter ratios for the continuous rise of the large particles when geometric segregation was dominant. Ahmad & Smalley [37] found that as the large particle size was increased it requires less time to reach the bed surface. Convection theories, however, predict that all particles will rise to the surface at the same speed irrespective of their size. The behavior of binary and single particle systems having the same particle diameter ratios could be quite different. Brone

and Muzzio [48] found that for a set particle diameter ratio and under certain vibrating conditions, segregation would occur in case of a single large particle, while mixing occurs in a binary system. Poschel and Hermann [45] observed that the presence of the large particle could "trigger" convection

The effect of the number of large particles in the hopper may also affect the formation of convection and convection velocity along the bed height. When geometric segregation is dominant, the upward velocity of the large particle is constant along the bed depth and is dependent on the particle size [40, 44, 46]. However, when convection rolls were present, the velocity of the particles depended on their depth below the bed surface, but was independent of their size, (i.e., all particles at the same depth had the same velocity [43]).

The initial position of the larger particles also significantly affects segregation. Ahmad and Smalley [37] found the position of the large particle inside the container affected its segregation. Poschel and Herrmann [45] also observed that the triggering of the convection rolls was very sensitive to the initial height of the large particle. Brone and Muzzio [48], however, observed that in case of a binary system the bed behavior was independent of the initial configuration of the system and that simply changing the frequency could drive the bed from a segregated mixture to a mixed.

In recent years, many researchers have tried to understand the effect of acceleration, frequency and the a/d ratio on segregation. Lan and Rosato [47] also found that at small *a/d* ratios, convection was minimal and that geometry plays an important role in size segregation. At higher acceleration values, the convection rolls start to appear and the convection mechanism becomes dominant. Knight et al. [34] however, in their

three-dimensional experiments, observed no segregation at accelerations below 1.2g. Lan and Rosato [47], using a three-dimensional system, found no long-term convection rolls for $\Gamma < 1.2g$. They also found that even at high accelerations, no convection was observed for $a/d < 0.25$. An increase in frequency is associated with an increase in a single particle's rise [1]. Brone and Muzzio [48] found that as the frequency was increased above 18 Hz, mixing instead of segregation occurred in a binary system of particles. Researchers have also examined the effects of cohesion on segregation. Harwood [51] observed that the particle cohesion has an effect on the behavior of binary systems. It was found that cohesion limits segregation and that greater vibrational energies are required to induce segregation.

1.7 Simulation Methods used to Study Granular Materials

Within recent years, with very powerful computers being developed, numerous researchers [55–66] have made attempts to study the behavior of granular materials using computer simulations. A review of the most common simulation techniques that are used to model the dynamics of granular systems is outlined in the following paragraphs. Molecular dynamics simulations are discussed in some details, since these will be used here to model granular materials. Among the most common simulation methods utilized in Granular Materials are the following techniques: molecular dynamics, Monte Carlos Method, Diffusing void Method, Method of Steepest Decent, and Cellar Automation.

As implied by the title, molecular dynamics simulations were initially developed for the simulation and molecular study of the liquids and gases [55]. When used in the

study of granular particles, this method is often referred to as a discrete-element method. Generally, there are two types of molecular dynamics simulations methods, referred to as time-driven simulations, and event driven simulations. The difference in these two methods is in their treatment of inter-particle reactions. In time driven simulations, a potential acts between the particles (repulsive when they overlap and zero otherwise in the case of grains), the equations of motion for all of the particles are integrated numerically, with a specific constant time step. The application of the time-step driven simulation to granular materials was first introduced by Cundall and Strack [56], and has been used in numerous studies [52, 57-59]. Details of the time-step driven molecular dynamics are outlined in detail in chapter 4 of this thesis.

In event driven molecular dynamics simulations, particles are treated as hard spheres, and collisions are taken as instantaneous. This technique is more often used in granular systems where the particles are of low density, and where there are no long-range interactions between particles. The particles will spend more time in free flight and it is more favorable to avoid using constant time steps, but rather to calculate all the collision times in the system and update all particle position, velocities and accelerations to the shortest time calculated. This is especially simple for hard spheres, where the collisions are instantaneous, that is, the contact time is zero, and only binary collisions occur. In event-driven simulations, instead of introducing a force between particles, a collision operator is defined which acts on the velocities of the colliding particles in event driven simulations, the trajectories between collisions are computed analytically if the forces acting on the particles allow.

Another popular numerical technique used to study the behavior of granular materials is the Monte Carlo method [55]. Initially, this method was used to study size segregation of binary materials undergoing vertical vibrations. In this technique, the influence of shaking is modeled by lifting the bulk of the material in the container then randomly displacing the particles while allowing no overlap. The use of this method is limited due to many limitations, namely the fact that no physical time scale enters the model since the collision time is zero and the normal restitution coefficient has to be zero in order to minimize the potential energy during each particle move. The Diffusing-Void Model [62] and the Method of Steepest Decent Models [40] have found very limited use in granular materials due to the many simplifications and limitations. The simplifications in these models make them inadequate to describe many of the particle properties.

1.8 Objectives

The motivation for this dissertation comes from the general lack of a reliable method for flow enhancements and characterization for cohesive materials, and inadequate information on granular flow of particles in vibrating hoppers. The major objective is the study of flow enhancement techniques, specifically, investigation of two techniques, magnetically assisted particle flow (MAPF) enhancement, and vibration based flow enhancement. With respect to the MAPF method, which is a recently developed technique at the Particle Processing Research Center, NJIT, the objective is to investigate in detail its applicability as an Angle of Repose (AOR) measurement technique. The study will examine the effects of various variables including the dropping height, mass of

the powder used in the hopper, magnetic field strength, hopper position in the magnetic field, mass of magnetic particles hopper outlet area and mesh size.

The research objectives for the other flow enhancement technique, which is the vibration based approach, include systematic investigations of; the flow patterns of mono-disperse particles in vibrated wedge shaped hopper, including the effects of the lateral vibrations induced due to system imperfections, the effects of various system parameters and identification of important regimes of behavior based on the state diagram of dimensionless amplitude and frequency of applied vibrations, examination of vibration effects on binary mixtures while in the hopper, and upon hopper discharge.

CHAPTER 2

MEASURING ANGLE OF REPOSE USING MAGNETICALLY ASSISTED POWDER FLOW SYSTEM

2.1 Introduction

In order to design silos, feeders, and flow promoting devices, it is necessary to know the flow properties of bulk solids. In contrast to pure fluids, the flow properties of bulk solids cannot be described only by knowing the name and the chemical structure under consideration. This is due to the large number of additional parameters, beside the chemical composition that can have an influence on the flow behavior of the bulk solid. These parameters include particle size distribution, particle shape, for example, spherical or plate-like, particle surface and moisture content. The characterization of powders are further complicated by the fact that the actual state of consolidation plays a very important role. A bulk solid behaves like a fluid in the fluidized state, whereas, it behaves like a solid if it has been compacted. During the storage and transportation of bulk solids, states may exists which lie between these two extremes.

In most technical applications, a consolidated bulk solid at rest has to be set to flow, that is, the yield point of the bulk solid has to be overcome. In order to measure the flow properties of fine-grained bulk solids, shear testers are used, of which the best-known example is the translational shear tester introduced by Jenike [65, 66], called the Jenike shear tester. The Jenike shear tester is often used, as a device by which the flow properties of a powder, in particular, the flow function can be measured. Details of the operation of this tester can be found in numerous references [65-67]. Schewedes [67] has given an overview of the different shear testers and divided them according to the way

the shear plane is formed. Although the Jenike shear tester has successfully been used in the design of silos and hoppers, it can be seen as a disadvantage that its operation is time-consuming and requires a certain level of skill. Additionally, the Jenike shear tester cannot be applied to all types of bulk solid, for example, if the products are too deformable or poor flowing. The Jenike tester is best suitable for use in cases where large batches of powder are available for testing.

Technologists handling powders on a day-to-day basis require a practical method of following the changes in powder flowability. Due to the need for the development of a quick, simple, reliable and reproducible test to characterize the flowability of powders, researchers have developed several empirical methods for the assessment of bulk solid properties. The measurement of angle of repose (AOR) has proven to be a quick, and attractively simple method of characterizing powders. Fayed and Otten [68] defined AOR in general as "the angle formed between the horizontal plane and the slope extending

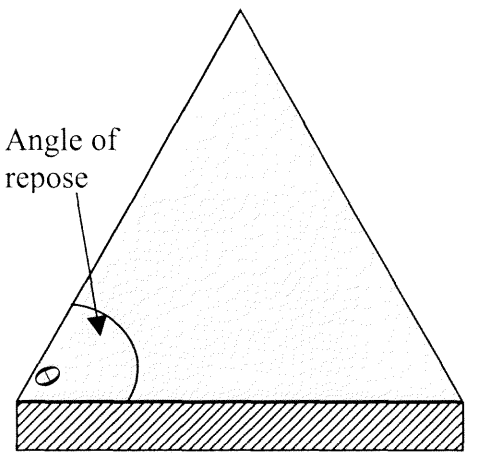

Figure 2.1.a Diagrammatic representation of the angle of repose

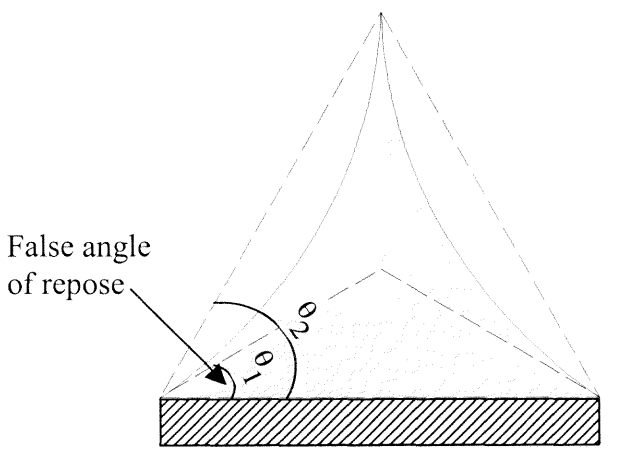

Figure 2.1.b Diagrammatic representation of false angle of repose

along the face of a heap formed by pouring material onto a horizontal surface". Figure 2.1.a shows a diagrammatic representation of the angle of repose. Unlike other flowability parameters, such as the cohesion, which requires the execution of a series of long test, the measurement of AOR can be finished within 15 minutes. The AOR-experiment also has the additional advantage that it is a simple procedure, while cohesion test needs an experienced operator.

Angular properties of powders are of significant importance since the natural angle of slip, the angle of repose, angle of internal friction, wall friction, all derived from the shapes of cones and heaps of powders, provide valuable information about their likely behavior in pipes, chutes, hoppers, tablets and capsule-filling machines [69]. However many researchers have found that the properties of powders, depend to some extent, on the details of the experimental techniques employed in measuring them. Also the current methods very often rely on the testers' skill. Hence, it is very important to understand the factors that ultimately affect the measurement and to devise a method that can avoid the deviation due to the testers' skill. Several researchers have concluded that angle of repose is a useful property for characterizing the flow of powders [69-79]. Unfortunately, values of AOR derived by various researchers using a variety of methods and different devices often yield different results. Particularly with cohesive powders, the cone formed may not be uniform in structure and may have a peak formed with irregular slopes. The angle of such a peak may result in inaccurate reading of the angle of repose, referred to as the false angle of repose shown in figure 2.1.b. Hence, it is not easy to compare the results often obtained. This greatly affects the confidence in the use of this value.

The increasing use and production of fine powders in pharmaceutical and chemical process industries have increased the need for quick and reliable methods for assessing the mechanical properties and the general handling characteristics. Craik [70] studied the flowability of cornstarch using angle of repose when magnesium oxide was added. He found that the manner in which the powder falls when using the standing cone methods affects the results. Train [71] compared several methods of measuring angle of repose and showed that the different variables involved in the measuring techniques affected the final value of θ. It was obvious from his work that for a given material a set procedure gave reproducible results. Carr [72] proposed a method for the evaluation of flowability of free flowing, and moderately cohesive powders. This method of evaluation was adopted by the American Society for Testing and Materials [15], and consisted eight measurements and two calculations to provide ten tests for Carr Indices. The first of the ten tests is the measurement of the angle of repose. In his work, Carr [72], noted that the angle of repose is a direct indication of the potential flowability of a material, and indirectly measures the following properties affecting flow: (1) shape, (2) size, (3) porosity, (4) cohesion, (5) fluidity, (6) surface area and (7) bulk.

The shape of the cone formed when measuring the AOR can significantly affect the accuracy of the results. Craik and Miller [73] found that when the angle of repose is large, irregular heaps are formed leading to variations in subsequent readings of as much as 10 to 20 percent. E. Teunou et al. [78] examined the different methods used and suggested that one of the main factors affecting the measurement of the AOR characteristic of a granular pile is the measuring method. Wouters and Gelddart [77] outlined that, in addition to the powder properties, the design of the equipment and the

measuring technique also play a very important role. Their findings confirm that the angle of repose corresponds only qualitatively to the flow of a powder. Also, great difficulties exist in obtaining consistent results using the existing methods especially when measuring the AOR of cohesive powders.

Jones and Pipel [74,76] studied the angular properties of magnesia and their relevance to material handling using different angle of repose measuring techniques. They found that the fixed based methods gave variable results due to non-uniform "broken flow". Neuman [75] outlined that the angle of repose is very useful in evaluating the properties of powders but stated, that when measuring the angle of repose using the popular methods, the results are generally affected by the impact of falling particles, and the sliding on wall supporting surfaces. Pipel [74] studied the variation that occurs in the AOR of different size fraction of magnesia when experimental conditions were varied. He outlined that AOR was mainly dependent on the extent to which the specimen had been consolidated.

When properly measured and interpreted, angle of repose can be a very useful method of characterizing the flow of powders [79]. Although this method does not give information about the behavior of the bulk solid under stresses which are present in hoppers, and some of the other influences which are important for the design of silos such as storage time and stress level, AOR is still popularly used since it is considered a practical method of assessment of inter-particulate friction and is measured in a standardized manner in the popular Hosokawa Powder Tester, which is based on the work of Carr [72]. It is a dynamic method of measuring flow and thus sometimes

preferred. With a more improved, reliable, and faster measuring technique, greater use can be made of this relatively simple measure of the properties of powders.

Due to the variations in the measurements by different methods and to the variety of parameters influencing the measurement of the AOR, there is the need for comprehensive work to be carried out to understand the factors that ultimately affect the measurement and to design a method that can reliably predict the flow properties of powders. In this work, a new type of device to measure AOR called the Magnetically Assisted Powder Flow (MAPF) that was developed at the New Jersey Institute of Technology for the flow enhancement of cohesive powders is used to measure facilitate the study of the AOR [80]. The MAPF method is based on a concept of multiple, point source, and internal excitation. This device has been investigated for discharging cohesive powders from a hopper. The operating principle of this device is different from conventional flow enhancement devices such as pneumatic, vibrational, or mechanical systems. Details of the operation of this new device can be found in work previously done [80, 81]. Different parameters that affect the measurements are studied including: the falling height, mass of magnets, the mass of corn starch, the magnitude of the magnetizing voltage, the size of the hopper opening, the mesh size and the position of the hopper in relationship to the center of the magnetizing field.

2.2 Experimental Method

The schematic of the experimental system is shown in Figure 2.2. The hopper is made of Plexiglas. The diameter is 5 cm, cylindrical section of the hopper is 15 cm long, and the

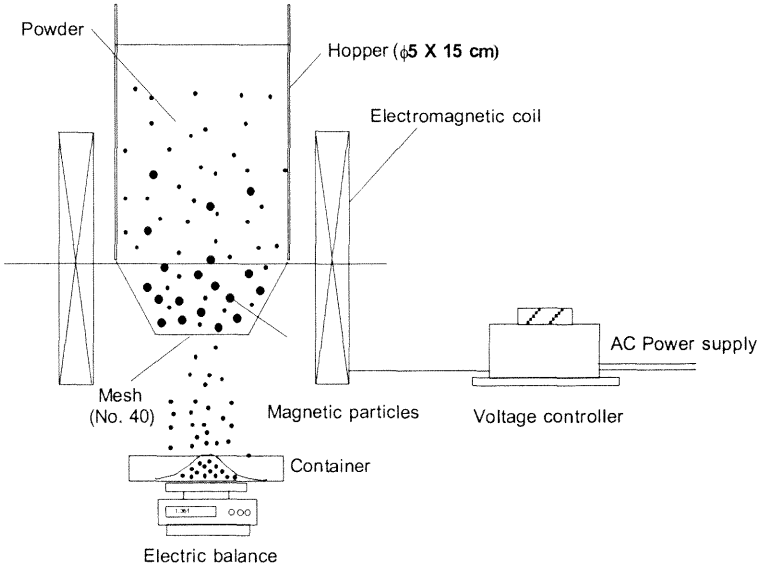

Figure 2.2 Schematic Diagram of MAPF

hopper angle is 60°. Hopper outlets of varying diameters are used for comparative purposes. A measured mass of magnetic particles are first placed in the hopper and held in place by a fine mesh. The magnetic particles are made of barium ferrite and coated with polyurethane to prevent contamination. Cornstarch, which was oven dried to constant moisture content, is then placed in the hopper. An external magnetic field is created using an electromagnetic field surrounding the hopper provided by field coil windings. When the magnetic particles are agitated by the external magnetic field surrounding the hopper, the powder is fluidized by the agitation resulting in flow through the base of the hopper and onto an electronic balance. Each individual test measurement is repeated three times. The angle of repose is measured with the use of a digital camera

that is connected to a computer. The images of the cones are transmitted to the computer where the angle is measured using the position coordinates of the outline of the cone. In addition to cornstarch, tests were carried out on three other different materials: sodium bicarbonate, sodium carbonate, and lactose. These materials were used so as to make comparisons with results obtained by Geldart and Wouters [77]. Table 2.1 below shows a list of the main materials tested. These materials differed widely in their mean particle size, sometimes resulting in different samples of the same material belonging to different groups in Geldart's classifications. Additional tests were also carried using carbon black and calcium carbonate.

MATERIAL TYPE	SHAPE/APPEARANCE	SIZE RANGE[(a)] (μm)	GROUP IN GELDART'S[(b)] CLASSIFICATION
Corn starch, commercial grade	Organic, disc like White	15	C
Sodium bicarbonate, commercial grade	White crystalline Powder	115-15	A/C
Sodium carbonate, commercial grade	Needle like shape, white granular solid	60-20	A
Lactose, of pharmaceutical quality	White crystallized Powder	60-15	A/C

Table 2.1 Characteristics of Materials used.

(a) Diameter measured using sieve analysis
(b) Group A powders are free flowing: Group C powders act cohesively, A/C powders show behavior of both group A and C powders

Experiment using a vibrated hopper were also conducted and the results compared with that obtained by the MAPF method. The tests using the vibrated hopper were carried out using test methods commonly used in the literature. That is, the fixed base method and the constant mass method were used. To further analyze the results, angle of repose tests were carried out using the Hosokawa Micron Powder tester commonly used in industry. Qualitative comparisons were made between results obtained from the Hosokawa Micron tester and the MAPF method. The various parameters that may affect the measurement and ranges of these parameters are listed in table 2.2.

Table 2.2 List of Experimental Parameters

	TEST	RANGE
1	Falling height	10cm – 35cm
2	Voltage	15V - 50V
3	Mass of Corn Starch	4g – 20g
4	Hopper position	-2 cm - 2 cm
5	Mass of magnets	1g – 10 g
6	Diameter of hopper	1.2cm – 5cm
7	Flow rate	0.2g/s – 2.3 g/s
8	Mesh size no. (US Standard)	30 – 50
9	Particle diameter	15μm – 105μm

Although tests were carried out using the materials listed in table 2.2, cornstarch was chosen as the base material for carrying out the testing of all of the experimental parameters. Cornstarch was chosen for several reasons. In addition to cornstarch being organic, it is widely used commercially and is easily obtained. Cornstarch also has poor flowability and high moisture absorption, thus providing a difficult test material hence

hence providing a suitable test to measure the efficiency of the MAPF system. Figure 2.3 shows a SEM micrograph of cornstarch highlighting the shape. When cornstarch was tested in a Jenike tester [80], the computation indicated a minimum outlet size of 1.2 m for a conical hopper further indicating that this is a very cohesive material.

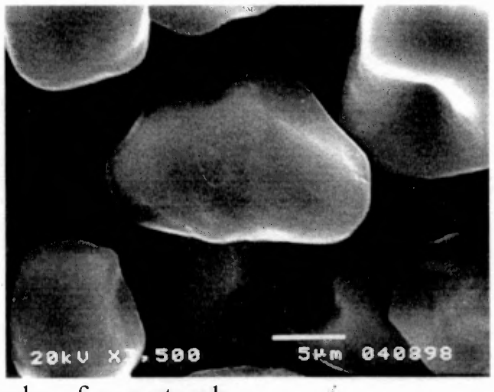

Figure 2.3 SEM micrographs of cornstarch

2.3 Results

One of the main criticisms of using the Angle of Repose as a measure of the flowability is the fact that many of the measuring methods currently used being used do not produce

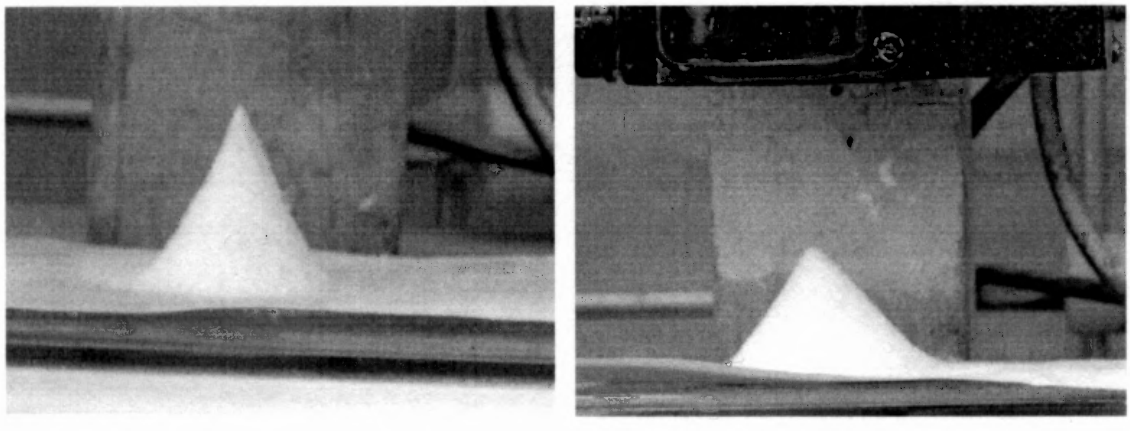

Figure 2.4 Cone shapes obtained using Magnetically Assisted Particle Flow (MAPF) for two types of powder: (a) cornstarch, (b) lactose

straight uniform slopes. This leads to false peaks or multiple peaks and as a result inaccurate or approximate values being measured leading to what is known as a false angle of repose [75]. A representative image of the powder cone obtained using MAPF is shown in Figure 2.4. The feature of this new method can clearly be observed in this figure. The rough surface and the varying slope commonly observed in other methods are no longer seen in this method. Instead, a surface with a constant slope is obtained with a single peak. As a result of this uniform slope, the angle of repose measurements are more accurate and easier to obtain.

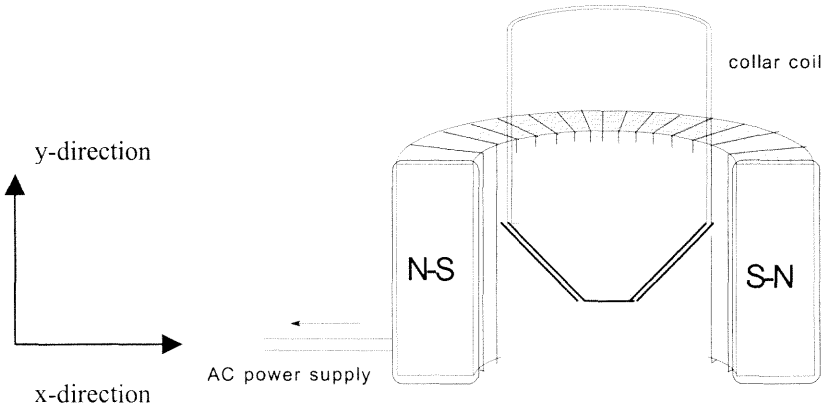

Figure 2.5 Schematic diagrams of the magnetic field coil and the hopper

A schematic of the magnetic field coil and hopper is shown in Figure 2.5. This diagram highlights the fact that the location of the hopper in the magnetic field can vary along the vertical and horizontal axis of the field coil windings. In order to determine the optimum location of the hopper within the magnetic field, measurements of the magnet flux density were carried out along the length of the field coils and across the axis. These measurements were made using a magnetic flux density meter held in placed along the vertical and the horizontal axis of the field coil. Measurements for the along the vertical

axis were taken considering the top of the field coil windings as the zero position. In considering the horizontal axis, measurements were taken moving the flux density meter across the internal diameter of the field coil moving from left to right. Figures 2.6 show plots of the magnetic field along the vertical axis of the coil for two values of voltage. This plot indicates that the field along the axis is strongest in the middle of the coil. A plot of the magnetic field strength along the horizontal axis is shown in figure 2.7. This

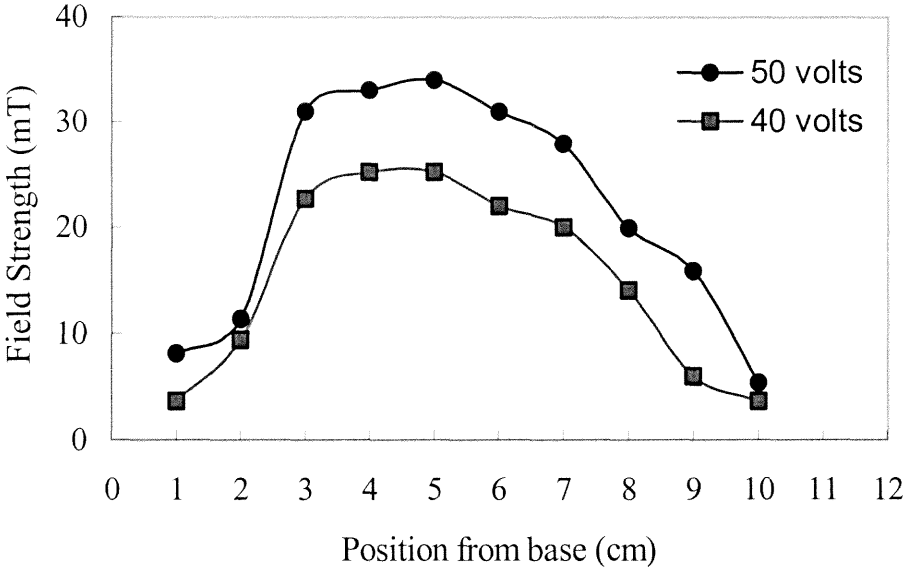

Figure 2.6 Strength of magnetic field as a function of position along the vertical axis.

plot indicates that the strongest magnetic field is closer to the wall of the coils and decreased to a minimum in the center as you move across the diameter of the coil, before increasing back to its maximum value close to the wall. The information obtained from these plots was used as a guide in the decision to place the hopper in the field with the base in the center of the coil along the vertical axis of the coil.

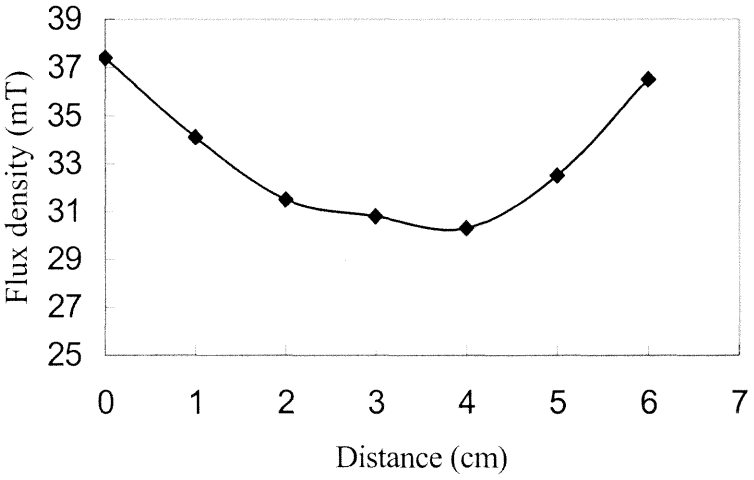

Figure 2.7 Strength of magnetic field as a function of position along the horizontal axis.

As reported by Craik, Train and Neuman, Train [70, 71, 75] the measurement of AOR is affected by the impact of the falling particles. The falling height is varied to investigate this effect. The results are shown in figure 2.8. As shown, the angle of repose

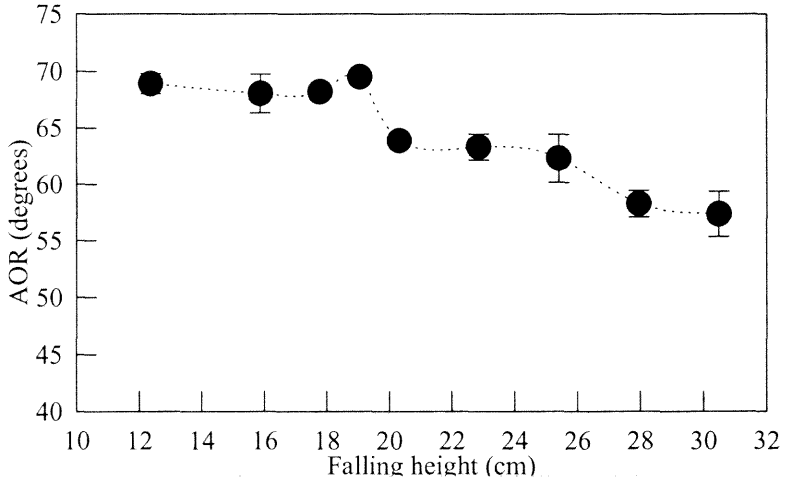

Figure 2.8 Angle of Repose as a function of falling height

decreases as the falling height increases above 19 cm for a given mass of cornstarch. The mass of cornstarch used was 20 grams. The decrease is due to the dispersion of the

powder flowing out of the hopper resulting in the spread in the powder over a larger area. Consequently, there were fewer particles falling onto the heap of cornstarch resulting in a heap that is not completely formed. That is, for the increased height, it takes a longer time for the cone formation due to the loss of powder particles to the surrounding area. This dispersion is influenced by the exposure of the light powder to the air while falling to the flat surface. The dispersion of the cornstarch above 19cm was linked to the presence air-drafts present. Reducing the presence of air currents reduces the dispersion of cornstarch. For a falling height less than 19 cm, the powder is confined to approximately the same area. Hence, the AOR measured does not change. The minimum falling height considered was 12cm. This height allowed enough clearance between the top of the cone and base of the housing for the field coil windings so as to allow to easy measurement of the cone angles.

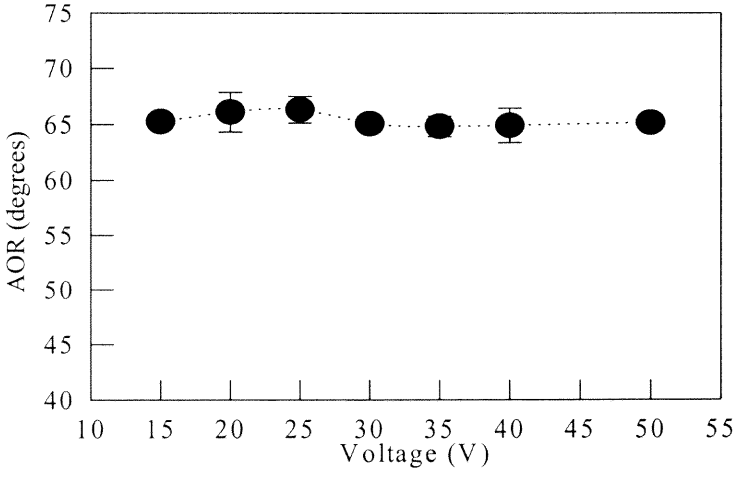

Figure 2.9 Angle of repose as a function of voltage

The measurement of angle of repose as a function of magnetic field strength is shown in Figure 2.9. Here, the mass of magnetic particles used was 4 grams, for 15 g

cornstarch, while the minimum voltage tested was 15 volts. Below 15 volts for this mass of magnet the rate of flow was very slow. Increasing the voltage supplied to the field coil windings resulted in a stronger magnetic field and as a result increased agitation of the magnetic particles. Although an increase in the voltage resulted in some increase of the powder discharge rate due to the increased fluidization of the powder, it can be seen in the figure that the AOR remained constant with voltage for the range of voltage used in this test. The voltage increase did not result in there being a significant effect on the momentum of the particles hitting the pile of cornstarch and as a result the AOR for this case was constant. The values obtained in this experiment were within 2.5 percent reproducibility. The upper range for the voltage reported in figure 2.8 is 50 volts. Using the MAPF system above 60 V in excess of 5 minutes, results in the automatic shutdown of the system due to overheating of the field coils of the MAPF system.

The measurement of the AOR has been reported to be very sensitive to the amount of powder, varying from one method to another [71] and hence choosing an appropriate amount is critical. The importance of the Angle of Repose in characterizing powders will be enhanced if a method is found to measure this quantity where it is independent of the mass of powder used. The amount of powder used is investigated and the results are shown in Figure 2.10. The applied voltage for these tests was 35 V, with 3 g of magnetic particles used. The results indicate that beyond 10 grams of cornstarch the value of the AOR maintains a relatively constant value, with a maximum variation of 3 degrees. Below five grams the shape of the cone was still developing and has not been formed completely hence it possesses a different value. Above 25 grams of cornstarch the cones formed by the cornstarch leaving the hopper crumbed. The fact that the AOR is

constant beyond 10 grams indicates that the new method is not affected by the amount of powder used once the cone is formed, thus making it a reliable method.

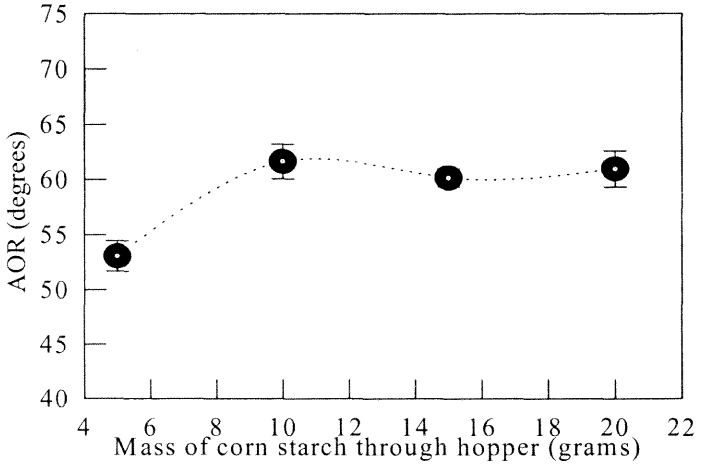

Figure 2.10 Angle of repose as a function of mass of cornstarch through hopper

Due to the fact that the strength of the magnetic field varies along the vertical axis of the field, the level of excitation of the magnetic particles in the hopper will vary with the location of the particles within the field. Figure 2.6 showed a plot of the magnetic field strength along the vertical axis of the magnetic field. In order to determine the effect of the strength of the magnetic field on the AOR, experiments were carried out varying the location of the hopper outlet location from the center of this field along the vertical axis. Figure 2.11 shows a plot of the AOR as a function of the position in the magnetic field. The center location of this field coil was considered the base point from which all measurements were made with distances above this point being considered positive, and distances measured below this point being considered negative. The AOR varies slightly as the position changes due to the corresponding small changes in the flow rate as a result

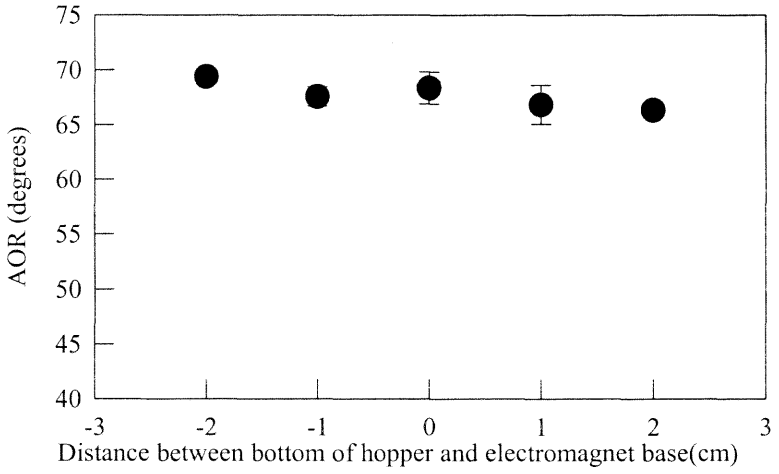

Figure 2.11 Angle of repose as a function of hopper position in magnetic field

of the variation in the magnetic field. Using a more consistent magnetic field can eliminate these minor variations.

The effect of the mass of magnetic particles used for a fixed quantity of powder

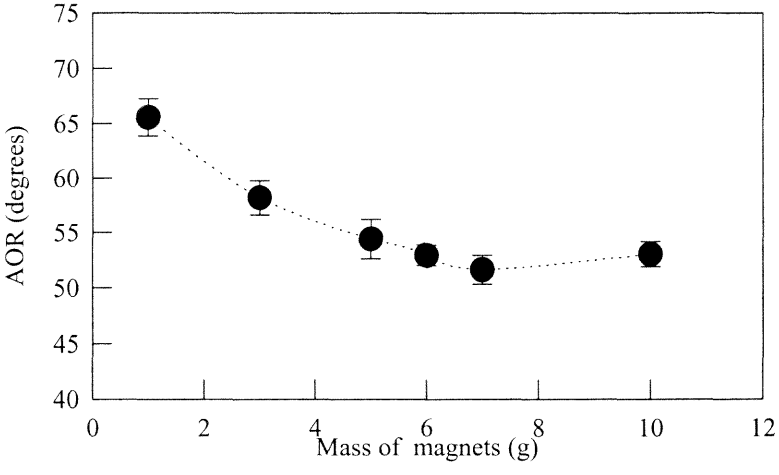

Figure 2.12 Flow rate as a function of mass of magnets

was investigated for a constant voltage of 35 g. Wu et al. [80] reported that the flow rate increases proportionally to the mass of magnet. The results obtained for values of the

angle of repose while varying the mass of magnetic particle shown in Figure 2.12. As illustrated in Figure 2.12 the mass of magnets significantly affected the value of AOR obtained. This significant change was due to the fact that changes in the mass of the magnets resulted in significant changes in the level of agitation of the powder, resulting in an increase in the flow rate of the cornstarch leaving the hopper. This increase in flow rate resulted in increases in the momentum of the particles and a flattening of the resulting cone formed. To obtain a reduced momentum of the powder leaving the hopper, with increases in the mass of magnetic particle used, it is necessary to reduce the applied voltage.

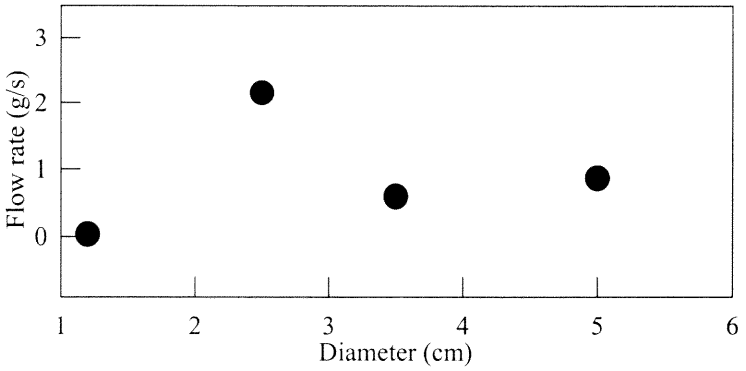

Figure 2.13 Flow rate as a function of diameter of hopper outlet

Figure 2.13 shows a plot of flow rate versus the outlet diameter of the hopper. Four different sizes of outlet diameters with dimension 1.2cm, 2.5cm, 3.5cm and 5cm respectively were used, with the mass of the cornstarch used kept constant, and a magnetizing voltage of 35 g. From figure 2.13 it can be seen that the highest flow rate was obtained with the 2.5cm diameter hopper outlet. This plot indicated that for a given hopper optimum flow rate is obtained from a specific outlet diameter size.

As seen from figure 2.13 the output size of the hopper was also studied, and showed that the flow rate was different for different size openings when used with a constant voltage and the same mass of magnets. In order to further examine the effects of flow rate on angle of repose, figure 2.14 shows a plot of the AOR as a function of the flow rate obtained from the different hopper outlet diameters. This plots shows that the diameter of the hopper with the fastest flow rate resulted in the lowest value of AOR whereas the outlet diameter of the hopper with the lowest flow rate gave the highest value of AOR. These results confirm that stated in existing literature in that increasing flow rate results in increasing momentum of the particles when the hit the pile and as a result a

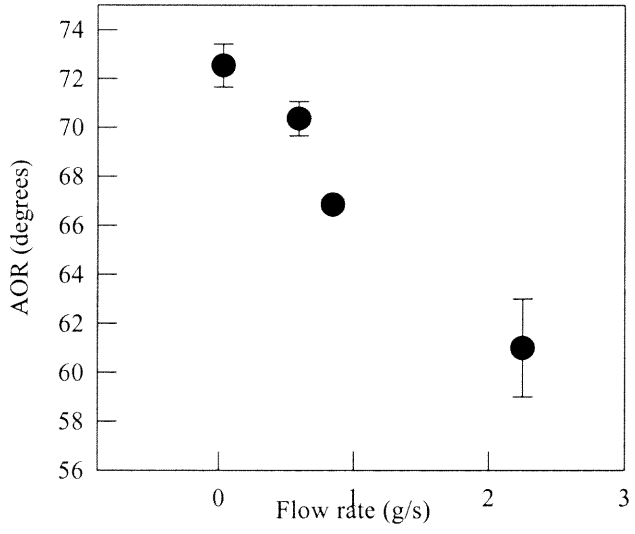

Figure 2.14 Angle of Repose as a function of Flow Rate.

decrease in the AOR. Choosing a low voltage thus reducing the agitation of the magnetic particle may easily eliminate the effect of the flow rate on AOR.

In addition to the diameter of the hopper being an adjustable variable in the MAPF method, the size of the sieves holding the magnetic particles in place may also

vary. The effect of the sieve opening on the AOR was examined. The mesh sizes considered consisted of sieve openings ranging from 600μm to 300μm. For these test the

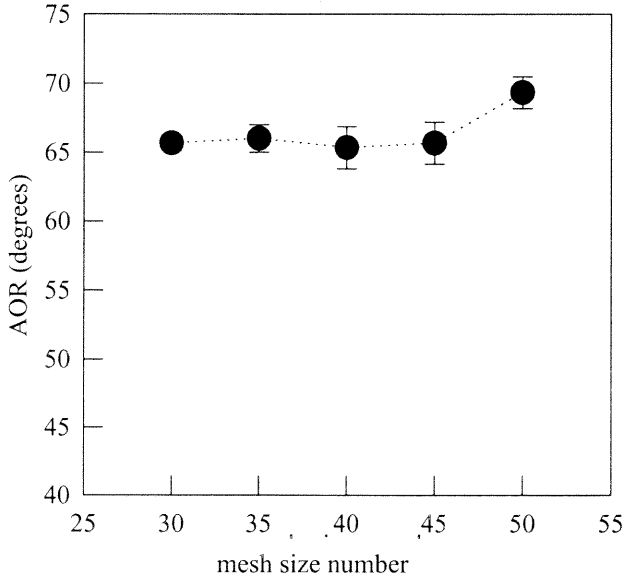

Figure 2.15 Angle of repose as a function of the mesh size

applied voltage used was 40 volts. Figure 2.15 shows a plot of the AOR as a function of mesh size. The results indicate that for the range of mesh size considered there was very little effect on the AOR values obtained.

Geldart and Wouters [77] carried out tests for the AOR for the same powders when materials move from "good flow" to "bad flow". The powders tested by Geldart and Wouters were sodium bicarbonate, fluid cracking catalyst, sodium carbonate and lactose. Figure 2.16 shows a plot of AOR versus particle diameter for materials sodium carbonate, sodium bicarbonate, and lactose using the MAPF method so as to compare with the results obtained with Geldart and Wouters. For all of the materials, a distinct increase in the AOR is observed as the diameter particles decrease. These results are as expected since as the diameter of these materials are reduce, the cohesive strength

increased, reducing their ability to flow. These results compare favorably with the results obtained by Geldart and Wouters [77] for the AOR for the same powders.

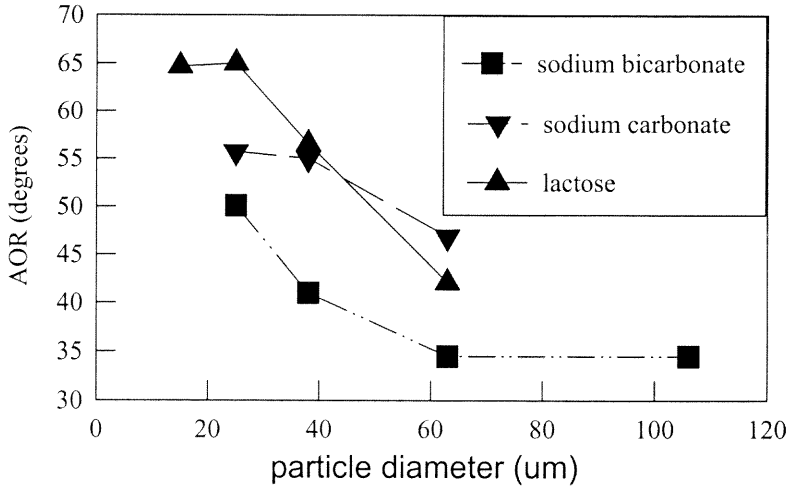

Figure 2.16 Angle of repose as a function of particle diameter for sodium bicarbonate, sodium carbonate and lactose.

TABLE 2.3 Values obtained for experiment comparing AOR for vibrated hopper and MAPF hopper

Mass flow rate = 2.6 g/s		
Height of hopper above surface = 6 ins. (15.24 cm)		
Mass of Cornstarch	*AOR MAPF (degrees)*	*AOR Vibrated Hopper (degrees)*
5 grams	58	56
10 grams	62	65

As outlined earlier in this dissertation, there are many different techniques to measure the Angle of Repose. Among these techniques the use of vibration to enhance

flow is very popular. To compare one such technique with the MAPF method, a vibrating funnel together with a fixed size base was used and compared with the MAPF method using a fixed size base. Table 2.3 shows a comparison between the values of the AOR between the vibrated hopper and the MAPF technique. For the vibrated hopper experiment, the same hopper was used, with vibration being provided by an unbalanced motor attached to the hopper. The same flow rate between the vibrated hopper experiment and the MAPF was used so as to make the comparison. Table 2.3 shows that very similar values were obtained, however, sharper images were obtained using the MAPF method, making the angles obtained easier to measure.

A very popular method used to test behavior of powders is the Hosokawa Micron powder Tester. This powder tester uses a mechanized method to measure the angle of repose together with other powder flow characteristics and is based on powder testing work done by Carr [72]. The Hosokawa micron tester was used to measure the AOR of the powders tested using the MAPF method.

Figure 2.17 shows snapshots of the cones obtained for using both the Hosokawa Micron and the MAPF powder testers. For the experiments carried out using the two powder testers, the results obtained by the Hosakaw Tester was generally between three degrees and five degrees smaller than the values obtained using MAPF. As can be observed, the slopes obtained by the MAPF were sharper and as a result less likely to give inaccurate results. The differences in the values for the AOR may have been due to the fact the MAPF has the capability of having smaller flow rates and as a result decreased momentum of the particles hitting the pile. This will result in larger values of

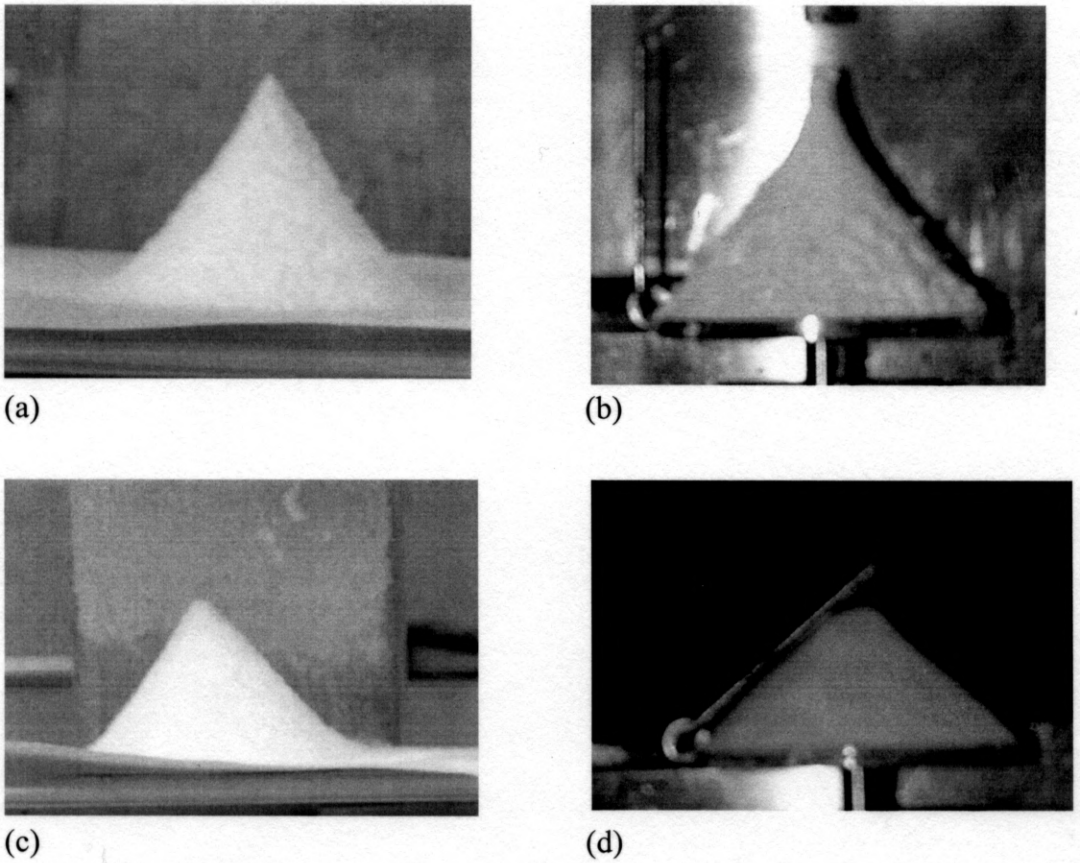

Figure 2.17 Angle of Repose snapshots of cornstarch using (a) MAPF, (b) Hosokawa Micron Powder Tester. Angle of Repose of lactose using (c) MAPF (d) Hosokawa Micron Powder Tester

AOR than that obtained from methods that cannot reduce their flow rates as low as the MAPF method.

2.4 Conclusions

In this study, an examination of the existing methods of measuring AOR was done, the problems encountered were observed and a new method called the MAPF method was proposed. The parameters that affect other AOR measuring equipment and those factors that may affect this new equipment were tested. The parameters tested included the

falling height, mass of powder, magnetic field strength, and hopper position in the magnetic field, mass of magnetic particles, hopper outlet area and mesh size and particle size. These tests indicate that for the range used, the magnetic field strength and the mesh size tested have no significant effects on the AOR. The factor that significantly affects the AOR is the momentum of the powder particles hitting the pile [70,71,76]. Using this new method, the velocity of the particles leaving the hopper is easily controlled hence factors such as the hopper outlet area which has some effect on the AOR due to the changing flow rate can be controlled. As a result, it is easy to control the momentum of the particles hitting the pile giving this method a significant advantage over other existing methods.

Other advantages of this method include the following:

- Mechanism is easy to operate thereby reducing errors due to inexperience operators.
- Sharp boundaries obtained for cones thus giving precise values for AOR.
- The occurrence of false peaks is eliminated.
- Very high degrees of reproducible results are obtained.
- Method can be applied to very cohesive bulk solids, which flow badly.
- Tests require very little time.
- Easy to control many of the parameters that affect AOR thereby enabling the effects of these parameters on AOR to be studied independently.

The MAPF system although suitable for the powders tested in this dissertation, may not be suitable for some of the powders often used in industry. Friable powders, which cannot tolerate the vigorous action of the magnetic particles, may break resulting in a

reduction in the particle size. Added to this, powders with magnetic properties may react to the presence of the magnetic particles and the magnetic field present. Mixtures containing magnetic and nonmagnetic material may also segregate, and the MAPF system will not operate satisfactorily. As outlined earlier, the powders tested were sieved to obtain the size range. If the powder being tested covers a wide cross section of particle diameters, the MAPF may not operate properly due to the fact that the particles are initially held in place by a mesh, placed at the bottom of the hopper. This presence of this mesh may result in the MAPF operating as a sieve when testing such powders.

The advantages listed above clearly easily offsets the disadvantages that affect may affect the use of the MAPF method for measuring the AOR. Test carried out on the magnetic particles used in the experiments did not show any attrition for the periods lasting thirty minutes. However, prolonged use in excess of this time may result in attrition leading to contamination of the tested powder. To verify the extent to which the MAPF method can be used, further testing is necessary.

CHAPTER 3

EXPERIMENTAL ANALYSIS OF FLOW PATTERNS IN WEDGE SHAPED CONTAINERS

3.1 Introduction

Many of the current popular devices for flow enhancement of bulk materials are based on vibration. While it is well known that vibration can facilitate granular flows, it can also cause size segregation. Moreover, the use of certain levels of vibrations in a storage container or hopper can lead to material compaction and hence, reduced flowability. Currently, vibration cannot be applied with confidence because its effects have not been characterized systematically and methods for selecting optimal values of frequency and amplitude of vibration have not been developed. It is important to carry out such an investigation to obtain better fundamental knowledge that will form a basis for design of industrial systems.

Flow pattern and segregation in bins and hoppers are not independent of each other. The influence of segregation can adversely affect the flow patterns in hoppers. Table 3.1 shows a partial listing of the main references on the two segregation dominant

Table 3.1 Segregation theories and their related references.

Theory/Model	**Experimental studies**	**Modeling / Simulation studies**
Geometric Method	38, 39, 41	40, 41, 42
Convectional Method	21, 42, 44, 45, 46, 48	47, 49

theories offering explanations for segregation in studies carried out by researchers both experimentally and using computer simulations. Arnold [36] indicated that the degree of

segregation present in the operation of a bin could influence significantly, and often adversely the flow and flow pattern exhibited in a bin or silo. Potentially mass flow bins can exhibit funnel flow and vice versa. Symmetric bins can display severely non-

Table 3.2 Segregation parameters and their related references.

No	Parameter	References
1	Frequency, acceleration, a/d ratio	37, 43, 46, 47
2	Form of Shaking	21, 38, 39, 40, 41, 43, 45, 48
3	Particle to Particle Friction	21, 50
4	Particle to Wall Friction	21, 46
5	Particle Size	37, 48, 49, 50
6	Number of Particles	40, 43, 44, 46
7	Position of Particles	37, 45, 48
8	Cohesion	51

symmetric flow patterns. Flow and flow pattern play a very important part on the pressure in bins. Segregation when it occurs in hoppers also greatly influence flow, and has a significant influence on bin wall loads. The variability in bulk solids exiting from storage systems is very important and as a result, segregation and flow pattern of the bulk solid prior to discharge must be understood, since this may this lead to an understanding of segregation upon discharge. A summary of some of the parameters found by researchers that seem to play very important part in segregation and flow pattern during vibration is listed in table 3.2. Sadler [82], in his chronology of silo problems leading to

structural distress, indicates that many of the problems were traced to non-symmetric flow patterns developing in silos.

Various researchers have examined the issue of pattern formation in vibrated granular materials. In a series of experiments Melo, Ubanhovar, and Swinney [83], reported a pattern-forming instability occurring in a layer of grains vibrating on a plate. Similar patterns were also observed in three-dimensional experiments done by Fauve, Douady, and Laroche [24]. Various theoretical models have been proposed to describe pattern-forming instability [15-19] but, although displaying a close pattern phenomenology, they do not give proper measured dispersion relation. Although they are many different approaches, there is still no clear understanding of the mechanism driving the instability.

3.2 Experimental Method

Several experiments were performed to investigate the behavior of the granular materials subjected to vertical oscillations in the container. The apparatus consisted of a wedge-shaped container and was constructed with a front plate of glass for observing the granular bed, a grounded back plate of aluminum for dissipation of electrostatic charges, and sidewalls of acrylic. The front height and width of the container were 23 cm and 17 cm, respectively. The width of container between the front (glass) and back (aluminum) was 6mm. These dimensions rendered pseudo two-dimensional in which the granular motion was basically confined in the front plane, and granular motion was essentially confined in one vertical plane. A snapshot of the apparatus is shown in Figure 3.1.

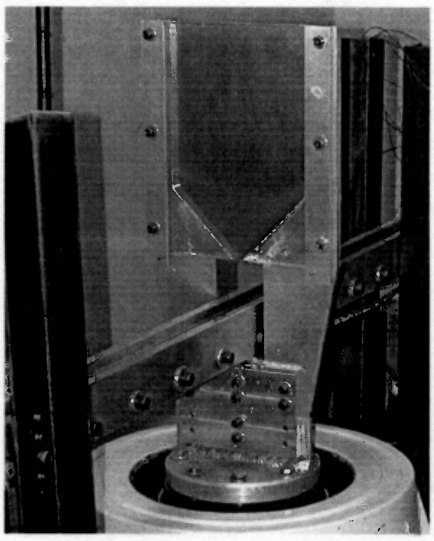

Figure 3.1 Snapshot of experimental setup

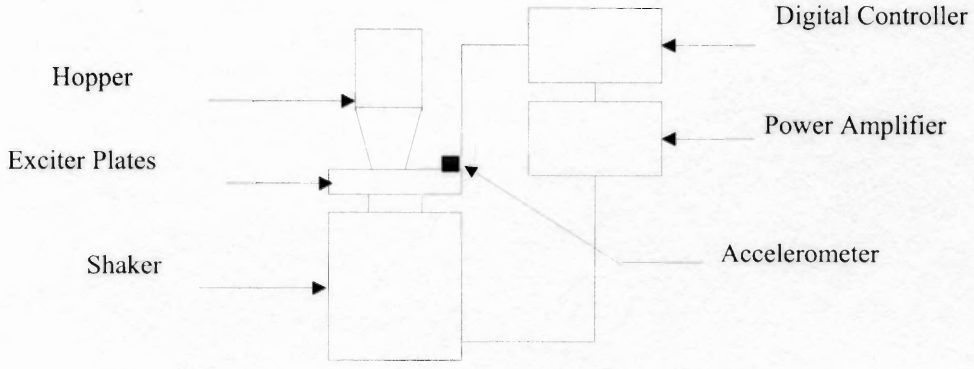

Figure 3.2 Schematic drawing of apparatus

With the gross dimensions remaining the same, hoppers with four included half-angles, namely 30°, 45°, 60°, and 90° were used. A schematic representation of the experimental facility and its controls is shown schematically in Figure 3.2.

The hopper is placed on a carefully leveled Ling Dynamics vibration exciter (model V651) that provides vertical displacement. Further care was taken so as to assure that the hopper arrangement is symmetrical to the vertical axis. A power amplifier (Model PA1000L, LDS) of up to 1400 VA output drives the vibrator. A digital sign controller (Model DSC 4, LDS) provides a sinusoidal signal and controls the amplifier. This control system can be used for both closed loop and open loop excitations. In a closed loop control, vibration parameters are monitored and corrected automatically through feedback. In this case, excitation builds up gradually to the desired values of vibration frequency and amplitude of acceleration. An open system, which is without feedback, provides excitation close to practical situations as, in this case, vibration builds up immediately. For this reason, the open system was used in the present study.

With the hopper closed, colored beads are carefully poured into the hopper to a height of 6cm, filling the conical section. The glass beads used were smooth, spherical,

Table 3.3 Properties of Glass beads

PROPERTIES	**QUANTITES**
Density (g/cc)	2.5
Specific gravity	2.45 – 2.50
Refractive index	1.51 – 1.52
Hardness, MOH	5 - 6
Coefficient of friction	0.9 – 1.0
Composition	Soda-Lime Silica Glass

and have a density of 2.5 g/cm^3. The properties of the beads are shown in table 3.3. The size of glass beads, and the range of frequency and amplitude of acceleration of vertical vibration used in the experimental studies are given in Table 3.4. Although the external excitation in vertical direction only and all possible care were taken for the geometric alignments, it was found that vibrations were always induced in the two horizontal directions. Consequently, vibration measurements with accelerometers were made in vertical as well as horizontal directions. Three Kistler 8702B50 accelerometers were used to measure the acceleration level accurately.

In order to understand if the results observed were unique, and as a result of the vibration system model utilized, some of the experiments were repeated using a different model vibrating apparatus. In this case, a Vibration Test Systems (VTS) vibration exciter (model VTS 100), that provides vertical displacement was used and similar tests carried out. A qualitative comparison was made between the results observed.

3.2.1 System Parameters

A list of the parameters studied for the Mono-disperse particle system is shown below in

Table 3.4 List of Experimental Parameters for the Mono-disperse system

Parameter	**Quantity**
Frequency range	20 Hz – 60 Hz
Acceleration range (Γ)	1.0 – 10
Particle size (mm)	0.3, 0.6, 1.0, 1.7, 2.4, 3.4
Hopper-wedge angles (degrees)	30°, 45°, 60°, 90°

table 3.4. The range of the particles sizes were selected so as to cover a wide cross-section as possible, so as to compare with results existing in literature. The frequency and acceleration amplitude range was selected so as to compare with results in existing literature, while maintaining the safe operation of the vibrator. Acceleration is normalized with respect to gravity, that is $\Gamma=a\omega^2/g$. In order to access if the shape of the hopper significantly affected the instability of the flow patterns in vibrated hoppers, hoppers with included angles varying form 30 degrees to 90 degree were chosen so to conduct the experiments. Selecting hoppers of different shapes also allowed comparisons to be made with a wider cross-section of work done previously by other researchers. The initial experiments were carried out using the 45° degree wedge shaped hopper. For each experiment, the granular bed was made with one uniform size of glass beads of the mean sizes specified in table 3.4. In the initial experiments, the layered depths were approximately 60mm. After each experiment, the glass beads were replaced by a fresh batch of beads so as to reduce the effects of static electricity. The grounding the aluminum back plate also allowed further dissipation of electrostatic charges. A fresh batch of beads for each set of experiments was used, and after each set of experiment the internal surfaces of the hopper was sprayed with a static guard. This was done so as to reduce the effects of electrostatic charges on the results of the experiments to a minimum.

Experiments were typically carried out by first fixing the frequency, f then varying the amplitude of acceleration. The flow convection pattern of the granular bed was characterized using a digital camera. Due to the limitations of the camera used, the motion of the particles was not observed at various phase angles. However, the phase was monitored be examining phase plots obtained from accelerometers connected to the

apparatus. To obtain the circulation time and observe overall flow fields, two particles of same dimensions but different color were initially placed on the base of the hopper and their motion followed over time.

3.3 Results

3.3.1 Mono-Disperse Particle

The first sets of tests were carried out for the range of sizes shown in Table 3.4. The effects of acceleration on the beads were first examined by first selecting beads of a certain diameter, loading the apparatus and varying the acceleration of the system for the

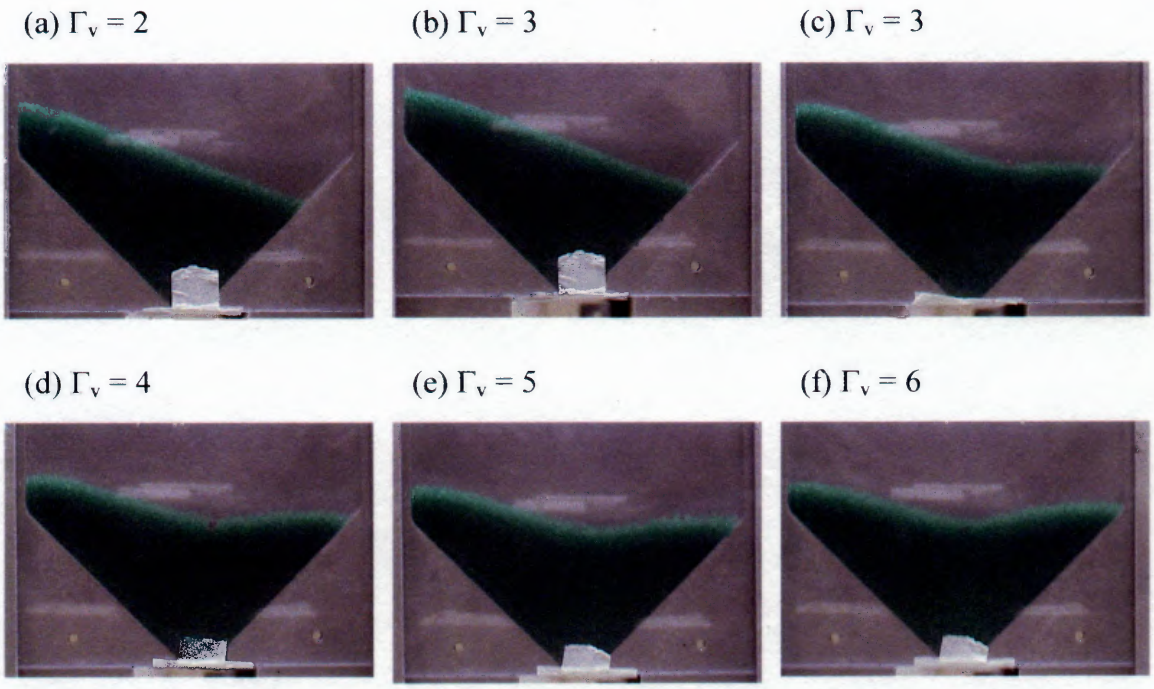

Figure 3.3 Snapshots of a typical set of experiments over a range of values with vertical acceleration $\Gamma_v = 2$, to $\Gamma_v = 6$. Diameter of the particles d = 1.0mm, f = 50 Hz.

fixed frequency. This process was repeated for all of the diameters outlined in table 3.4. Figure 3.2 shows examples of the snapshots for the behavior of glass beads of diameter 1.0mm as the dimensionless acceleration was varied from two to six for a frequency of 50

Hz. The corresponding horizontal accelerations that were measured are also shown in the figure. The snapshots show that for the selected frequency as the amplitude is increased, the shape of the free surface changed from that of being inclined in (a), to that where the free surface was symmetrical with surface waves (d). Below a certain value ($\Gamma \approx 1$) the particles in the hopper remained stationary. During the changes in the value of the

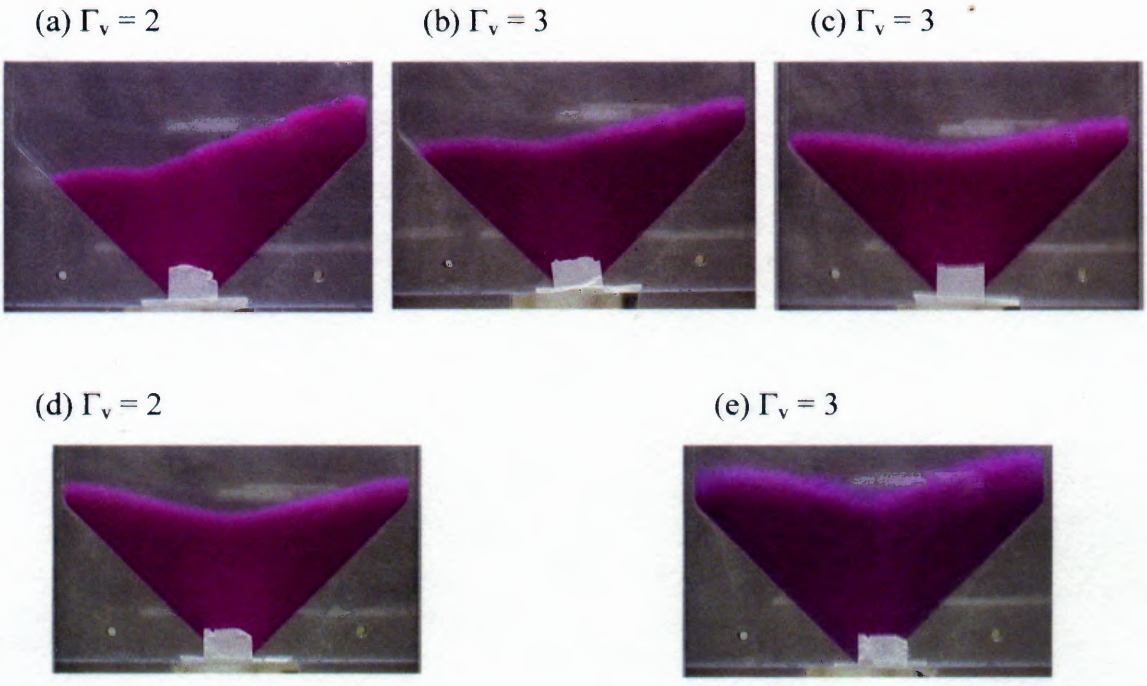

Figure 3.4 Snapshots of a typical set of experiments over a range of values with vertical acceleration $\Gamma_v = 2$, to $\Gamma_v = 5$. Diameter of the particles d = 0.60mm, f = 20 Hz.

acceleration amplitude, the particle made the transition from a bed that was inclined with heaping, to a symmetrical flow pattern, then finally to random motion with surface waves. Experiments were repeated for the complete range of the particles in table 3.4 and the flow pattern, and transitions generally followed the same trend outlined in figure 3.2. However, for test conducted at frequencies 20 Hz and less, the slope of the free surface

changed direction for low values of vibration acceleration. Figure 3.3 shows snapshots for the behavior of glass beads of diameter 0.60mm as the dimensionless acceleration was varied from two to five for a frequency of 20 Hz. This figure shows the free surface of the beads sloping towards the left. The formation of the inclination always appeared to one side of the container regardless of the initial condition of the bed and perturbations of the surface using a rod. This indicates that the reason for the slope or inclination may have been due to the forcing frequency. It is observed that in this case the snapshots of the particles also made the transition from a bed that was inclined with heaping; to a symmetrical flow pattern, and then finally to random motion with surface waves. The depression that forms in the center of the hopper is due to the convective motion up the sides of the hopper and down the center of the bed.

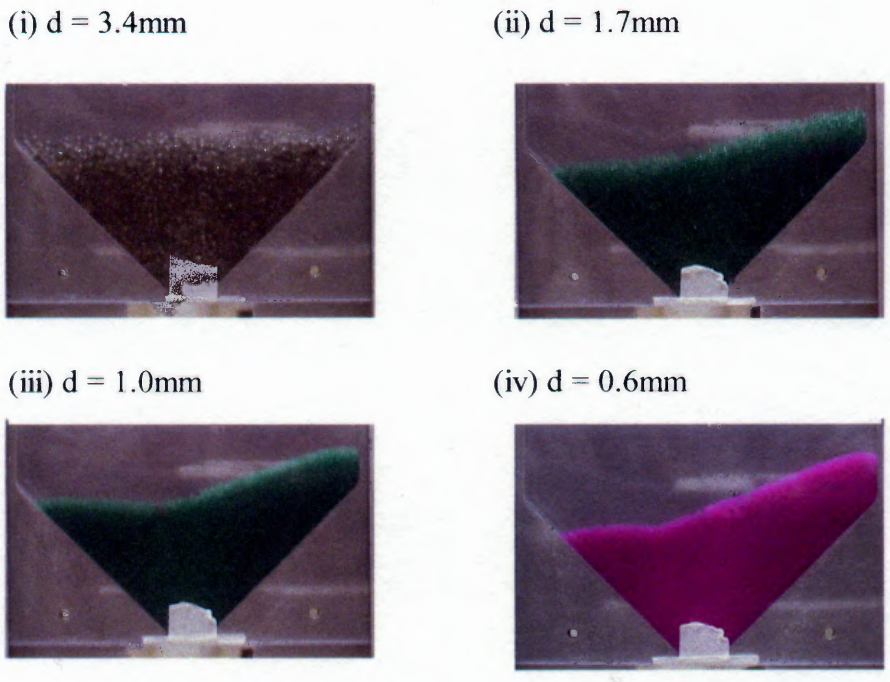

Figure 3.5 Snapshots of sets of glass beads with diameter (i) d =3.4mm, (ii) d =1.7mm, (iii) d = 1.0mm, and (iv) d = 0.6mm. Vertical acceleration $\Gamma_v = 2$, and $\Gamma_h = 5.$, and $f =$ 20Hz.

Examination of the snapshots shown in both Figure 3.2 and Figure 3.3 show that the heaping instability disappeared with an increase in Γ.

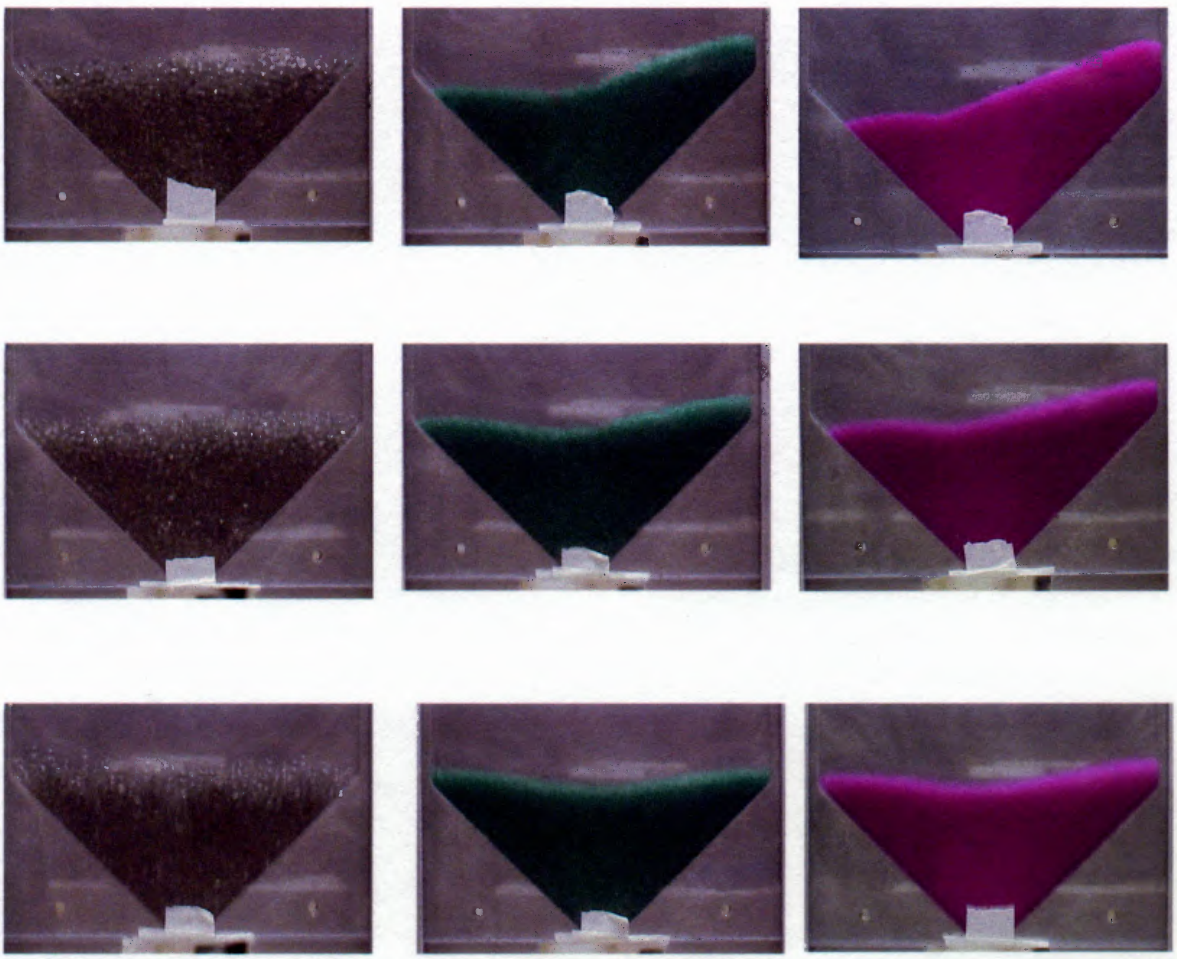

Figure 3.6 Snapshots of sets of glass beads with diameter (i) d =3.4mm, (ii) d =1.7mm, (iii) d = 1.0mm, and (iv) d = 0.6mm. Vertical acceleration $\Gamma_v = 2$, and $\Gamma_h = 5.$, and $f =$ 20Hz.

3.3.2 Effects of Diameter of the Particle on Instability

The asymmetric heaps and inclination seen here were observed by Evesque and Rajchenbach [19] in their study with rectangular hoppers. In their work, they outlined that the instability occurred beyond a certain threshold, where the horizontal surface

became unstable, exhibiting a slope with the horizontal which was present with glass spheres of 0.2, 0.4, 1 mm diameter but was not present with 2 mm diameter particles. The effect of the diameter of the particle on heaping and the inclination of the free surface was examined. Figure 3.4 shows that the slope of the inclination varied with the diameter of the particles, with the smallest particles having the largest angle of inclination. As can be seen in figure 3.4 (i), this inclination was not present for the larger size particle. The snapshots shown in figure 3.5 further illustrate the effect of diameter and vibration amplitude on the slope of the free surface. This diagram shows that in addition to the particle diameter affecting the slope of the free surface, the vibration amplitude also

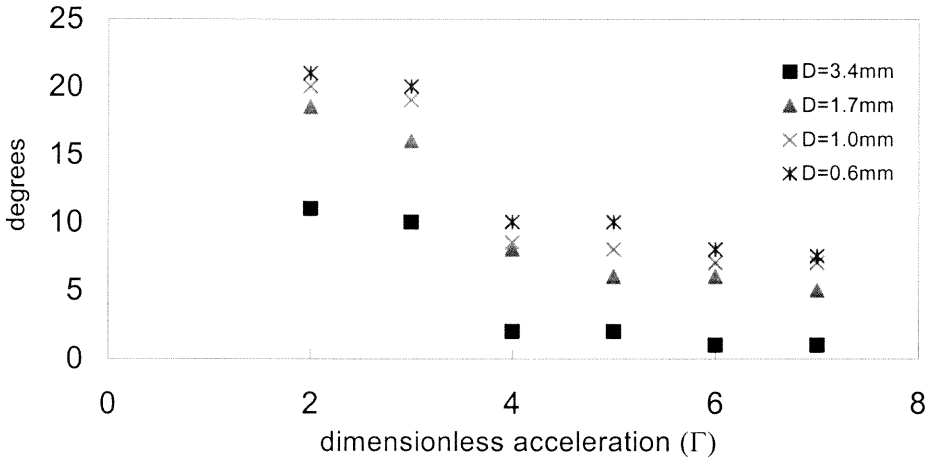

Figure 3.7 Angle of Slope as a function of dimensionless acceleration (Γ)

affects the slope. Figure 3.6 shows a plot of the change of the slope of the inclined surface of the glass beads of four different particle diameters for a frequency of 50Hz. From the plot shown in figure 3.6, it can be observed that the slope of the angle of inclination of the free surface was reduced as the diameter of the particles tested was increased.

3.3.3 Effects of Vibration Acceleration and Frequency on Flow Pattern Instability

In order to gain incite of the variation of the rate of convection of the particles in the bed, the circulation time as a function of changing velocity (v =A * ω) due to the increasing amplitude was measured. Figure 3.6 shows a plot of the circulation rate versus velocity amplitude. The circulation time is measured as the time it takes for the two colored particles to rise to the top. Since the two particles placed initially at the bottom of the hopper move slightly off the walls of the container, this plot gives some quantitative measure as to how the convection velocity increases with both increasing Γ at a fixed frequency and with decreasing frequency at fixed Γ. This plot shows that as the velocity

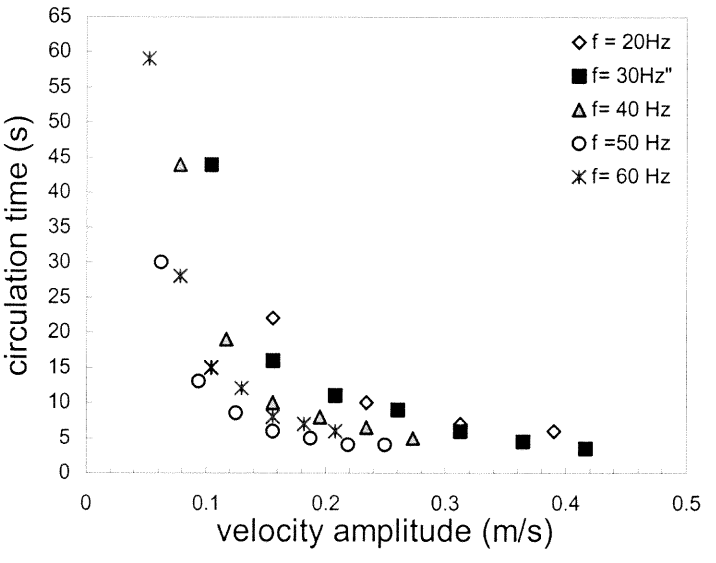

Figure 3.8 Particle circulation rate as a function of velocity for different frequencies

amplitude increases, the circulation time decreases with the particles rising faster to the surface of the bed of beads.

The transition for each particle diameter was further highlighted using bubble plots.

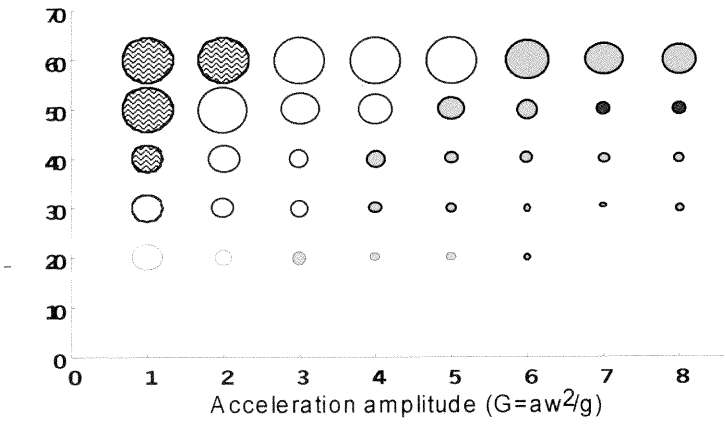

Figure 3.9 Effect of frequency and acceleration on convection pattern in a vibrated hopper (particle size = 3.4mm)

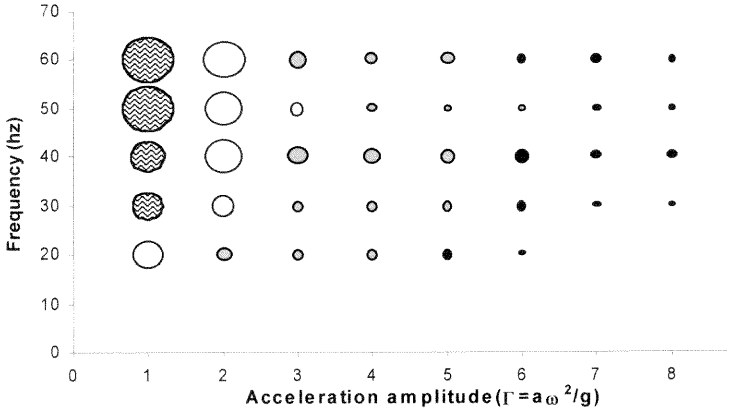

Figure 3.10 Effect of frequency and acceleration on convection pattern in a vibrated hopper (particle size = 1.7mm)

Figures 3.7 and 3.8 show two such plots of frequency versus dimensionless acceleration amplitude for particles with diameters 3.4mm and 1.7mm respectively. The diameter of the circles give an indication of the relative time it takes for the particles to circulate to the free surface. The large diameter circles indicate a longer time for the particle to reach the surface that is, a slower rate of convection. The different shades of colors indicate the

four different regimes observed. Generally, it was observed that at constant frequency the circulation rate of the particles moving to the free surface of the materials increased with the increase in acceleration. The circulation rate of these particles to the free surface is a measure of the convection rate [58]. It can be observed that although the size of the particle changed, the trend of the flow pattern continued to be the same. However, as frequency increased for the range 20hz to 50hz, at constant acceleration there was no significant increase in the convective motion. Bubble plots similar to that shown in figures 3.7 and 3.8 were done for the complete range of particles, diameters shown in Table 3.4. When mapped onto each other resulted in a phase diagram shown in figure 3.9.

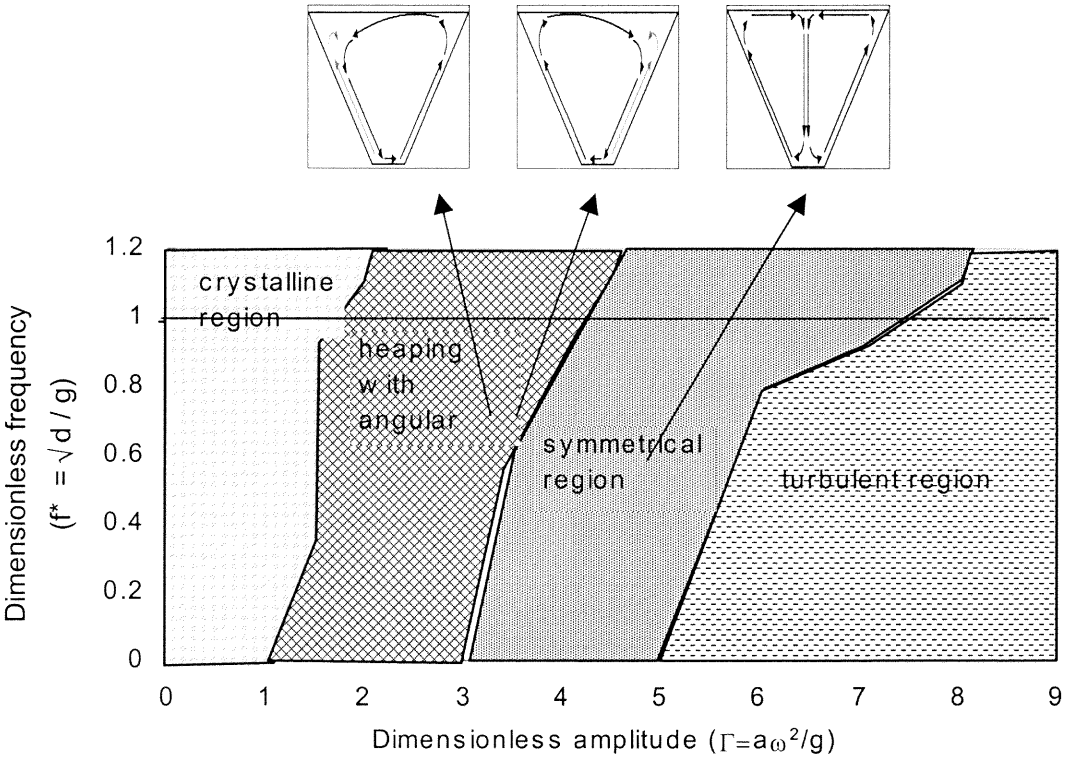

Figure 3.11 Phase plot showing the phase space diagram of the bed behavior appearance as a function of oscillation acceleration amplitude $\Gamma = a\omega^2/g$, and frequency $f^* = f\sqrt{d/g}$.

The different regimes that were observed are highlighted in this figure. The first regime was observed with the bed existing in a crystalline state for the frequency range considered (30hz – 60hz) and acceleration amplitude below 1.2g. For this range, the higher frequencies showed no relative movement between the particles. As the acceleration increased to a value above approximately two for the complete range shown in Figure 3.10, a second regime is observed where the horizontal free surface became unstable and inclined at an angle θ with the horizontal. Particles continuously rolled down this free surface forming one big continuous loop, and a smaller less active loop (see figure 3.2 and 3.3). This loop may be to the left or right depending on the acceleration amplitude but is repeatable for the specific frequencies and acceleration applied. The slope of the free surface varied, depending on the amplitude of vibration. This slope was not present for particles above 2.5mm. As the acceleration was increased, the surface gradually approached a horizontal state, indicating a third regime, with the particles forming two almost symmetrical convective loops. Further increases in acceleration resulted in the gradual destruction of the uniform convective motion, with the formation of surface waved. In the fourth regime, the motion of the particles is somewhat random, although occasionally, clear convective cycles can be observed. In addition to this, the surface waves became larger as the acceleration increased. The faster rate of convection was close to the container walls. As the convection increased, the band of faster moving particles increased in width, extending outwards from the inclined surfaces of the hopper.

3.3.4 Effects of Mass of Beads on Surface Instability

Experiments examining the effect of the mass of the beads on the slope of the free surface of the beads showed no variation in the slope of the free surface. Figure 3.11 below shows an example of the results obtained for snapshots of the free surface of the beads for masses of 45g, 25g, and 15g respectively for beads of diameter 1.0mm. These snapshots revealed that there were no significant changes in the slope of the free surface as the mass of the beads was varied.

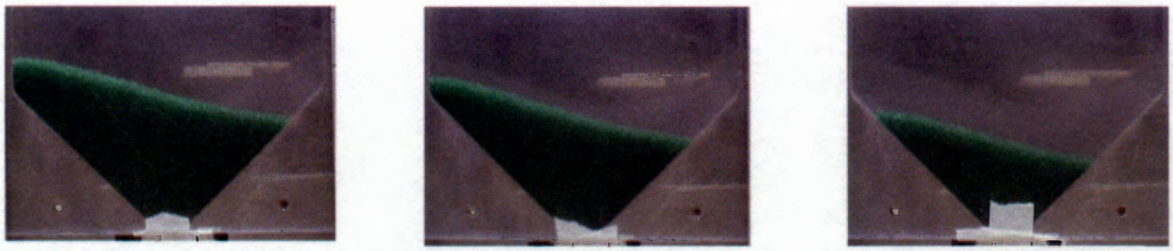

Figure 3.12 Snapshots of sets of glass beads with diameter d =1.0mm, and (a) mass = 45g, (b) mass = 30 g, (c) mass = 15g

3.3.4 Effects of Shape of Container on Pattern Flows

For a container with rough vertical walls and an aspect ratio of order one, the convection rolls are such that the particles move up the center of the container in a wide swat and down the sides in a narrow band. In containers where the walls have been tilted outwards, motion can be seen in which the particles move down the center of the container and up the sides. It has been noted that that the shape of the container in which the granular material is shaken, as well as the condition of the containers' surfaces, affects the direction of the flow pattern. Earlier work done [27] has established the fact that for containers sloping upwards, particles vibrated in a container moves up the sides and

down the center. As the outward slope of the container is reduced, that is as the walls become vertical the direction of convective motion changes.

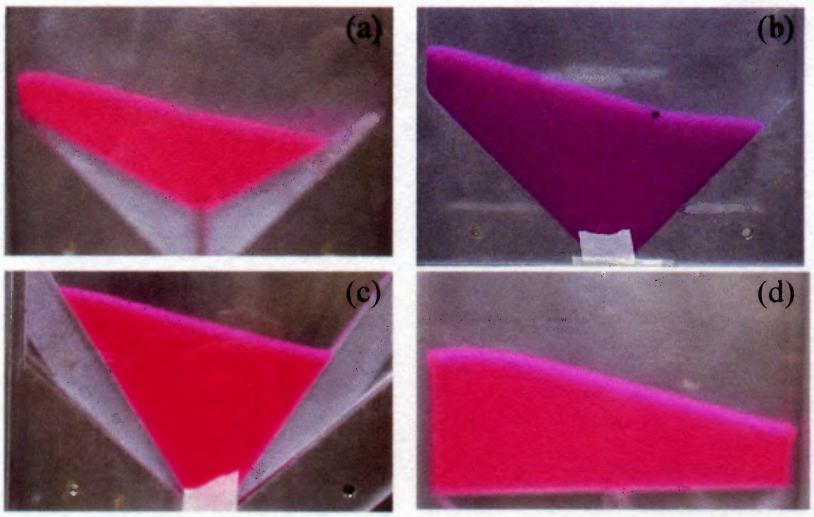

Figure 3.13 Snapshots showing the slopes of the free surface for hopper half-angles (a) 30°, (b) 45°, (c) 60° and (d) 90°. Frequency f = 30 Hz, and $\Gamma = 3$ for all cases.

Hoppers with different sloped angles were also investigated to determine what effect this would have on the slope of the free surface of the material. Diagrams above show particle size 0.6 mm for four different shaped hoppers. Figure 3.12 shows the slopes of the free surface for particle size 1.0 mm for four different shaped hoppers. In addition to using the 45 degree shaped hopper to carry out most of the experiments, hoppers of included half-angle 30 degrees, 60 degrees and of rectangular shape (included angle 90 degrees) were also used in experiments. These diagrams show that the angle does not significantly affect the direction of the slope of the instability. Although the angle of the hopper affected the rate of convection and the direction of flow in the rectangular hopper, the slope of the free surface was generally the same for the

parameters tested. This seems to indicate that the inclination is independent of the shape of the hopper.

Figure 3.13 shows snapshots of the slope of the free surface of three different sizes of particles when vibrated using a hopper made of Perspex and a Vibration Test Systems (VTS) vibration exciter (model VTS 100) that provides vertical displacement. In this case, it can also be observed that the diameter of the particles affected the slope of the free surface. It can also be observed that although in this case a significantly lighter

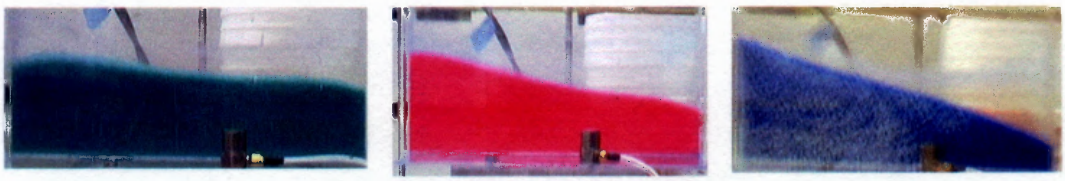

Figure 3.14: Snapshots showing inclined free surface for particle size (a) 1.7mm (b) 0.6mm (c) 1mm. Frequency f = 30 Hz, and $\Gamma = 3$ for all cases

hopper was used, thus reducing the effects misalignment moments, the inclination of the free surface is still obvious. In this case, the inclination of the free surface was also greater for the smaller sized particles. This fact indicated that the inclination of the free surface is not restricted to large vibration equipment.

3.4 Conclusions

Convection flow patterns and instability in a wedge shaped hopper is investigated for different shaped containers. In the experimental system, four regimes were observed for the convection flow patterns, with instabilities being observed at low acceleration amplitude similar to that reported in the literature. The convective instability was linked

to acceleration of the system in the lateral planes, which may have been due to unavoidable alignment problem in the apparatus. Tests and measurements indicate that heaping instability is very sensitive to small horizontal lateral vibrations. When vertical vibrations are applied to a hopper even on a laboratory scale, small lateral vibrations may be close to impossible to eliminate. These lateral vibrations may be due to the difficulty in making a perfect system. For smaller values of vertical vibrations, the effects of the lateral vibrations are greater. This was partly due to the fact that the particles are still in contact with the boundary of the container, and for smaller values of vertical vibration, the ratio of the vertical vibrations to the lateral vibration is higher. This effect is minimized as the applied vertical vibration is increased, and the particles begin to separate from the boundary of the container, destroying the inclination of the free surface upon increased collision force with the hopper bed. The inclination of the free surface changing from sloping to the right to sloping in the opposite direction is linked to the phase of the horizontal component of the acceleration amplitude changing in phase in relation to the vertical component.

CHAPTER 4

COMPUTER SIMULATION ANALYSIS OF FLOW PATTERNS IN WEDGE SHAPED CONTAINERS

4.1 Introduction

In recent years, due to enormous growth of computing power and computer visualization techniques, computer simulation has become an increasingly popular tool for studying the behavior of vibrated granular materials. The areas of concentration of researchers may be broadly classified as: (1) characterization of the particulate behavior inside the vibrating bed, vessels, or hopper-like containers; (2) effect of vibration on segregation of particulate mixtures of two or more types of particulate solids; and (3) effect of vibration on segregation of particulate flows from hoppers. The parameters involved are many, and include the size and shape of the granules, the size and shape of the containers, the direction, amplitude and frequency of vibration [32-44]. The large number of parameters makes experimental studies very difficult and as a result computers have increasingly been used in this field of study. Over the years, although computer simulation seems to provide a powerful tool for studying granular flow, the use of computers have in some cases been limited, due to the fact that it is exorbitantly expensive in terms of computation time. As a result, the reported studies in the subject are dispersed and somewhat at variance. Over the years, two simulation methods have been used more than the others. These two methods are often referred to as the hard sphere and the soft sphere models, respectively. In this dissertation, the soft sphere method is be used.

4.2 The Basics

The simulations are designed to allow us to look at a granular material in a variety of enclosures. The aim of the simulations is to recreate the experimental system, and as a result, the parameters were chosen to match those used in the experiments. This fixed the size of the particles and the frequency of oscillations. In this work, a two-dimensional granular system is modeled on a computer, using a molecular dynamics simulation code. Essentially there are two types of molecular simulation methods, namely time step driven and event driven. The fundamental difference in the two methods are that in time driven simulations, the equations of motion of all the particles are integrated numerically with a specified constant time step, while in event driven simulations, the trajectory between the collisions termed events, are computed analytically and the simulation is advanced from event to event.

4.2.1 Time -step Driven Simulations

Cundall and Strack [56] first introduced the application of time-step driven molecular dynamics simulation to granular materials. This method is one of the most popular simulation methods for granular materials, and has been used in numerous studies [55-59]. The reason for its popularity lies in the fact that it can be adapted to granular systems in a relatively straightforward manner as outlined below. Using this method, one seeks a description of the dynamics of the granular system on a particle basis for each individual grain.

The Governing equations of motion are,

$$\vec{F}_i = m_i \ddot{\vec{r}}_i \qquad \text{(i =1,N)}, \qquad (4.1)$$

where, N is the number of particles, $\vec{r}$ their positions and $\vec{F}_i$ the force acting on the particle i. If there are also rotational degrees of freedom is taken into consideration, the equation below has to be added,

$$\vec{M}_i = I_i \dot{\vec{\omega}}_i \qquad \text{(i =1,N)}, \tag{4.2}$$

where $\vec{M}_i$ is the torque of the particles, I_i the moment of inertia, and $\dot{\vec{\omega}}_i$ the rotational velocity of the particle.

In addition to molecular dynamics simulation having the capability to model granular systems, there is the advantage that soft sphere particle molecular dynamics simulations can simulate many types of interactions. The forces considered in such a model are generally of two general types, namely body forces, and contact forces. Body forces, which generally act on flowing particles, include gravitational forces and electromagnetic forces. While contact forces, are forces that act when particles are in contact, and include traction due to contacting surfaces, and cohesive forces. In this model presented here, only gravity body force is considered while the electromagnetic forces are neglected. The contact forces considered are acting between particle-particle and particle-boundary. From Newton's law the equation for a force acting on particle *i* due to gravity, equation (1) becomes,

$$\vec{F}_i = m_i \vec{g} \tag{4.3}$$

4.2.2 Collisions

There are a variety of approaches to model particle collisions [55, 62]. The model chosen in this dissertation has the advantage that it allows particle rotation, and includes frictional effects, which are both recognized as key elements in granular convection.

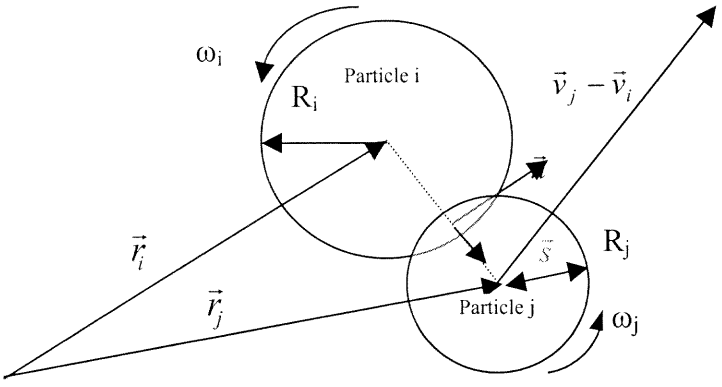

Figure 4.1 Sketch of impact geometry in 2-dimension showing the coordinate system used in the simulation.

The model used is two-dimensional. Figure 4.1 shows a sketch of contact between two particles of radii R_i, and R_j, position $\vec{r}_i, \vec{r}_j$ velocities $\vec{v}_i, \vec{v}_j$, and angular velocities $\vec{\omega}_j, \vec{\omega}_i$. Two particles are considered to interact only when they are in contact, i.e. their "virtual overlap" Δ_{ij} is larger than zero. Where,

$$\Delta_{ij} = (R_i + R_j) - |\vec{r}_j - \vec{r}_i| \geq 0 \tag{4.4}$$

Δ_{ij} is the amount of overlap between particles i and j. In this model, if the particles do not overlap then $\Delta_{ij} = 0$.

There are two key characteristics considered in this granular systems. First, there are no interparticle forces; the only way one particle interacts with another is through physical contact, that is, a collision. Second, the collisions are energy dissipative. The dissipation in the system occurs both from velocity loss in collisions and from frictional losses. This characteristic is explicitly accounted for in the simulation by including a dissipative mechanism in the model. The collision of the two spheres shown in figure 4.1 can be described in a local coordinate system with unit vectors $\hat{n}$, $\hat{s}$. The two unit vectors $\hat{n}$, $\hat{s}$ are used to decompose the forces and velocities into normal and shear components, with the normal component acting along a line connecting the center of particle *i* to the center of particle *j*. Normal vector $\hat{n}_{ij}$, is give by,

$$\hat{n}_{ij} = \frac{\vec{r}_j - \vec{r}_i}{\left|\vec{r}_j - \vec{r}_i\right|} \tag{4.5}$$

The tangential unit vector, $\hat{s}_{ij}$ is rotated 90 degrees from the normal component such that $\hat{n}_{ij} \times \hat{s}_{ij} = \hat{k}$ where $\hat{k}$ is the direction of the third dimension. Considering the particles also in general may have rotational velocities $\vec{\omega}_j, \vec{\omega}_i$, the relative velocity at the point of contact of particle *j* with respect to particle *i*, $\delta \dot{\vec{r}}_{ij}$, is given by,

$$\delta \dot{\vec{r}}_{ij} = \dot{\vec{r}}_j - \dot{\vec{r}}_i - (\omega_j R_j - \omega_i R_i)\vec{s}_{ij} \tag{4.6}$$

where $\dot{\vec{r}}$ is the translational velocity of the particle center and ω is the rotational velocity of the particle. The relative normal velocity component $\delta \dot{\vec{r}}_{ijn}$ and relative shear velocity $\delta \dot{\vec{r}}_{ijs}$ are thus given by,

$$\delta \dot{\vec{r}}_{ijn} = (\dot{\vec{r}}_j - \dot{\vec{r}}_i) \cdot \vec{n} \tag{4.7}$$

$$\delta \dot{\vec{r}}_{ijs} = (\dot{\vec{r}}_j - \dot{\vec{r}}_i) \cdot \vec{s} - (\omega_j R_j - \omega_i R_i) \tag{4.8}$$

If the shear of the velocity $\delta \dot{\vec{r}}_{ijs} = 0$ at the beginning of contact, the impact is direct. If $\delta \dot{\vec{r}}_{ijs} \neq 0$ at the beginning of the impact it is oblique. The angle of the impact is measured by,

$$\delta\theta = ar\cos\left(\frac{(\dot{\vec{r}}_j^{\,i} - \dot{\vec{r}}_i^{\,i}).\vec{n}}{\left|\dot{\vec{r}}_j^{\,i} - \dot{\vec{r}}_i^{\,i}\right|}\right) \tag{4.9}$$

where the superscript *i* in the previous quantities denote velocity before impact.

4.2.2.1 Normal Impact. Modeling a force that leads to inelastic collision requires at least two terms: repulsion and some sort of dissipation. Hertz to derive the expression for the repulsive force acting in the normal contact of two perfectly spheres elastic [62]. He established that the normal force (F_n) acting on particles that are in contact varies with the relative normal displacement. In this simulation, the normal contact is modeled as a

linear spring with dashpot element (see figure 4.2). The dashpot included in the normal force model accounts for the dissipation of energy when particles collide. The force acting on particle i due to particle j in the normal direction $\vec{F}_{nij}$, is given by,

$$\vec{F}_{nij} = (-k_n \Delta_{ij} + \nu_n \delta \dot{\vec{r}}_{ij} \cdot \hat{n})\hat{n} \tag{4.10}$$

where k_n and ν_n are the normal spring constant and normal dashpot coefficient, and Δ_{ij} is the amount of overlap between the particles (see equation 4.4). This model was used in computer simulations by Cundall and Strack [56], and has the advantage that its analytical solution allows the calculation of important quantities shown later.

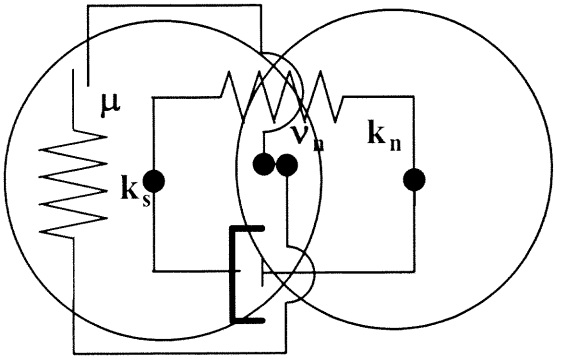

Figure 4.2 Normal contact and tangential model

4.2.2.2 Oblique Impacts and Frictional Contacts. In oblique impacts, there is a tangential component of the force, or shear force. The shear force is connected to the normal force by the Coulomb laws of friction. The simplest shear force [55] just applies the Coulomb lay of dynamic friction so that

$$F_s = -\mu \cdot |F_n| \cdot sign(v_s) \tag{4.11}$$

This simple approach cannot provide a reversal of the tangential velocity, but can only slow it down to zero. Equation (4.11) above is discontinuous at $v_s = 0$. Various authors use viscous friction force relationships that avoid this discontinuity. However, the force often yields impractical results. There are a number of force schemes [57, 62], however, many of them do not account for tangential elasticity. Stability would require that a finite shear force act between particles also at $v_s = 0$, in order to withstand gravitational force components in shear direction of contacts.

Tangential elasticity was first introduced by Cundall and Strack [56] and used by many other researchers [60, 86-88]. This model consists of a spring in series with a Coulombic friction-sliding element. The spring allows the particle to respond elastically, while the sliding friction element allows the particle to slide against each other. The magnitude of the tangential force is limited by the sliding element. This model compares favorably with more complicated models developed by Maw et al. [87]. The tangential spring force acting on particle *i* due to a particle *j*, due to the spring $\vec{F}_{s,s}$ is given by,

$$\vec{F}_{s,s} = (k_s \delta s_{ij})\hat{s}_{ij} \tag{4.12}$$

where k_s, is the tangential spring constant and δs_{ij} denotes the displacement in the tangential direction that took place since time t_o when the contact was first established, and is given by,

$$\delta s_{ij}(t) = \int_0 (\delta \dot{\vec{r}}_{ij} . \hat{s}_{ij}) dt' \tag{4.13}$$

The inclusion of the sliding element makes the model more complicated. This sliding element becomes active when the magnitude of spring force exceeds the magnitude of the sliding force, that is, where $\left|\vec{F}_{s,f}\right| = \mu \left|\vec{F}_{nij}\right| < \left|\vec{F}_{s,s}\right|$ and the force applied to the particle is,

$$F_{s,f} = -\mu \cdot \left|F_n\right| \frac{\vec{F}_{s,s}}{\left|\vec{F}_{s,s}\right|} \tag{4.14}$$

This force is implemented by changing the tangential spring displacement, δs_{ij}, to give a spring force equal to the sliding force,

$$\delta s_{ij}(t) = \mu \left|\vec{F}_{nij}\right| / k_s \tag{4.15}$$

Thus, the tangential force, when the sliding force is active has a magnitude of $\mu \left|\vec{F}_{nij}\right|$, and acts in the same direction as the spring force. Furthermore, the spring extension is

changed in order to give the magnitude of the sliding force. If the tangential displacement is active once again, $\left|k_s \delta s_{ij}\right| < \mu\left|\vec{F}_{nij}\right|$, the initial value of the tangential displacement will be given by equation (4.15).

4.2.3 Time-integration Scheme

Knowing the forces that enter the equations, the equations can be integrated numerically to determine the acceleration of the particles in the system. Similarly, the updated particle states are then determined by integrating the particle accelerations in time, so as to determine the new velocities and positions. The equation of motion for a particle is given by,

$$m_i \ddot{\vec{r}}_i = \vec{F}_{gi} + \sum_{j=1, j\neq i}^{N} \vec{F}_{cij} \tag{4.16}$$

$$I_i \ddot{\vec{\theta}}_i = \sum_{j=1, j\neq i}^{N} (\vec{R}_i \times \vec{F}_{cij}) \tag{4.17}$$

where $\vec{r}$ and $\vec{\theta}$ are the translational and rotational positions of the particle *i*. N the number of particles in the simulation, m_i and I_i the particle mass and rotational moment of inertia, $\vec{F}_{gi}$ the gravitational force acting on the particle *i*, and $\vec{F}_{cij}$ the contact force due to the particle j. The particle velocities are then determined by integrating in time. There are a number of methods available for numerical integration, here a center-difference scheme

utilizes by Cundall and Strack [56], and Walton [60] is used. This scheme is given by the following equations,

$$\dot{r}_{n+\frac{1}{2}} = \dot{r}_{n-\frac{1}{2}} + \Delta t \ddot{r}_{n-1}$$
$$r_{n+1} = r_{n-1} + \Delta t \dot{r}_{n+\frac{1}{2}} \tag{4.18}$$

This process is the most time consuming part of the simulation, since each iteration requires that the forces acting on each of the particles to be calculated. There are a number of different techniques available for numerical integration [55].

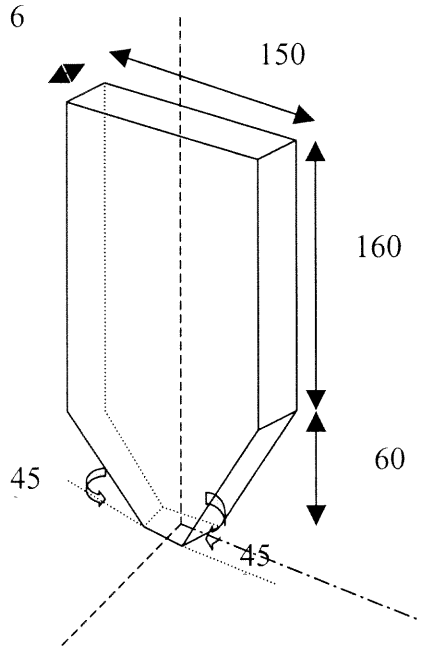

Figure 4.3 Geometry of Simulation space

4.2.4 Parameters and Assumptions of the Simulations

The simulation parameters were divided into two groups [64]: parameters that were taken directly from experiment, and parameters that are based on the force contact model. The table below shows a list of the simulation parameters.

SIMULATION PARAMETERS		
	Parameters Based on Experiments	**Parameters Based on force Contact Model**
1	Gravity ($\vec{g}$)	Simulation time step (Δt)
2	Coefficient of restitution (i) particle/particle (ε_{pp}) (ii) particle/wall (ε_{pw})	Normal spring constants (i) particle/particle ($k_{n,pp}$) (ii) particle/wall ($k_{n,pw}$)
3	Coefficient of sliding friction (i) particle/particle (μ_{pp}) (ii) particle/wall (μ_{pw})	Dashpot coefficients (i) particle/particle ($\nu_{n,pw}$) (ii) particle/wall ($\nu_{n.pw}$)
4	Hopper dimensions (i) hopper width (W) (ii) hopper height (h) (iii) hopper slant (θ)	Tangential spring constants (i) particle/particle ($k_{s,pp}$) (ii) particle/wall ($k_{s,pp}$)
5	Vibration amplitude $\Gamma = a\omega^2/\lvert\vec{g}\rvert$	
6	Mean particle diameter (d)	
7	Particle density (ρ)	
8	Vibration frequency (f = ω/(2π)	

In general, the simulations were designed to match the experiments wherever possible. Figure 4.3 shows a sketch of the general hopper dimensions used for the two dimensional simulations, the width was not used. The value for the acceleration due to gravity was the standard value generally used g = 9.81 m/s). When energy dissipation is introduced, possible mechanisms for energy dissipation, that is, the transformation of kinetic energy into other forms of energy, which finally transform into heat are, plastic deformation, viscoelasticity of the material, and elastic waves excited by the impact. The energy due to the elastic waves excited by the impact, although present, carry so little energy, that they are generally neglected. The elasticity is described by the coefficient of restitution, ε, which is defined as the relative velocity after the collision, divided by the ratio before collision, and defined by

$$\varepsilon = -v_n^f / v_n^i \in [0,1] \tag{4.19}$$

Here the subscript *i* refer to pre-collision (initial) and *f* to post-collision (final) quantities. Johnson [81] indicated that the necessary critical yield velocity causing plastic deformation is given by,

$$v_{yield}^2 \approx 107 \frac{R_{eff}^3}{m_{eff}} \frac{Y^5}{E_{eff}^4} \tag{4.20}$$

where $m_{eff} = (m_i m_j)/(m_i+m_j)$ and $R_{eff} = (R_1 R_2)/R_1+R_2)$ are the reduced mass and radius, Y is the yield strength of the softer sphere, and E_{eff} is related to the Young's modulus E, and

the Possion's ratio ν of both spheres. For the case of plastic deformation, a simple theory [83] predicts ε to fall off like $v_n^{b^{-1/4}}$ with increasing velocity impact. Experimental studies by Goldsmith [89], Bridges et al. [90], Kuwabara and Kono [91], and Sondergaard et al. [92] for spheres made of a large class of different materials all show a monotomoc decrease of the coefficient of restitution with increasing impact velocity. Using the linear spring–dashpot model has the advantage that its analytical solution (with the initial conditions) allows the calculation of important quantities such as the coefficient of normal restitution. Analysis shows that the damped spring model gives a constant coefficient of restitution. The effective normal coefficient of restitution for the collision of two particles is given by,

$$\varepsilon = \exp\left(\frac{\pi}{\left(\frac{4(k_n / m_{eff})}{(\nu_n / m_{eff})^2} - 1 \right)^{1/2}} \right) \tag{4.21}$$

Rearranging the equation above gives an expression for the dashpot coefficient, ν_n, based on the spring constant, k_n and the coefficient of restitution, ε

$$\frac{\nu_n}{m_{eff}} = \sqrt{\frac{4\dfrac{k_n}{m^2{}_{eff}}}{1+\alpha^2}} \tag{4.22}$$

In reality, the force equation has no free parameters, since k_n and ν_n can be set by adjusting ε and τ to the corresponding experimental values exhibited by a given material in a velocity range relevant to the simulation. Due to the advantages of this model, it has

been used in numerous works. Foerester et al. [93], measured $\varepsilon_n \approx 0.87$ in a velocity range 0.29 m/s $\leq v_n^b \leq$ 1.2 m/s. There is no generally accepted theory that describes the energy loss in a normally collision adequately. Although there are strong indications that the coefficient of restitution for normal impacts depends on the impact velocity, this dependence is weak enough that for a typical range of relative velocities occurring in a specific situation, a constant coefficient of restitution seems to be a good approximation. In most of the simulations conducted the value for ε_{pp} and ε_{pw} used in this work is 0.8. This value was used so as to compare some of the results with work done by Wassgren [64]. This value is lower than the experimental values which of 0.83 and 0.97 for two colliding 3mm glass spheres [93]. With a 2D system less energy will be dissipated than in a 3D system due to the decreased number of contacts and as a result a smaller value for the coefficient of restitution. The sliding friction parameter, μ, also has a range of values varying from frictionless, $\mu = 0.0$, to highly frictional particles, μ=1.0. Foerster et al. [93] indicated that a typical value for μ between two 3mm particles is 0.01 while μ for a 3mm glass sphere and aluminum wall is 0.13. The glass beads used are of a constant density of 2500kg/m^3, but the particles can be set to varying sizes.

Mindlin and Deresiewicz [94] examined the tangential friction forces between two elastic spheres for the case of several distinct loading-unloading histories. Assuming that Hertz theory holds, Maw et al. [87], and Walton [60], carried out analysis for the case of oblique impact of spheres. In Mindlin's elastic theory [94] the initial and final tangential stiffness k_s is related to the normal stiffness by,

$$k_s = k_n(1-\upsilon)/(1-\upsilon/2) \tag{4.23}$$

Where υ the Poisson ratio, is of the order 1/3 for most materials, such that k_s/k_n = 2/3. Based on Mindlin and Deresiewicz's analytical models of tangential contacts Cundall and Strack [56] recommended that

$$\frac{2}{3} \leq \frac{k_s}{k_n} \leq 1 \tag{4.24}$$

Following the work done by Wassgren [64], the simulation time step t, was chosen so that the highest frequency in the system corresponding to the smallest period, could be integrated accurately. The highest frequency in a system consisting of identical spheres constrained to move in 2D is for a particle in contact with six other particles. The translational period of oscillation, τ_{trans}, for the period of oscillation is,

$$\tau_{trans} = \sqrt{\frac{m}{3k_n + 3k_s}} \tag{4.25}$$

While the rotational period, τ_{rot}, is,

$$\tau_{rot} = 2\pi\sqrt{\frac{I}{6k_s r^2}} \tag{4.26}$$

When k_s/k_n =1 and I = 2/5 mr^2, and $\tau_{rot} = \sqrt{\frac{2}{5}\tau_{trans}}$. As a result, the smallest period in the system is given by τ_{rot}. Since the computation time increases with decreasing computation time step, very often a compromise has to be found between realistic

stiffness and reasonable computation time. The simulation time step is chosen in order to ensure integration stability and accuracy.

The values used for the vibration frequencies, accelerations, are the same as the values for these parameters in for the experiments in table 2.2.

In this model, that is, in the damped linear spring model, the maximum overlap of a two-particle system is given by,

$$\Delta_{ij} = \left(\delta\dot{\vec{r}}_{\max,ij} \cdot \hat{n}_{ij}\right)\sqrt{\frac{m_{eff}}{k_n}}\left(\exp\frac{\arctan - \alpha}{\alpha}\right) \tag{4.27}$$

where $\alpha = \pi / \ln\varepsilon$. If the particle i collides with a wall, $m_{eff} = m_i$, since $m_j \to \infty$.

Rearranging the equation (4.27),

$$\frac{k_n}{m_{eff}} = \left(\frac{(\dot{\vec{r}}_{\max,ij} \cdot \hat{n}_{ij})}{\Delta_{\max} / R}\right)^2 \left(\exp\frac{\arctan - \alpha}{\alpha}\right) \tag{4.28}$$

The duration of collision is given by the relationship

$$\tau = \frac{\pi}{\sqrt{\left(\frac{k_n}{m_{eff}}\right)\left(1 + \frac{1}{\alpha^2}\right)}} \tag{4.29}$$

This duration of the collision is the most important time scale in the simulation. It fixes the time step for the integration of the equations of motion, and thus the real time that can be simulated. To get a good integration of the collision, the time step in the simulation should be at least $\tau/50$ [55]. Thus, the value of k_n/m_{eff} is very important, since if a large

value of k_n/m_{eff} is used, the time t will be small as a result the simulation time step will be small, resulting in increasing computation time. To reduce computation time, a smaller value of k_n/m_{eff} is preferred; however if the spring constant is too small particles overlap significantly affecting the transport properties of the material. Thus a compromise has to be found between realistic stiffness and reasonable computation time.

4.2.5 Boundary Conditions

The system is made up of a horizontal bottom, and two walls that can be set at varying angles to allow the examination of granular material in a variety of enclosures. The wall boundaries consist of smooth, rigid, but frictional walls. The vertical position of the hopper is given by $y(t) = y_o \sin(2\pi ft)$, with the amplitude y_o and the frequency f, similarly the horizontal position is $x(t) = x_o \sin(2\pi ft)$ with the amplitude x_o. The strength of the motion is characterized by Γ, the ratio of the container acceleration to gravity.

4.3 Simulation Method

In this numerical work, initially the particles are placed in the hopper with a random velocity within a prescribed range. So as to be certain that the initial condition for each set of parameter studied was the same, prior to each simulation the bed conditions were made the same by allowing the particles to sell freely due to gravity.

The numerical simulation code used in the present study is written in C programming language following the flow of a code initially designed by Wassgren [64], This was further developed by Dr. M. Malik [95]. In the present work necessary changes

were made to enhance the speed of the simulations. Modifications were also made to account for both vertical vibrations and horizontal vibrations of the hopper, different shape containers, and to carry out diagnostic calculations of a wide variety of parameters. The flow chart of the code is given in the APPENDIX. The operation of the code is briefly described below. The initial conditions for the particles are generated after the input data is read from the input file. The parameters read from this file are as follows:

- Density of the particles in the granular mixture
- Depth to which particles must be filled in the
- Mean diameter of the particles
- Coefficients of restitution (particle/particle and particle/wall)
- Normal friction coefficients (particle/particle and particle/wall)
- Stiffness coefficients (particle/particle and particle/wall)
- Tangential friction coefficients (particle/particle and particle/wall)
- Hopper dimensions
- Maximum simulation time or number of cycles
- Gravity acceleration
- Frequency and g-level acceleration of hopper vibration in the vertical and horizontal directions

In addition to the above information, the range of simulation time over which the various outputs are plotted to files, is also defined in the input data file. To ensure that the initial condition for each simulation is the same, the zero-time setting of the particles is configured. This is done by allowing the particles to fall under gravity and settling

loosely into the simulation space; this is equivalent to pouring and setting of the granules in the hopper in an actual experiment. The hopper is set in vertical vibration and numerical simulation begins with the solution of the equations of motion of the interacting particles (modeled as soft spheres). The code comprises of a number of functions. Using the force subroutine, the forces acting on each particle in the system is first determined using the contact model described earlier.

The forces are utilized to determine displacements and velocities by integrating the equations of motion. Next, the appropriate measurements are made and the particle states are recorded to an output file. The loop repeats until the ending condition, which is set upon completion of a predetermined number of cycles. Parameters measured in the output file includes the following:

- Translational granular temperature
- Rotational granular temperature
- Particle and hopper trajectories

As the simulation of a physical system may involve a very large number of particles, efficient management of computation and the available memory is of utmost importance in the development of the computer code. For this purpose, the entire space of the hopper is divided into an array of square cells with the length of each side being greater than the largest particle in the system. This technique was drawn from work done by Wassgren [64], where each cell is a pointer that points to a particle with its center located in that particular cell. All of the other particles are linked together using a double-linked list of pointers. This use of double linked-list allows particles to be easily included

and removed from cells as particles pass through them. The advantage of monitoring the cells in which the particles are located is that a given particle only needs to check for collision with particles in the neighboring cells. Checks do not need to be made with particles located in cells far from the current cell. This technique results in there the overall speed of the simulation being increased when the simulation involves many particles. Other techniques for reducing the number of contacts checks exist, however this method is straightforward, easily implemented and is considered very robust. Using this technique plays an important role in achieving the objectives of memory management and computation time reduction. Both monodisperse and binary disperse system of particles were examined and studied.

A deep bed model of the hopper similar to experimental system was constructed. In order to study the behavior, a monodisperse system is initially taken and the parameters like frequency and amplitude was varied and studied. The complete range of the frequency, acceleration and diameter of particles used in the simulations was shown earlier in table 3.1. The motion of the particle was visually observed using a visualization tool developed in OpenGL. The initial simulations experiments were carried out using the 45° degree wedge shaped hopper. The base parameters used in the simulations are shown in table 4.2. Each simulation experiment granular bed was made with one uniform size of glass beads. The convection flow pattern of the simulations of the granular material was characterized by plotting the results in MATLAB to study the behavior of the particles in the bed. The output for the average displacement vectors of the particles was printed to a file after every twenty cycles of oscillations from where the average displacement vectors of the particles were plotted.

Parameter	Value
ε_{pp}	0.80
$k_{n,pp}$	$5.289*10^{3}$ N/m
$v_{n,pp}$	$8.337*10^{-3}$N/(m/s)
$k_{s,pp}$	$5.289*10^{3}$ N/m
μ_{pp}	0.1
$k_{n,pw}$	$1.058*10^{4}$ N/m
$v_{n,pw}$	$1.667*10^{-2}$N/(m/s)
$k_{s,pw}$	$1.058*10^{4}$ N/m
μ_{pw}	1.0
ρ	2500kg/m^3
Δt	$2.552*10^{-6}$

Table 4.2 The base simulation parameters used in simulations

4.4 Results

4.4.1 Flow Pattern and Surface Stability: Vertical Shaking

The first set of test were carried out for the using frequencies used in the experiments together with the vertical accelerations but neglecting the horizontal accelerations

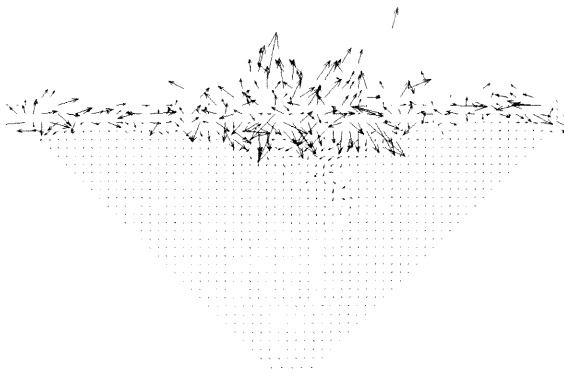

Figure 4.4.a Displacement vectors of the mono-disperse particles at frequency of 20Hz and 2g acceleration

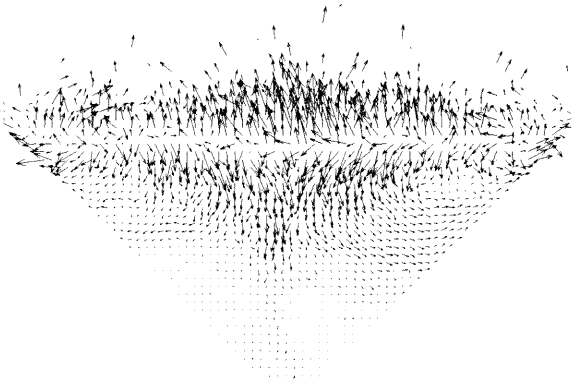

Figure 4.4.b Displacement vectors of the mono-disperse particles at frequency of 20Hz and 3g acceleration

measured in the experiments. Figure 4.4.a and Figure 4.4.b show sample plots of the flow patterns observed for the mono-disperse system. Figure 4.4.a show that there was very little movement of the particles within the bed, however there was some movement on the surface of the particles. As the acceleration was increased, the motion moved further down into the bed and convection flow patterns could be observed as shown in figure 4.4.b. These convection flow patterns were symmetrical, with the particles moving up the sides of the hopper and own the center. Further increases in the acceleration to 4g, at the same frequency resulted in the flow rate of the particles increasing as observed by the longer displacement vectors shown seen in figure 4.4.c. As the acceleration was increased to 5g, the motion of the particles were less symmetrical and with the flow patterns

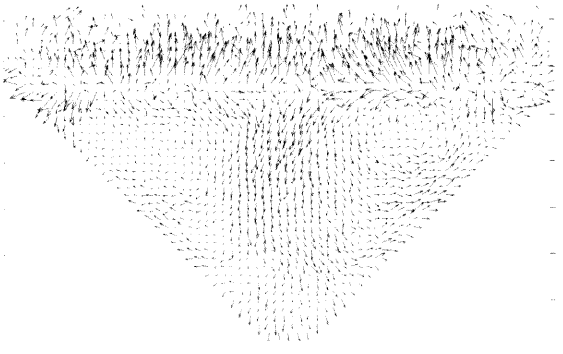

Figure 4.4.c Displacement vectors of the mono-disperse particles at frequency of 20Hz and 4g acceleration.

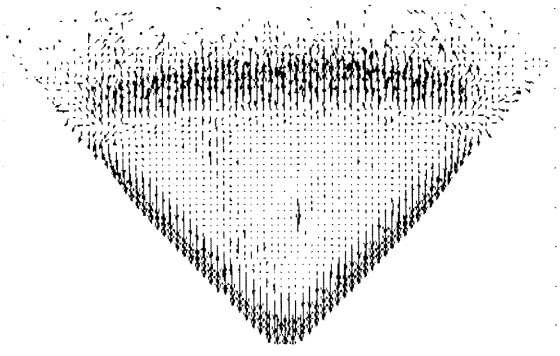

Figure 4.4.d Displacement vectors of the mono-disperse particles at frequency of 20Hz and 5g acceleration.

becoming more random and dispersed (see figure 4.4 d).

In vibrated granular systems, the energy input occurs mainly at the base of the container. Collision transfers energy up through the bead pack. Since the collisions are inelastic, the energy is continually dissipated during the process. In large or very inelastic

or weakly forced systems, all of the driving energy is dispersed among the particles or lost through collisions. As the energy input into the system is increased, the system is unable to absorb all of the input energy and as a result the particles at the top of the bead pack receives a disproportionate amount of energy resulting in the uppermost layers becoming fluidized.

Simulations were completed for the entire range of particles and the behavior generally followed the trend shown in figures 4.4.a to 4.4.d. The patterns observed in the MATLAB particle displacement plots, were also visually observed using a visualization tool developed in OpenGL. With the increasing values of acceleration amplitude, the behavior was observed for the entire range of particles studied and summarized as follows:

1. It was found that in the initial stage, with gravity force alone acting on the particles, the depth of the bed is reduced due to compaction, with the particles showing a small amount of relative motion.
2. Motion of the particles initiated on the surface along the sides, gradually moving towards the center with a small amount of heaping and surface fluidization.
3. Symmetrical motion occurred about the vertical axis of the simulation space with the particles seen to be rolling up sidewalls of the hopper and down the center.
4. Random motion of the bed, highlighted by large displacement of the particles and large surface waves.

That the rate of convection increased with increases in acceleration, and decreased with increases in frequency; this is indicated by the size of the displacement vectors. The parameters used to obtain the results shown in figure 4.4.a to 4.4.d are shown in table 4.3.

Parameter	Value
f	20 Hz
ε_{pp}	0.80
N	1258
d	1.7 mm
H/d	35
$k_{n,pp}$	$2.5984*10^{4}$ N/m
$v_{n,pp}$	$4.09600*10^{-2}$N/(m/s)
$k_{s,pp}$	$2.5984*10^{4}$ N/m
μ_{pp}	1.0
$k_{n,pw}$	$5.1967*10^{4}$ N/m
$v_{n,pw}$	$1.667*10^{-2}$N/(m/s)
$k_{s,pw}$	$5.1967*10^{4}$ N/m
μ_{pw}	1.0
ρ	2500kg/m^3
Δt	$2.500*10^{-6}$
Hopper angle	45°

Table 4.3 The simulation parameters used in simulations to obtain the sample result shown in figures 4.4.a to 4.4.d

4.4.2 Flow Pattern and Stability: Vertical Shaking and Horizontal Shaking

The initial results although similar to the experimental results, showed no inclination of the free surface for small values of acceleration as seen in the experiments. It was this difference that prompted the measurement of the vibrations in the horizontal planes. The parameters although generally the same in as that applied to the experiments did not include the horizontal component of the acceleration measured by accelerometers. In an effort to make the simulations as similar to the experiments as possible, the simulations were repeated with both the vertical components of the acceleration, along with the horizontal component of the acceleration measured in the experiments also being simultaneously applied. Sample plots of the flow patterns are shown in Figures 4.5.a to 4.5.c. For the system with both the vertical acceleration, and the experimentally measured horizontal acceleration applied the results clearly showed the inclination seen in the

experiments and described by Evesque and Rajenbach [19]. The parameters for the results in figure Figures 4.5.a to 4.5.c are the similar to that in table 4.3 with the addition of the horizontal acceleration of 0.4g, 0.9g and 1.1g respectively, corresponding to applied vertical acceleration of 2g, 3g, and 4g respectively. In this case, the changes in

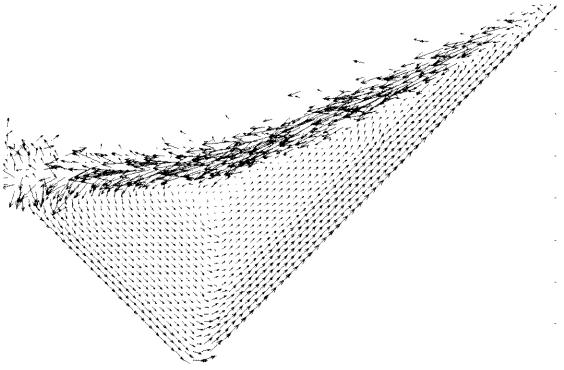

Figure 4.5.a Displacement vectors of the mono-disperse particles at frequency of 20Hz and $\Gamma_v = 2$ and $\Gamma_h = 0.4$

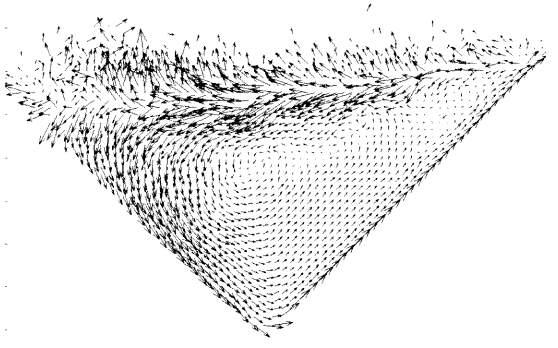

Figure 4.5.b Displacement vectors of the mono-disperse particles at frequency of 20Hz and $\Gamma_v = 3$ and $\Gamma_h = 0.9$

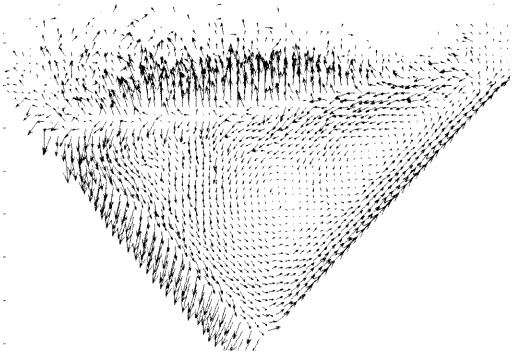

Figure 4.5.c Displacement vectors of the mono-disperse particles at frequency of 20Hz and $\Gamma_v = 0.4$ and $\Gamma_h = 1.1$

the value of the acceleration amplitude resulted in flow patterns and heaps, which closely matched that observed in experiments. The values used for the coefficient of friction was $\mu = 1$. This value is higher that the actual value, however with a high value of μ resulted

in fewer oscillation cycles being required for averaging, thus saving simulation time. The complete range of the particles was tested and the flow pattern transition generally followed the same trend. The behavior of the particles with both components of the acceleration applied to the bed may be summarized as follows:

1. It was found that in the very initial stage, from the initial position, the depth of the bed is reduced when the particles were allowed to settle under gravity.
2. Initially there was motion of the particles on the surface accompanied by the sloping of the free surface inclined with the horizontal. The convection vectors indicated that the particles were forming one loop, or in some cases two loops that were non-symmetrical.
3. Longer displacement vectors, indicating faster motion of the particles, accompanied by the surface approaching a horizontal state with the increase in acceleration.
4. Random motion of the bed, highlighted by large displacement of the particles. As acceleration increased the slope of the free surface was reduced, until the slope was no longer apparent. The free surface of the displacement vectors also gave the indication that surface waves were being formed.

For all of simulations, it was observed that the convective motion was weaker at higher frequencies and smaller values of acceleration amplitude.

4.4.3 Effects of Shape of Container on Instability

In prior work, it has been noted that that the shape of the container in which the granular material is vibrated, affects the direction of the flow pattern. Figure 4.6.a to figure 4.6.d

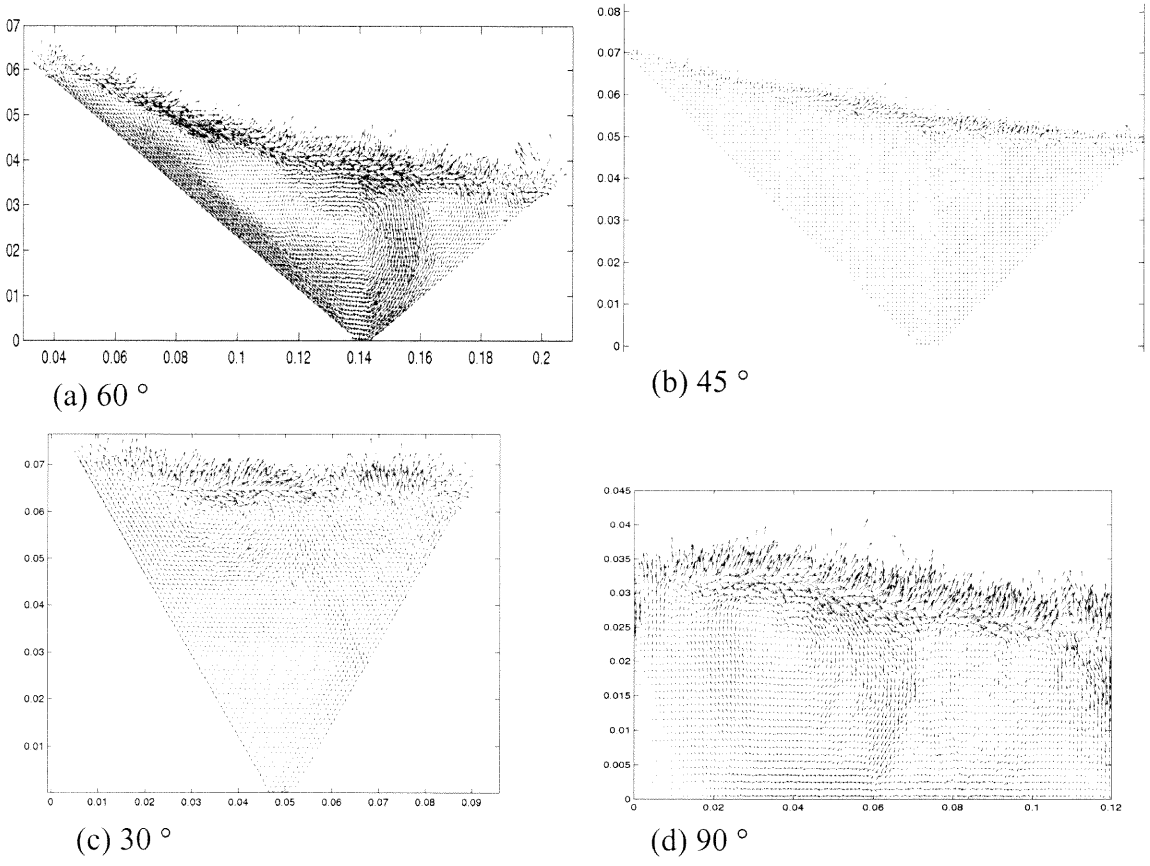

Figure 4.6.a - 4.6.d Displacement vectors of the mono-disperse particles at frequency of 30Hz and $\Gamma_v = 3$ and $\Gamma_h = 0.8$ for hoppers of different angles

show snapshots of the effect of the shape of the container on the surface stability. It was observed in the experiments that the shape of the contained did not show any significant effect on the values measures for the horizontal acceleration. Figure 4.6 show snapshots of the slopes of the free surface for particle size 1.7 mm for four different shaped hoppers with different wedge angled. Although the difference observed for the different angles were not significant, the displacement vectors indicate that for the 30 degree included

angle, and the rectangular hopper the angle of inclination of the free surface was less. From figure 4.6.a to 4.6, it can be observed that as the slope of the hopper sides became steeper, the rate of convection reduced. That is, the faster rate of convection of the particles along the hopper walls corresponded with the greatest slopes of the free surface. The parameters used for to obtain the results shown if figure 4.6.a to 4.6.d are shown if table 4.4.

Parameter	Value
f	30 Hz
ε_{pp}	0.80
No of cycles	120
d	0.10 mm
$k_{n,pp}$	$5.2890*10^{3}$ N/m
$\nu_{n,pp}$	$8.33706*10^{-2}$ N/(m/s)
$k_{s,pp}$	$5.2890*10^{3}$ N/m
μ_{pp}	1.0
$k_{n,pw}$	$1.0578*10^{4}$ N/m
$\nu_{n,pw}$	$1.667*10^{-2}$N/(m/s)
$k_{s,pw}$	$1.0578*10^{4}$ N/m
μ_{pw}	1.0
ρ	2500kg/m^3
Δt	$2.500*10^{-6}$
Hopper angle	60°, 45°, 30°, 90°

Table 4.4: Simulation Parameters used in Simulations to obtain the Sample Result shown in figures 4.4.a to 4.4.d

4.4.4 Effects of Diameter of Particle on Slope of Surface

Similar to the experiments, the slope of the free surface was either tilted to the left or the right when both the vertical and the horizontal acceleration parameters were applied to the simulations. The experimental analysis indicated that as the particle diameter increased the slope of the free surface was reduced. Figure 4.7 shows a plot of the

inclination of the free surface as the acceleration increased for different diameter particles. The plot indicates that as the acceleration increased, the slope of the free surface was reduced. Also, as the diameter increased, the results obtained from the simulations indicate a reduction in the slope of the free surface.

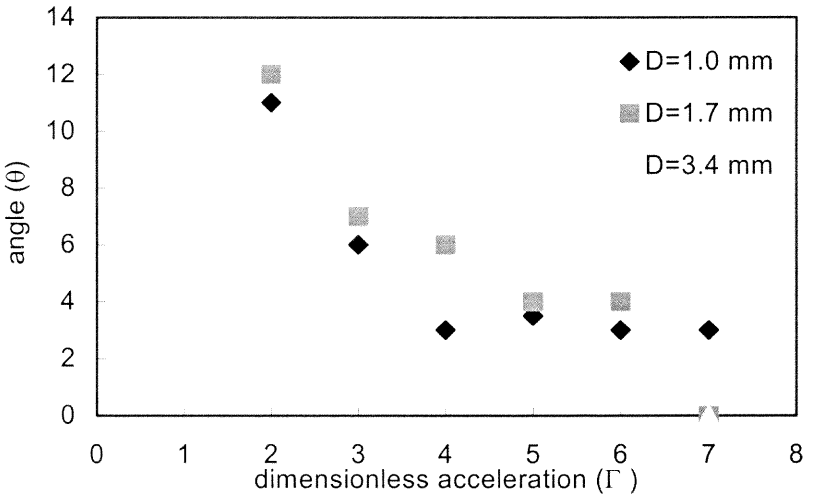

Figure 4.7 Slope of surface plotted as a function of dimensionless acceleration amplitude (Γ)

In order to quantitatively investigate the behavior of the particles in the hopper, another other properties of the bed investigated was total flow of the particles as a function of the dimensionless acceleration amplitude Γ. The experimental results indicated that the rate of circulation or the time it took for a particle at the bottom of the hopper to rise to the surface decreased as the acceleration increased. By averaging the displacement per cycle for many shakes, the simultaneous convective velocities can be calculated. The goal of the exercise is to examine the direction and the strength of convection. This measurement of this quantity for different values of vibration acceleration also gives some indication of the starting point of convection flow.

The movement of the particles along the walls of the container is also an indicator of sidewall convection. Grossman [32] used this technique to determine the transition angle of convective flow for containers with a variety of wall angles. This rate of convection is obtained by measuring the strength of flow of convection, done by measuring the cell-to-cell flow ζ. By counting the number of particles that go out of and come into a cell, the cell to cell average [58] is obtained. To measure the cell-to-cell convection, the simulation space is first divided into grid of squares each with the length of the side slightly greater than the particle diameter. The mass average particle displacement per cycle for each cell for each cycle is determined by the following relationship,

$$\Delta\vec{r}_{(i,j),c} = \frac{1}{M_{(i,j)}} \sum_{n=1}^{n=N_{(i,j)}} m_n (\vec{r}_{n,c} - \vec{r}_{n,c-1}) \tag{4.30}$$

where (i, j) refers to a particular cell, c is the oscillation cycle, $\Delta\vec{r}_{(i,j),c}$ the mass averaged particle displacement for cell (i, j) from cycle c-1 to cycle c, $M_{(i,\,j)}$ the total mass of particles in the cell (i, j), $N_{(i,\,j)}$ the number of particles with centers located in cell (i, j), m_n the mass of particle n, and $\vec{r}$ the particle's position vector. The average mean motion over several oscillation cycles is given by,

$$\overline{\Delta\vec{r}_{(i,j)}} = \frac{1}{C-1} \sum_{c=2}^{c=C} \Delta\vec{r}_{(i,j),c} \tag{4.31}$$

where C is the total number of oscillations cycles.

In order to obtain information on the strength of convection at various points in the simulation space, the cell-to-cell flow along the sidewalls, and along the vertical axis

through the hopper was also measured. For the side wall convection behavior, only the cells near the walls are considered, while for the convection along the vertical axis of the hopper the only the cells on both sides of the vertical axis are considered. The average displacement over one cycle near the walls is found by

$$\Delta y_w = \frac{1}{N_w} \sum_{n=1}^{n=N_w} (\overline{\Delta \vec{r}_n} . \hat{j}) \tag{4.32}$$

where N_w is the number of cells bordering the walls, and $\hat{j}$ is the unit vector in the vertical direction. The average displacement along the center of the hopper is divided into components. One component acts along the left center of the axis and is found by the following relationship

$$\Delta y_{lc} = \frac{1}{N_{lc}} \sum_{n=1}^{n=N_{lc}} (\overline{\Delta \vec{r}_n} . \hat{j}) \tag{4.33}$$

Where N_{lc} is the number of cells bordering the left side of the center axis walls. While the second component acts along the right center of the axis and if found by the relationship

$$\Delta y_{rc} = \frac{1}{N_{rc}} \sum_{n=1}^{n=N_{rc}} (\overline{\Delta \vec{r}_n} . \hat{j}) \tag{4.34}$$

where N_{rc} is the number of cells bordering the left side of the center axis walls

Figure 4.8 shows the average flow in the hopper over the entire container with respect to

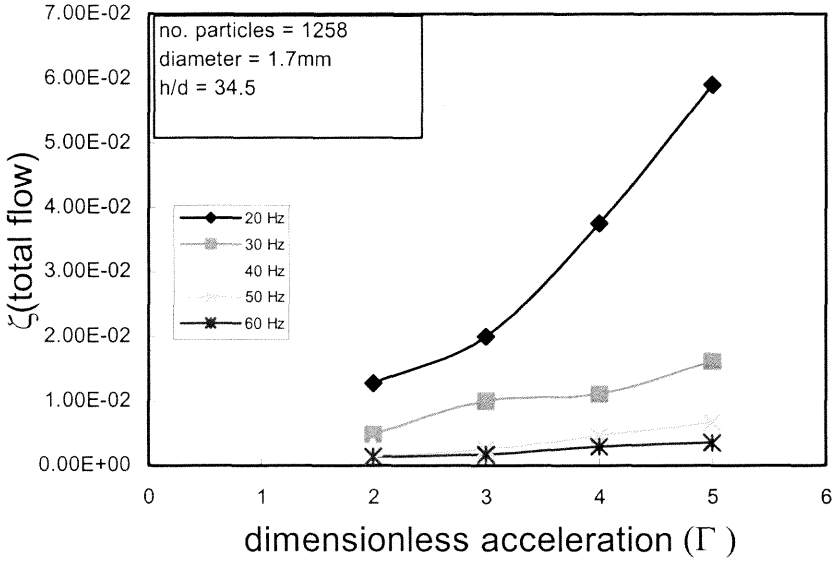

Figure 4.8 Total flow ζ as a function of Γ

the dimensionless acceleration amplitude. The simulations showed that there was no motion below $\Gamma = 1$ and clearly that there is motion of the particles above $\Gamma = 2$. Taguchi [58] defined the threshold value for the onset of motion as $\Gamma_c = 1.2$ similar to the present results. Figure 4.9 shows the dimensionless flow along the walls of the hopper for particle size of 1.7 mm in a hopper with purely vertical vibration applied. This graph shows that for a purely vertical acceleration the motion up the sides of the hopper is uniform and of approximately the same values. This probably accounts for no inclination being present on the free surface of the particles when the horizontal acceleration is not applied.

Figure 4.10 shows the case with both the vertical and the horizontal acceleration is applied. Here, it would be noticed the direction of the hopper flow although initially the same headed in opposite directions. This is as a result of there being one loop formed in the simulation space, with the particles flowing up along the left wall of the hopper and

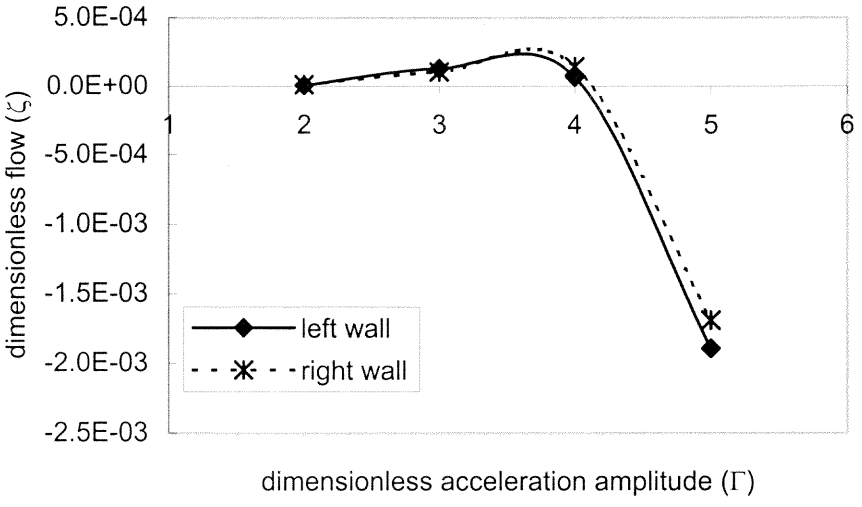

Figure 4.9 Flow along the hopper walls as a function of dimensionless acceleration (Γ) without horizontal component of acceleration.

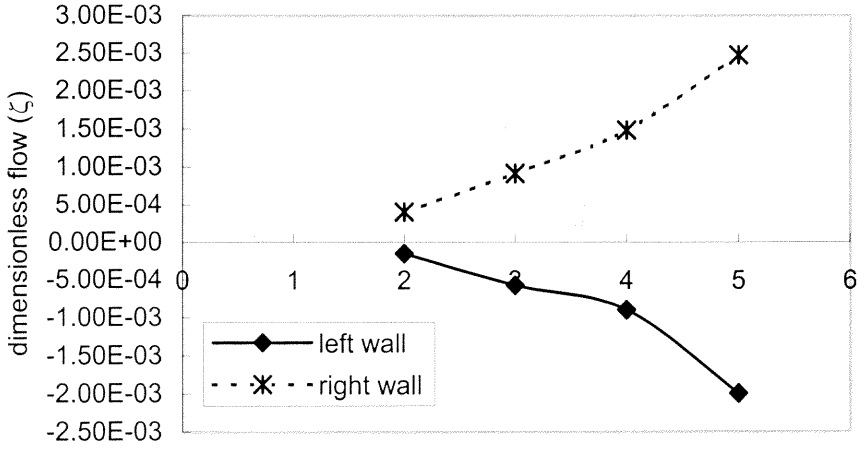

Figure 4.10 Flow along the hopper walls as a function of dimensionless acceleration (Γ) with horizontal component of acceleration and vertical acceleration applied.

down the right wall. In this case, the convection flow is not uniform result in the inclination of the free surface. It can also be observed that in both cases the rate of convection flow increased with the increase of the acceleration amplitude of vibration.

As the acceleration increased the inclination of the free surface was reduced similar to that observed in the experiments. This may be due to the fact that as the convection speed increases the magnitude of the force of the collision between the bed and the particles also increased resulting in the destruction of the slope of the free surface. As the acceleration increases in the experiments, surface waves were observed. The occurrence of these surface waves may also be a contributing factor to the disappearance of the slope on the free surface.

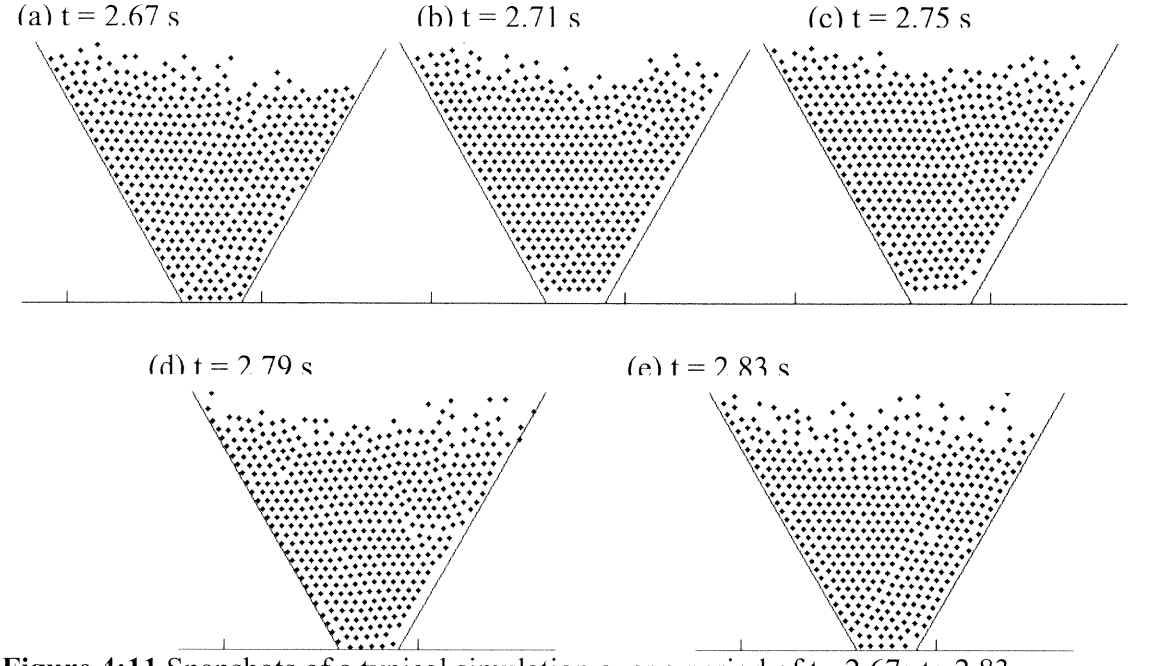

Figure 4:11 Snapshots of a typical simulation over a period of t =2.67s to 2.83s. Diameter of the particles d = 1mm, f = 30 Hz, with vertical acceleration 2g, and horizontal acceleration 0.44g.

The MATLAB plots discuss so far do not refer to the actual motion of the particles at a given moment time, but actually measures the average displacements of the particles. As the hopper rises and falls, the particles may explore a wide range of space,

but the change in the average position of a particle at a fixed point in the cycle is what defines convective motion [60]. In the figure 4.11, a time series for a range of the position of the hopper over one cycle is presented. These are snapshots of the relative motion of the particle and the hopper. Initially, the particles are horizontal see (Figure 4.11.a). When the hopper moves up to the top, there is greater separation between the particles and the base. The largest separation is just when the hopper is on its downward motion and the particle are momentarily still moving upwards, see (c) and (d), and the greatest contact occurs when the hopper is moving upwards and the particles are just completing their downward motion still moving down, see (e) and (f). Note that there is more separation between the particles and the container wall on the right boundary, which is due to the horizontal vibration acceleration. As a result of this, there is greater contact between the particles and the left wall, thus more movement of the particles up this wall, due to a smaller area in which to fall downwards.

Lee [85] emphasizes that the variation in density over the course of a cycle, and the effect that it has on the shear force exerted by the walls, play a significant part in the direction and magnitude of the convection. He observed that at higher densities, the sides of the container could exert a larger drag force on the particles. There are two distinct phases that make up the oscillation: when the beads are moving up relative to the container and when they are moving down. During the upward motion of the beads relative to the container, the force is downward; in the second part, the particles are moving down into the container, so the shear force due to the walls is directed upwards. Due to the fact that the walls are tilted outwards, as the particle rise, the horizontal space available to them increases. This means that, in the first phase of the cycle, the particles

near the wall can expand into the space aerated as the grain pack lifts away from the walls. On the way down, the particles must be packed into the narrower space at the base of the container and hence the density is higher. Since the density is greater when the particles are moving downwards, the magnitude of the drag force exerted during this phase of the cycle will be larger and the net force over the course of the cycle will be upwards. Due to the fact that the particles are closer to one of the walls as a result of the horizontal acceleration, the force on this wall will be greater resulting is the particles being further up this wall.

Another parameter that was used to access the bed behavior properties quantitatively is the time of flight of the particle. Plots of the particle and base trajectories are shown in figures 4.12.a to 4.12.c. These plots give an analytical indication of the bed behavior for different values of vibration acceleration. The top figure show the trajectories for a frequency of 20 hertz while the vibration acceleration was varied from $\Gamma = 2$ to $\Gamma = 4$. The other two figures showed the same thing for frequencies of 40Hz and 60 Hz respectively. From these plots, it can be observed that for the small values of Γ the particle collides with the base after a time of flight that is less than the oscillation period. As the value of the acceleration increased at constant frequency, the plots indicate that the particle collides with the base at a later stage of the oscillation period eventually moving to the state where the plots show the particle motion exhibiting a period of two motions.

The results indicated by these plots are consistent with the experimental behavior that was observed in the time series of range of motion of the particles. For small values of vibration acceleration, the particle bed does not leave the base. However, as the value

of the acceleration increases the particles in the bed leaves the bed for longer time periods. The plots seems shown above seems to indicate that the particle did not touch the

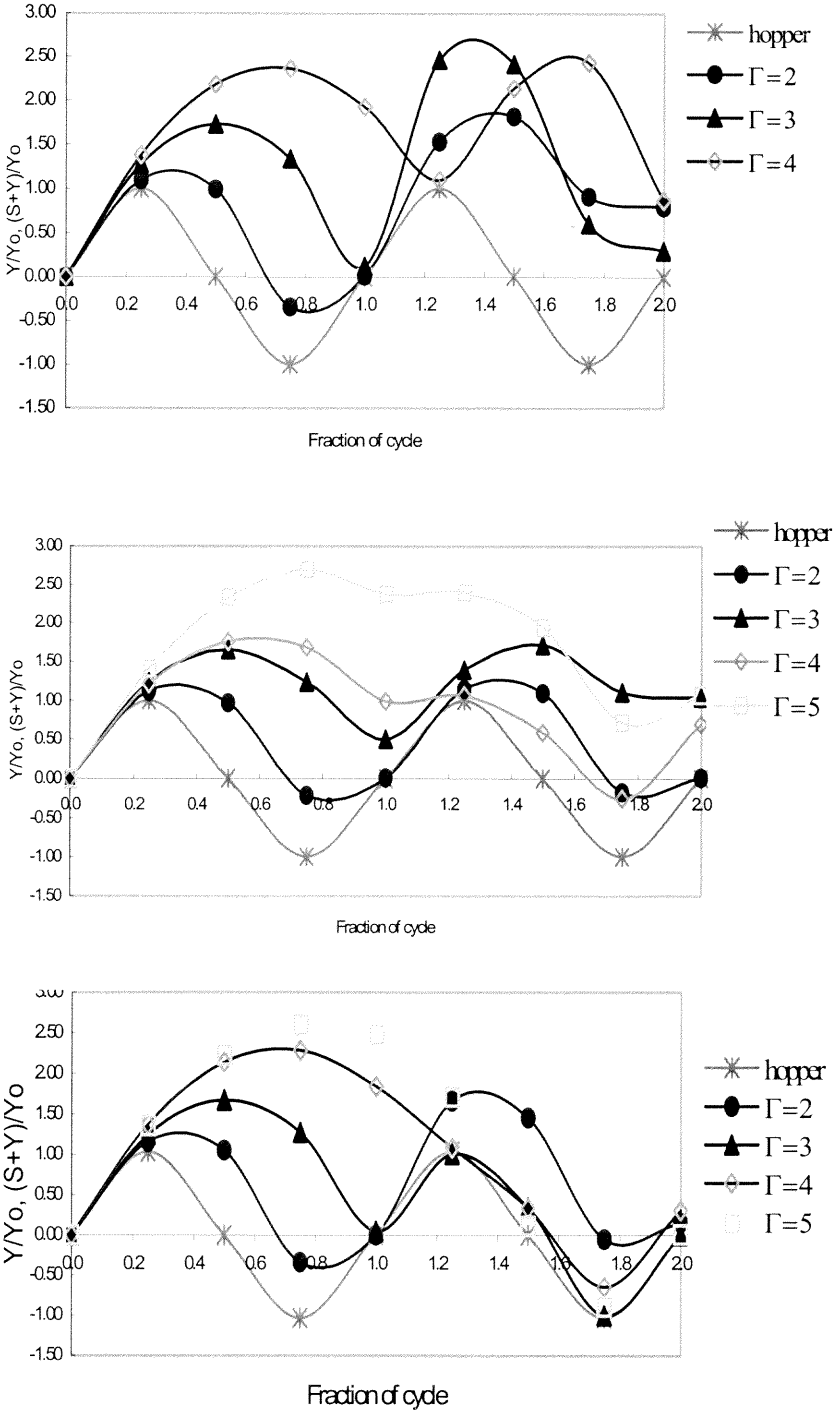

Figure 4.12 Particle and base trajectories as functions of oscillation phase angle. The coefficient of restitution for the calculations is e = 0.25. The figures show the trajectories for three different frequencies, (a) f = 20 Hz, (b) f = 40 Hz, (c) f = 60 Hz.

plotted were chosen from the hopper containing many particles just off the base of the container and as a result was colliding with other particles already touching the base rather than the hopper base.

Another measure of random particle motion in the bed is the granular temperature per unit mass, γ, defined as the kinetic energy per unit mass in the bed due to particle fluctuation velocities. This quantity can be measured by the following relationship,

$$\gamma = \frac{1}{2M} \sum_{n=1}^{n=N} m_n ((\dot{x}_n')^2 + (\dot{y}_n')^2) \tag{4.35}$$

where M is the total mass of the particles, N the number of the particles, m_n the mass of the particles n, and $\dot{x}_n' = \dot{x}_n - \dot{x}_{cm}$, $\dot{y}_n' = \dot{y}_n - \dot{y}_{cm}$ are the fluctuating particle velocities $\dot{x}_n$ and $\dot{y}_n$ are the velocity components of particle $\dot{x}_{cm}$ and $\dot{y}_{cm}$ are the bed's center of mass velocity component. Figure 4.12.a to 4.12.c shows the granular temperature per unit mass plotted as a function of oscillation cycles for Γ = 2, 3, and 4 plotted for values of frequencies of 30Hz, 40Hz, and 50Hz. For each cycle of vibration, it is observed that there is a sudden increase in the granular temperature. This sudden increase in the granular temperature once each cycle corresponds to the particle bed impacting the base. The temperature then decreases as collisions between particles occur. These plots also reflect the behavior of the particles during the vibration of the hopper. For small values of vibration acceleration, the granular temperature value is very small for a larger part of the cycle. This indicates the fact that the particles remain in contact with the base of the container, as is reflected by the plots for the particle base trajectories shown if figure 4.11.

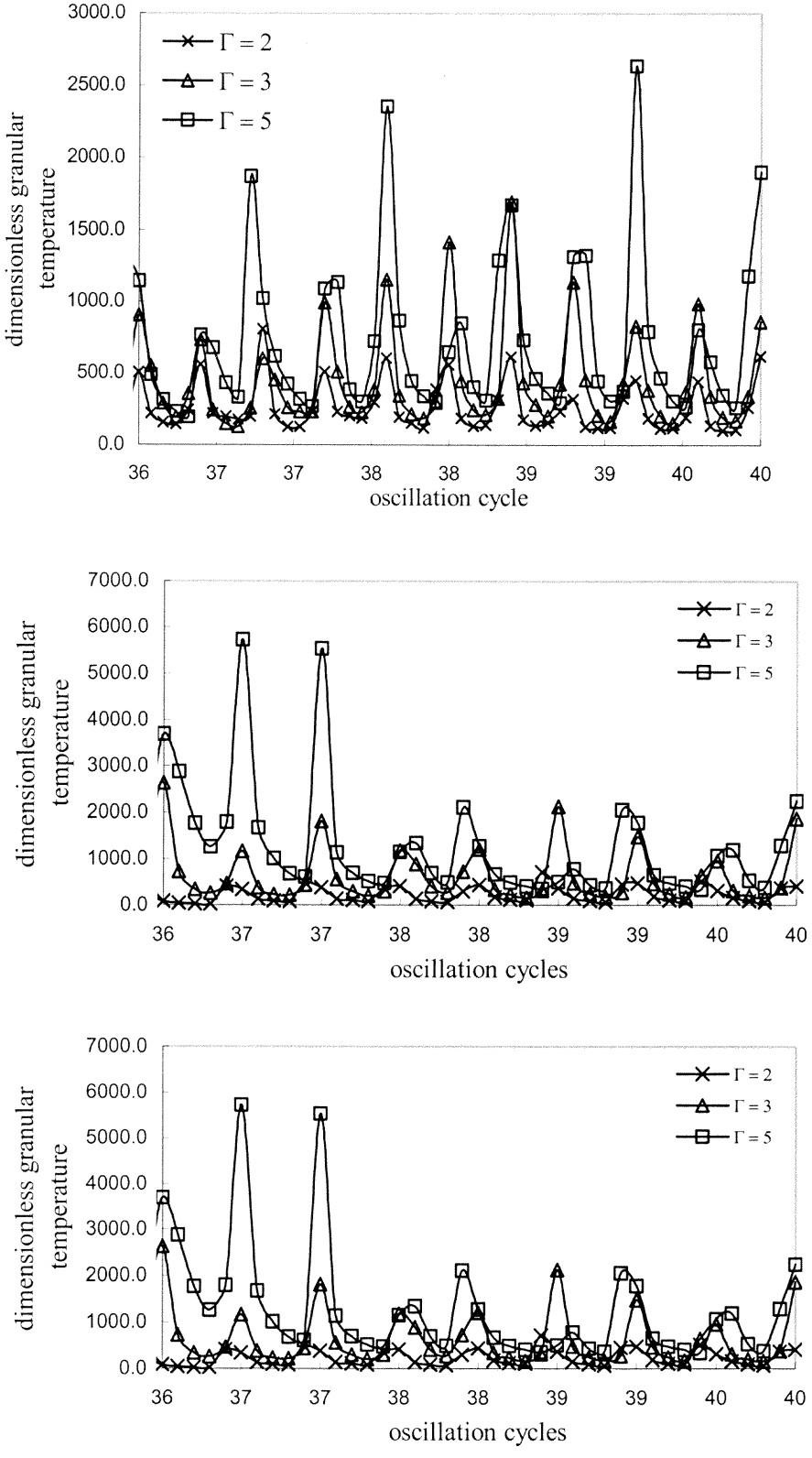

Figure 4.13: The dimensionless temperature per unit mass, $\gamma\omega^2/g^2$ plotted as a function of the oscillation cycle for $\Gamma = 2$, 3, and 4, for $f = 40$ Hz, 50 Hz, and 60 Hz.

Grossman [32] examined the reversal of convection flow patterns and indicated that a key role is to look at how convection changes when the container is shaken at different frequencies, with the forcing strength measured by Γ kept constant. As can be seen from the plots in figure 4.13, the strength of the convection rolls decreases with

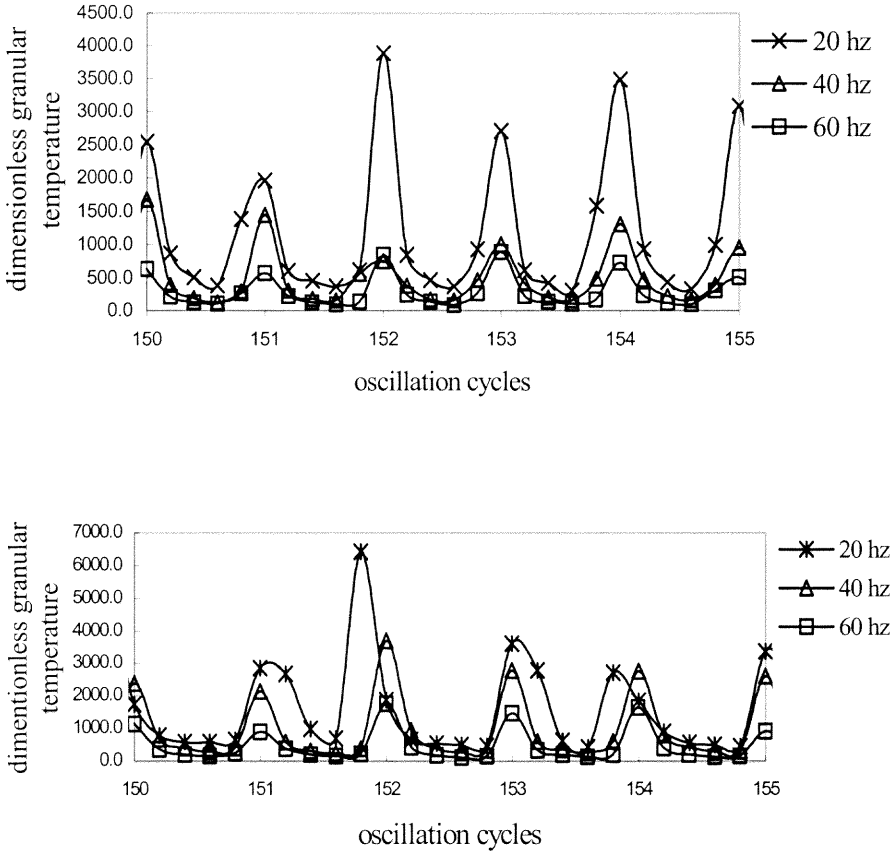

Figure 4.14 The dimensionless temperature per unit mass, $\gamma\omega^2/g^2$ plotted as a function of the oscillation cycle for (a) $\Gamma = 2$, (b) $\Gamma = 3$, for $f = 20$ Hz, 40 Hz, and 60 Hz.

increase frequency. This is due to the fact that at higher frequencies the period is shorter and the range of density explored is narrower. Since the magnitude of the net force exerted by the walls over the course of the cycle is determined by the difference between

the densities on the upward and downward phases of the cycle, the smaller range produces a lower net shear and therefore weaker convection rolls.

In figure 4.13 and figure 4.14, the plots of the dimensionless temperature were not taken from the initial time that the vibration was applied to the hopper. Instead, in both cases the hopper was allowed to vibrate for some time so as to enable the vibrating particles to attain a stable vibrating condition. As a result, the starting cycles were chosen as 36 cycles and 150 cycles respectively. The unusual spikes in the values of the granular temperature observed in these plots were due to some of the particles on the surface of the bed occasionally rising higher than usual. This larger relative displacement of some of the particles on the free surface was observed in figure 4.5.c.

4.5 Comparison between Experimental and Simulation Results

The simulations done in this work, shown in chapter 4, closely matched the experimental analysis done in chapter 3. The geometry utilized for the two-dimensional hopper used in the simulations matched that used in the experiments. A comparison of the results in chapter 3 and chapter 4 indicates, that when same magnitude of acceleration amplitudes that were used in the experiments is applied in the simulations, the flow pattern and flow pattern directions were the same. In addition to the flow patterns being similar, the sloping of the free surface was observed in both the experiments and the simulations. Graphs plotting the slope of the free surface in both cases (see, figures 3.2 and 4.8) showed a similar trend with the angle of inclination being reduced both with increasing velocity amplitude and particle diameter. The snapshots shown in figures also confirm

that one possible reason for the inclination observed in the experiments was most likely due to lateral components of acceleration being present. This conclusion can be made since the effect of air was not considered in the simulations. After examining these plots from the experimental and simulation results, it can be concluded that the heaps formed along whichever wall is pushing on the material during the negative vertical acceleration portion of the cycle.

4.6 Conclusion

Due to the fact that the simulation is two-dimensional, only the two larger values of accelerations were applied in the simulation. The simulation studies have shown, that when lateral vibrations are applied to a vertical vibrating hopper, even very small values of lateral amplitude can result in surface instability and heaping. The application of the actual values measure in the experiments to the simulations resulted in very similar results, illustrating that the simulation model adequately represented the experimental system. This matching inclination seen here both in the experiments and the simulation, seem to indicate that the inclination may be as a result of imperfections in the alignment of the apparatus that may be impossible to practically eliminate.

The small differences between the experimental analysis and the simulation analysis may be due to the fact that the computer model was two dimensional, and the fact that some of the parameters could not be modeled exactly as in the experiment. As proven by this work, minor lateral vibrations will result in particle surface instability leading to heaping and the inclination of the free surface. These inclinations, which are

present, may be one of the reasons why inclination of the free surface was observed by previous researchers. The inclination observed indicates that the air effects may not be the governing factor responsible for heaping indicated by some researchers [22-24].

CHAPTER 5

EXPERIMENTAL ANALYSIS OF SEGREGATION OF A BINARY SYSTEM OF PARTICLES

5.1 Introduction

A common industrial practice is to mix different types of particles before processing, for example, to produce pills. However, it is well known that particles of different kinds often tend to segregate that is, particles with similar properties collect is some region of the apparatus. Although the existence of size segregation in the handling, storage and the reclaim of granular materials have long been recognized, there have been few attempts to investigate the phenomenon quantitatively. Extensive literature review revealed that only quantitative study of segregation in silo discharges is by Standish [96] and Arteaga and Tuzun [97] who measured the volume ratio of a bidisperse mixture as a function of time but did not visualize the internal flow. In both cases, the behavior of the polydisperse granules was examined while subjected to gravity flow through the hopper. Currently, there are no acceptable theories that would predict quantitatively the amount of segregation in the ideal system, thus indicating the difficulty in obtaining theoretical explanation of segregation in systems of industrial complexity. Brown [4] did early work on segregation and gave qualitative explanations identifying two types of segregation, the first due to vibration and the second segregation down a free surface.

When dealing with hoppers, segregation may occur during filling of the hopper, in the hopper, or upon discharge from the hopper. In the filling and emptying of hoppers, size segregation can be troublesome and, in some industries critical. Over the years, more efforts has been devoted to the design of hoppers from the position of stress distribution

to ensure safety and flow requirements while paying less attention to the problems relating to size segregation.

5.2 Segregation During Filling

Due to the fact that particles of different size or density have a strong tendency to segregate during flow, care must be taken to avoid unwanted segregation during the filling of bins and hoppers. In previous work, it has been noted that most of the segregation problems encountered after storing in silos are already introduced during the filling process. Gray et al. [98] showed that stratification patterns are present when filling silos with different sized particles from a point source, which is the method most commonly used in industry. They referred to the patterns formed to as a pine-tree pattern that builds up through successive avalanches. Segregation during the filling of hoppers can be reduced by not loading material through a point source but rather through a whole region. Various manufacturers have developed special loading devices, for example, using pipes with flaps at different heights that will open successively, or egg shaped inserts for use in industry to reduce segregation during filling.

5.3 In-bin Segregation and Flow Pattern

Another important effect of size segregation is in relation to the flow properties within the hopper and the onset of stoppage. Vibration is usually applied to hoppers so as to enhance flow and stop stoppage. When vibration is utilized to enhance flow, although segregation may be avoided during filling, the use of vibration may result in segregation

in the hopper. This may result in varying, unpredictable flow patterns, leading to excess stresses being set up in the container.

Ristow [86] examined the flow pattern in hoppers by loading alternate layers of colored and non-colored beads. Without vibrations, the glass beads showed funnel behavior, where the discharge mainly came from the central region and material avalanched down the top surface inclined at an angle of $\theta \approx 60°$. The flow pattern was reversed by applying horizontal vibrations with $\Gamma = 2.0$, and at 20 Hz. He examined the flow patterns with the hopper closed, and found two small triangulation regions with the material flowing down along the side vertical walls. With the hopper open and the horizontal vibrations applied Hunt et al. [17] found that the flow patterns were almost inverted to that without the vibrations applied, referred to as inverted funnel flow by the authors. In this case, the central region discharged last, and it was found that the transition from the funnel flow to the inverted funnel pattern, occurs over a range of vibration velocity and acceleration, affecting the inclination of the upper free surface and coinciding with an increase in the discharge rate [17].

5.4 Segregation During Outflow and Upon Discharge

It has been noted that depending on the flow characteristics of granular materials in the hopper, segregation during outflow may or may not be present. It is often clearly visible when the silo is operated in the funnel-flow regime, where most of the material is transported along the surface and flows through a central channel. Hunt et al. [17] investigated the discharge rates of 1.1 mm and 2.0 mm glass beads in a planar hopper that was horizontally vibrated. They found that the discharge rate increased with vibration

acceleration, with the lowest frequencies giving the highest discharge rates for fixed vibration amplitudes. However, it was found that for the highest frequencies, the acceleration had to be greater than $\Gamma = 1$ in order for the discharge rate to increase with vibration acceleration.

5.5 Experimental Method

The experimental setup for the segregation study consists of one additional component, namely, a granules collection system that was not used in the earlier studies for the flow pattern of the mono-disperse systems. In the present study, the conical or wedge-type hoppers used earlier is utilized. This may be seen from Figure 5.1, which shows the dimension of one of the hoppers used. With the gross dimensions remaining the same, hoppers with four included half-angles, namely 30°, 45°, 60°, and 90° were used to cover both the conditions of core flow and mass flow hoppers for the experiments. The hopper exits were approximately the same for all of the various angles of hoppers used.

The present study was divided into two sections: One examining the flow patterns and segregation in the hopper, and the seconds study examining the study of segregation upon discharge for different in-bed segregation, and flow patterns conditions. The experiments to carry out the in-hopper segregation and flow pattern study was done basically on binary mixture of granules, using two types of glass beads of different diameters. The details on the parameters used in this study are shown in table 5.1. For all of the experiments, equal masses of the two beads were placed in the hopper. In order to have consistency in the initial conditions, the settings of the binary mixture of the glass beads comprised the layer of the smaller beads poured over the layer of the larger size

beads in all of the experiments involving vibration prior to discharge. To study in-bed segregation, with the hopper closed, vibration was applied for a period of time that allowed the to achieve a stable state. This was done so as to make the initial condition for

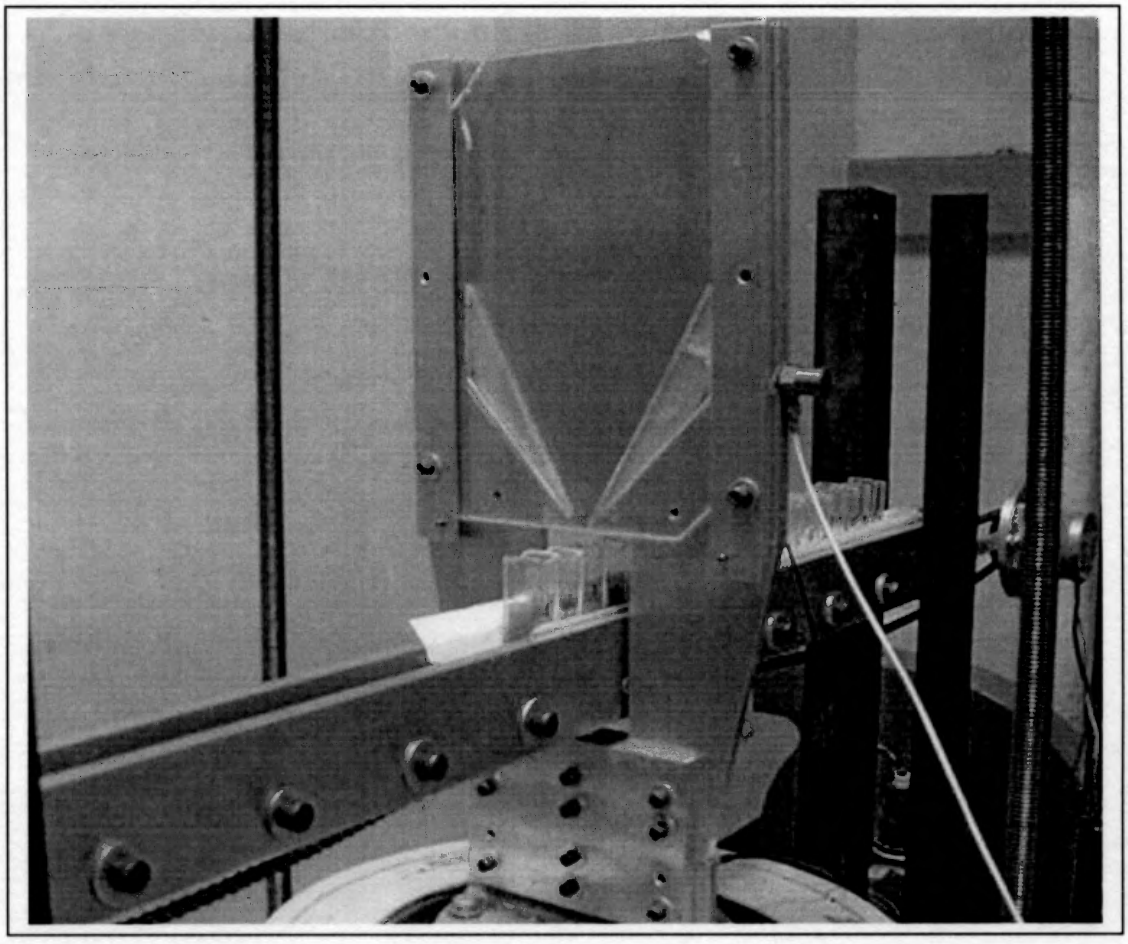

Figure 5.1: Snapshot of experimental setup

the first set of experiments constant. The convection rate was studied by examining the behavior of two beads of the larger sized particles that had a different color from the other beads in the particle bed that were initially placed at the bottom of the be and measuring the time taken by this bead to complete the convection cycle. This flow patterns were determined by visually observing the movement between the binary

particles of the glass beads that chosen with two contrasting colors that facilitate better visualization. Several experiments were performed to investigate the behavior of the granular materials of varying size ratios and subjected to vertical oscillations in the container. For each chosen frequency, the vibration acceleration was varied from $\Gamma = 2$ to 7.

In the study of segregation upon discharge from the hopper the hopper was set up as shown if figure 5.1. This diagram shows the hopper that is attached to the Ling vibration system together with a collection system. This system has a chain pulled track, operated by a computer-controlled electric motor. The tracks can accommodate approximately thirty collection cups. These cups are designed with a parabolic profile at the top so as to increase the collection efficiency of the particles coming out of the hopper exit. Three different initial conditions of the particles in the hopper were examined for the segregation upon discharge. These conditions are as follows:

(i) Segregation upon discharge with material in the hopper initially layered and the hopper opened simultaneously with the starting of vibration.

(ii) Segregation upon discharge with the after the material in the hopper had already been vibrated for some time and the material in the hopper achieving a stable state.

(iii) Segregation upon discharge with the material in the hopper initially layered and without vibration applied to the system.

The three different initial conditions were examined due to difficulty in quantitatively establishing the same initial conditions. Currently, there is no universally acceptable method that measures segregation. However, the initial conditions covered included

conditions established after characterizing the segregation in the hopper. For all of the cases (i) and (ii) mentioned above, a wide range of frequencies and vibration amplitudes was examined. For the measurements, the gate valve at the bottom of the hopper was opened and the discharge stream collected in the train of sampling boxes. The contents were then subjected to standard sieve analysis. Each experiment was repeated three times.

5.2.1 System Parameters

A list of the parameters studied for the binary disperse particle system is shown below in table 5.1. The initial experiments were carried out using the 45° degree wedge shaped hopper. The properties of the glass beads used are shown in table 3.3.

Table 5.1 Lists of Experimental Parameters for the Binary System of Particles

Parameter	**Quantity**
Frequency range	20 Hz – 60 Hz
Acceleration range	1.0g – 10 g
Particle ratios (ϕ)	2.1, 3.4, 5.7, 11.3
Hopper wedge angles	30°, 45°, 60°, 90°

For each experiment, the granular bed was made with two uniform sizes of glass beads of different color. The experiments were typically carried out by first fixing the frequency *f*, while varying the amplitude of acceleration. The flow convection pattern and the segregation of the granular bed were characterized using a digital camera.

5.6 Results

5.6.1 Segregation in the Vibrated Hopper

The first set of test were carried out for the range of size ratios shown in Table 5.1 the effects of acceleration on the beads were first examined by first selecting the desired diameter ratio, by choosing the combination of two particles and layering the particles

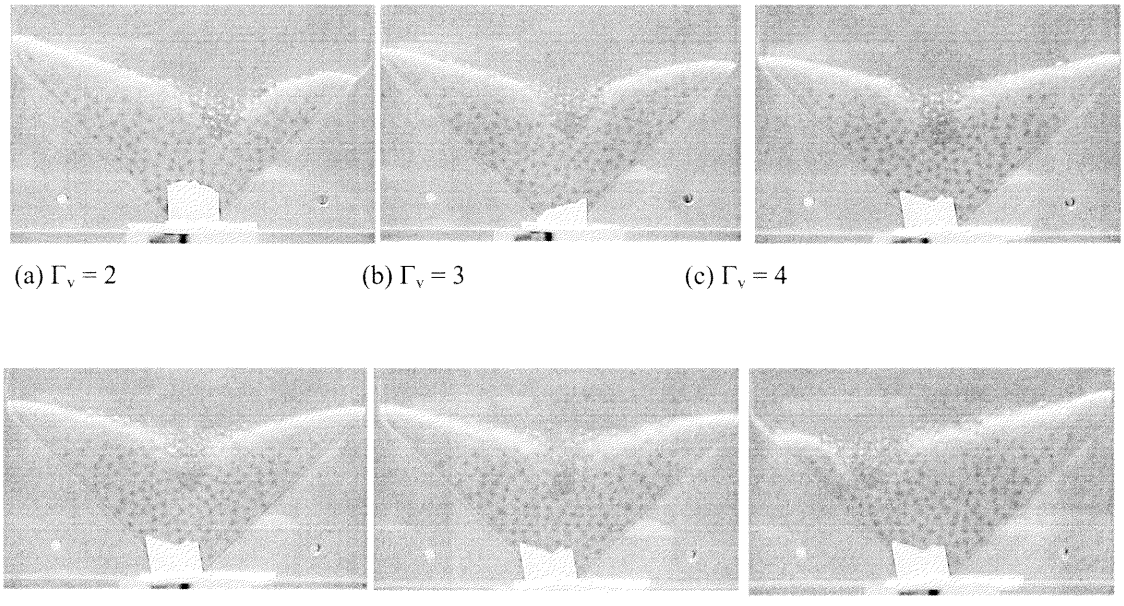

(a) $\Gamma_v = 2$ (b) $\Gamma_v = 3$ (c) $\Gamma_v = 4$

(d) $\Gamma_v = 5$ (e) $\Gamma_v = 6$ (f) $\Gamma_v = 7$

Figure 5.2 Snapshots of a typical set of experiments over a range of values with vertical acceleration $\Gamma_v = 2$, to $\Gamma_v = 7$. Diameter ratio of the particles $\phi = 11.3$ mm, f = 50 Hz.

with the larger particle initially placed at the bottom and the smaller particle placed on top. Equal masses of each particle were selected for all of the experiments conducted. The mass of each particle was chosen so as to fill the hopper up to the tapered section of the hopper. In these experiments the binary bed mixture were always deep in the sense of conventional terminology. The effects of acceleration on the flow pattern on the binary

system were first examined varying the acceleration of the system for a selected fixed frequency. This process was repeated for all of the diameters diameter ratios outlined in table 5.1 for the 45° degree hopper.

Figure 5.2 shows examples of the snapshots for the behavior of glass beads of diameter ratio $\phi = 11.3$ as the dimensionless acceleration Γ was varied from 2 to 7 for a frequency of $f = 50$ Hz. Similar snapshots are shown if figure 5.3 for the same diameter

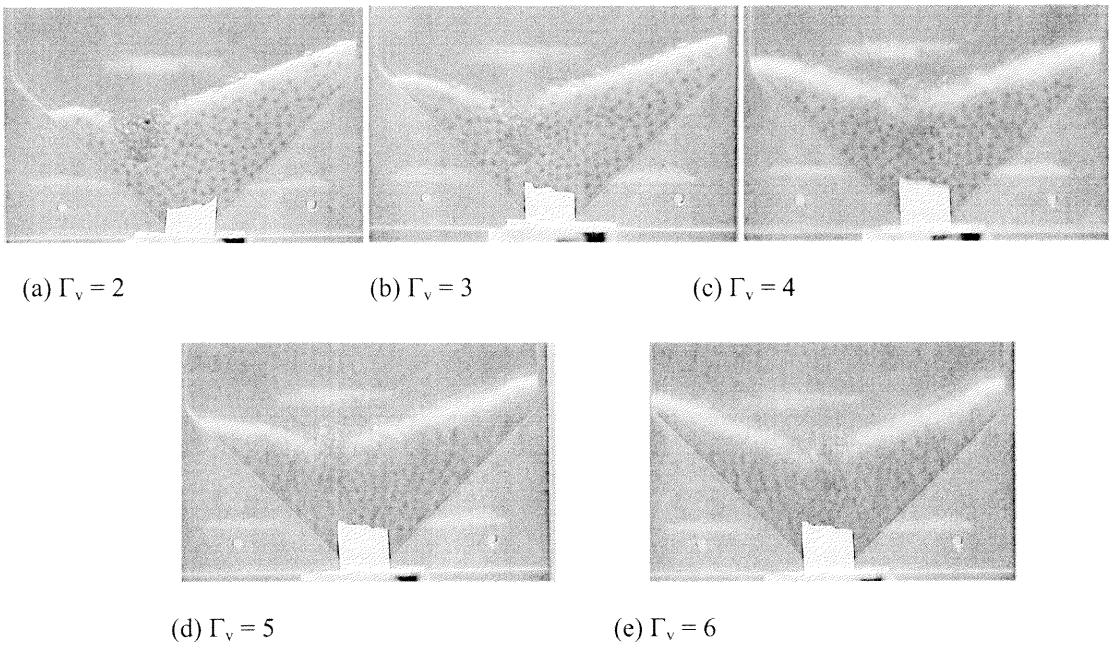

Figure 5.3 Snapshots of a typical set of experiments over a range of values with vertical acceleration $\Gamma_v = 2$, to $\Gamma_v = 6$. Diameter ratio of the particles $\phi = 11.3$ mm, $f = 20$ Hz.

ratio of glass beads but this time for a frequency of $f = 20$ Hz while the vibration amplitude $\Gamma = 2$ to 6. The results examining the flow pattern showed the following trend:

1. At very low acceleration amplitude $\Gamma \leq 1.0$ there was no convection flow movement within the bed of binary particles. For the larger size ratios $\phi \geq 5.7$ the

smaller particles moved down in-between the larger particles in the bed in a sieving motion filling the gaps between the larger particles.

2. At higher acceleration amplitudes, $\Gamma \geq 1.5$ convection patterns begin to form at the top while the rest of the bed remains stationary. As the acceleration amplitude increased, the convective motion moved deeper down into the bed. These convection flow patterns at low amplitudes were generally two offset loops sloping to the left or right of the hopper, see Figures 5.2 a. and Figure 5.3 a.
3. The convection cells formed at low amplitude comprised of the smaller and larger beads moving up the sides of the hopper and down the center. Heaping was observed where one of the two convection cells dominates, with the top surface being inclined at an angle with the horizontal. The acceleration amplitude influences the size of the angle of inclination with the horizontal. The direction of the inclination was the same as that observed for the mono-disperse system.
4. There was a great degree of segregation accompanying the heaping, with the larger particles moving to the surface of the bed of hopper particles. The larger particles found it difficult to renter the bed once they reached the surface, and accumulated as the lowest point of the heap or at the point of re-entry into the bed.
5. As the acceleration amplitude increased to $\Gamma \geq 3.0$, the convection flow pattern loops became symmetrical with the particles moving up the sides of the hopper and down the center. The increase in vibration amplitude resulted in an increase in the rate of convection and a decrease in the accumulation of the larger particles on the surface of the bed.

6. Increases in the acceleration amplitude $\Gamma \geq 4.0$ resulted in the formation of surface waves and the flow pattern in the hopper becoming unstable; particles continue to move up the sides of the bed but the flow patterns varied from symmetrical to non-symmetrical at random intervals. Here although segregation was still evident the level of segregation was less than that seen at the lower vibration amplitudes.

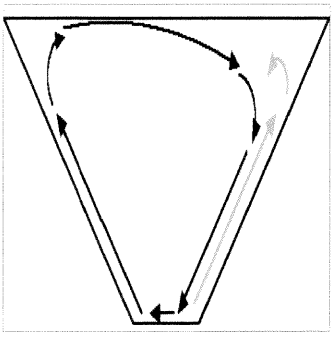

Figure 5.4 Convection Flow pattern with heaping and segregation sloping to the right

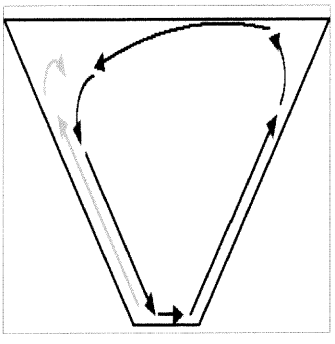

Figure 5.5 Convection Flow pattern with heaping and segregation sloping to the left

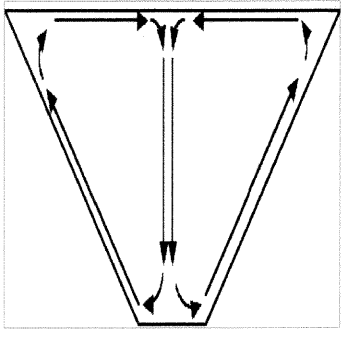

Figure 5.6 Symmetrical convection flow pattern

Figures 5.4 to 5.6 shows sketches of the convection patterns observed. Figure 5.4 and 5.5 shows sketches of the flow patterns observed at low acceleration amplitudes, while

Figure 5.6 show the symmetrical convection patterns observed at higher acceleration amplitudes.

Frequency range	Acceleration amplitude	Convection flow pattern	Segregation
20-60 Hz	$\Gamma < 1.5$	No convection flow.	Geometric segregation present for size ratio $\phi >$ 5.7. Smaller particles move in-between larger particles in a sieving motion.
20-60Hz	$\Gamma > 2$	Slow unsymmetric flow.	Heaping, high degree of segregation, with larger particles separating out on surface.
20-60 Hz	$3.5 \leq \Gamma \leq 4.5$	Symmetric flow, small surface waves.	Reduced segregation, more uniform mixing of particles within the bed.
20-60 Hz	$\Gamma \geq 4.5$	Varying random motion, ranging from symmetric to non-symmetric motion with surface waves.	Segregation still apparent but less than for the case with heaping.

Table 5.2 Summary of observed convection plow patterns and segregation levels

Table 5.2 gives a summary of observations based on the experiments carried out for the range of diameter ration for the parameters listed in Table 5.1. From the summary outlined in table 5.2, the granular flow and segregation behavior can be characterized by the following four regimes:

- Large particles stationary with the smaller particles sifting between the spaces in the larger particles due to geometric segregation

- Unsymmetrical convection pattern, accompanied be heaping due to sloping surface and a high degree of segregation with the accumulation of larger particles on the surface.
- Symmetrical convective motion with uniform mixing within the bed of particles and a reduced degree of segregation of the larger particles at the re-entry point into the bed.
- Unstable motion of particles ranging from symmetrical patterns to nonsymmetrical pattern with large surface waves. Segregation present at the point of re-entry of larger particles into the bed. The location of this segregation varies with the point of re-entry of the larger particles into the bed.

It should be noted that that for the range of frequency considered, except at low frequency the observed convection patterns were independent of frequency. As the acceleration amplitude increased at a given frequency, the rate of convection increased; this increase resulted in the convection patterns forming more streamlined bands of beads as the particles re-entered the bed. The rate of the re-entry of the larger particles significantly affected the degree of segregation with the accumulation of larger particles on the surface being reduces as the rate of motion of the particles into the bed increased. The inclination of the free surface observed in the experiments reported earlier was also observed in the mono-disperse system of particles. The inclinations of the free surface that occurred may also have been be due to the presence of lateral vibrations. The inclined surface of the materials resulted in increased heaping and segregation of the particles.

5.6.2 Segregation upon Hopper Discharge

Segregation during outflow, and upon discharge may be present depending on the flow characteristics of the material in the hopper. The first sets of experiments were conducted for the binary system of particles vibrating within the regime of uniform mixing of particles defined above in table 5.2. Four different size ratios were examined and for each size ratio frequencies of 20 Hz, 40 Hz, and 60 Hz were examined. Size segregation was investigated by monitoring the change in weight fraction of the beads upon discharge.

5.6.2.1 Segregation upon Hopper Discharge without Layering. The loading of the hopper for first set of segregation upon discharge experiments were done by layering the larger particles followed by the smaller particles. After being placed in the hopper, the

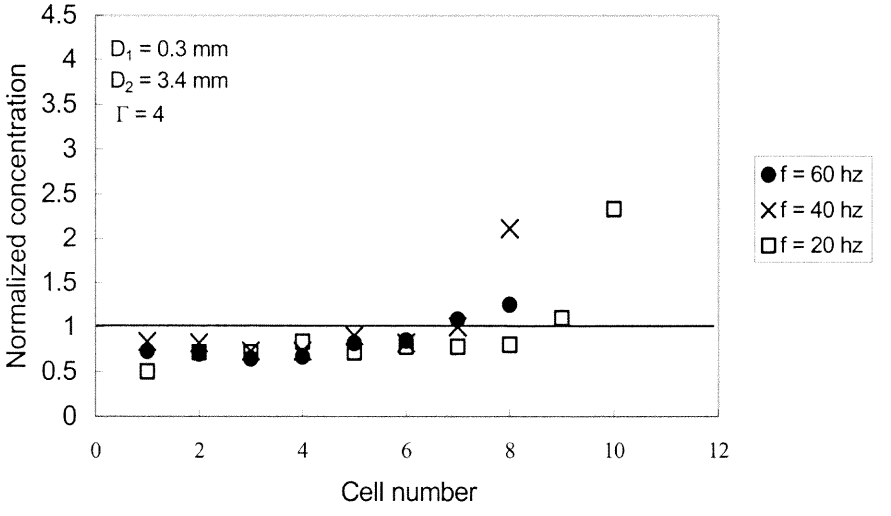

Figure 5.7: Plot of discharge segregation for particles size ratio $\Phi = 11.3$, and $\Gamma_v = 4$

material in the hopper is vibrated with the hopper closed for a period that allowed the particles to achieve a stable state. With the hopper vibrating, the base was opened and the particles emptied as a continuous stream into the collection cups into

the collection cups passing below on the computer controlled track system. Plots of the normalized concentration versus the cell number are shown in figures 5.7 to figure 5.10.

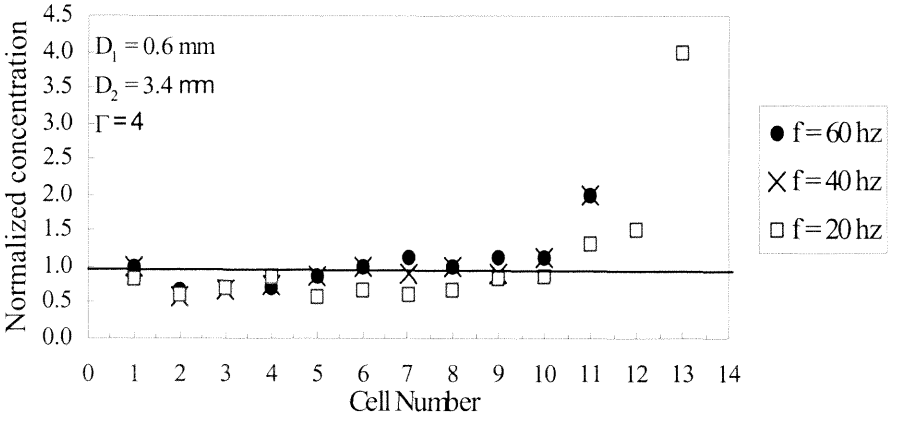

Figure 5.8 Plot of discharge segregation for particles size ratio Φ = 5.7

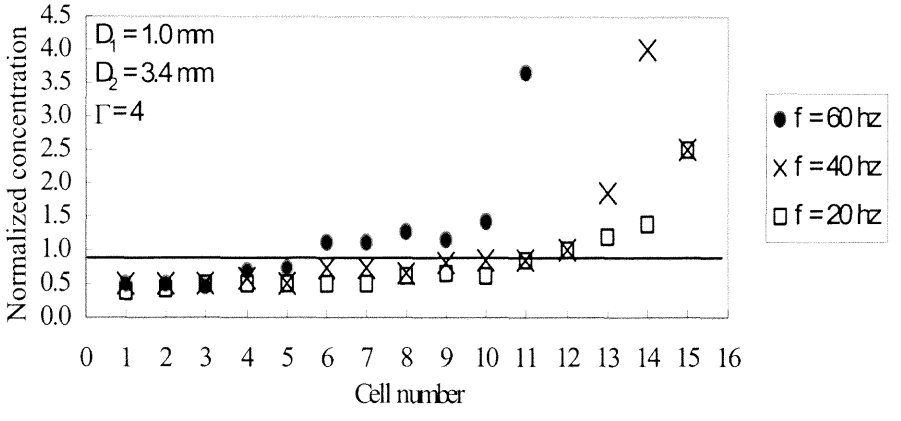

Figure 5.9 Plot of discharge segregation for particles size ratio Φ = 3.4

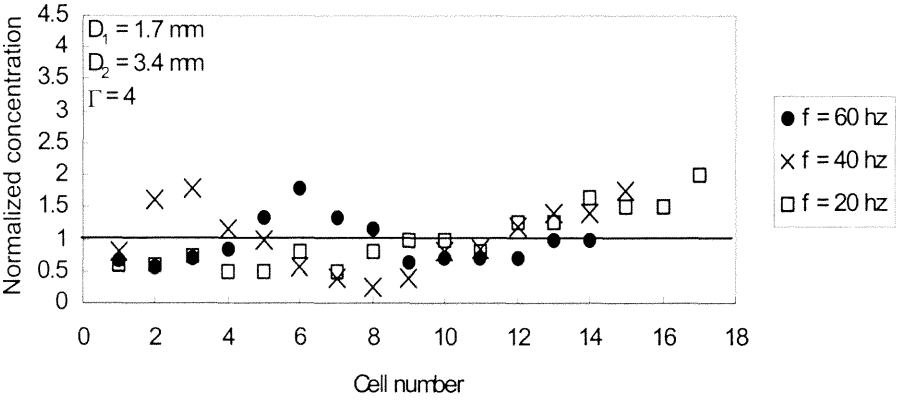

Figure 5.10 Plot of discharge segregation for particles size ratio Φ = 2.1

These plots indicate that there was not much segregation within the region of uniform mixing within the hopper bed. Examination of the above plots indicates that generally initially there were more large particles than small particles in the material flowing out of the hopper. However, as flow progressed the situation changed becoming less showing less segregation except for the smallest size ratio considered. For the last ten percent of the hopper material flowing out of the hopper, there was increased segregation with a much higher percentage of smaller particles in the mix. The fact that the results size ratios of ϕ = 11.2, 5.7 and 3.4 did not show any notable segregation for the first seventy percent of the material exiting the hopper may be explained by the fact that the in-bin concentration for the regime chosen was essentially uniform for a large part of the feed. In the case of the 2.1 size ratio, whose discharge segregation shows a sinusoidal pattern. This may be due to the fact that for the combination of larger size particles the flow rate of the particles out of the hopper was reduced. That is, for this size ratio, the flow out of the hopper was less fluid than in cases where the size difference between the particles were larger. Standish [96] is similar work also observed this and indicated that this may be due to the fact that there is a lower concentration of particles and is most probably explained by size separation, and the effects of retarded particle motion or retention. However, in his work the particles were not being vibrated. The slightly higher percentage of larger particles may also be explained by examining the flow patterns in the vibrated hopper. Although the regime considered above was the best-mixed regime, there was still some segregation as can be noted in figures 5.2 and 5.2 c. where there was an area down the center of the hopper had a slightly higher percentage of larger particles. Similar plots were also completed with the acceleration amplitude Γ = 5. These plots

displayed the same characteristics of the plots listed above further establishing the fact size segregation in the discharge stream is a function of size segregation in the hopper and the material flow pattern in the hopper.

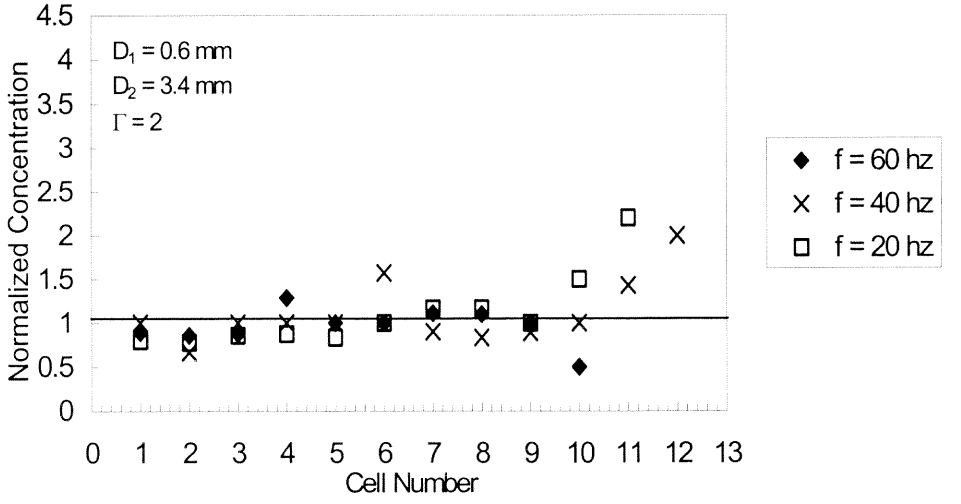

Figure 5.11 Plot of discharge segregation for particles size ratio Φ = 5.7

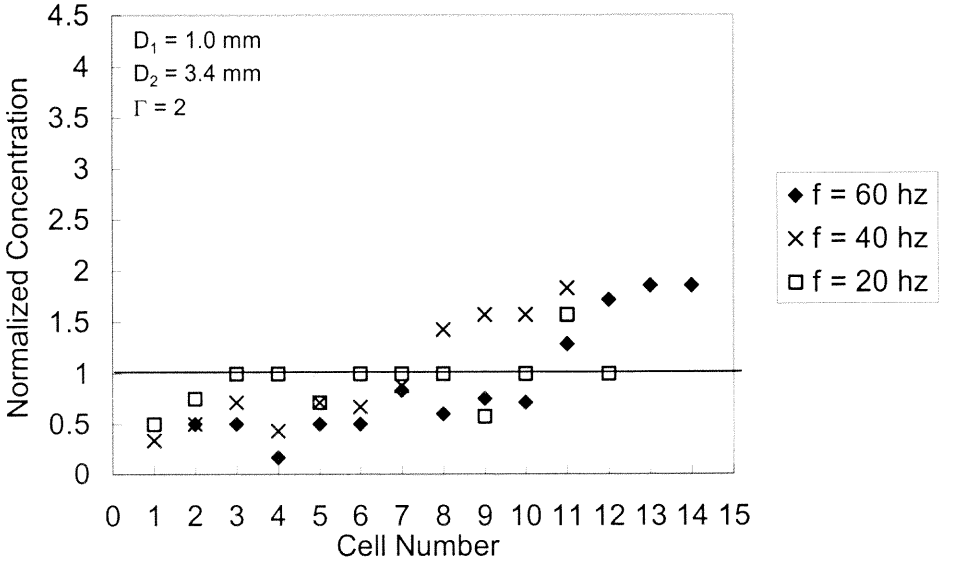

Figure 5.12 Plot of discharge segregation for particles size ratio Φ = 3.4

Segregation plots of the discharge particles at low vibration amplitude, that is, $\Gamma = 2$ are shown in plots 5.11 and 5.12, below. These plots are in the regime where the particles when vibrated in the closed hopper showed the highest degree of segregation and heaping. When figures 5.11 and 5.12 are compared with figures 5.8 and 5.9 of the corresponding size ratios it can be observed that 5.11 and 5.12 shows more segregation upon discharge. The plots of segregation upon discharge in the above figures also follow a sinusoidal pattern that was not obvious in the earlier plots.

5.6.2.2 Segregation upon Hopper Discharge with layered beads. Plots of the segregation upon discharge of the materials in the hopper where the large and small beads were layered in alternate strips are shown in figures 5.13 to 5.18. Comparing plots for the particle ratio 5.7 and 3.4, in figure 5.13 and 5.14, for the particles that were initially

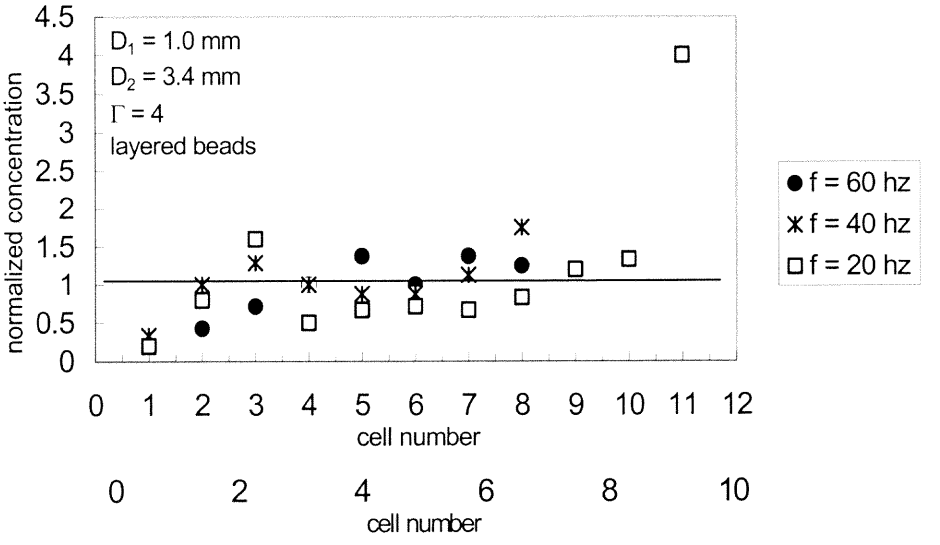

Figure 5.13 Plot of discharge segregation for layered particles size ratio $\Phi = 5.7$, $\Gamma_v = 4$.

layered with figures 5.8 and 5.7 of the same size ratio but initially vibrated until stable, show that the segregation upon discharge for the particles that were not layered is less.

That is, the particles that were allowed to vibrate until a steady state was achieved in the mixing regime were more uniformly distributed upon discharge than the layered particles vibrated at the same acceleration amplitude $\Gamma = 4$.

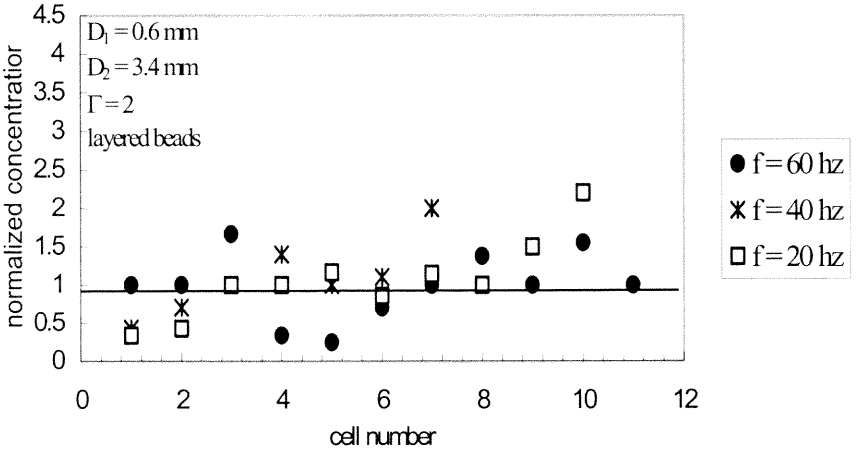

Figure 5.14 Plot of discharge segregation for layered particles size ratio $\Phi = 3.4$, $\Gamma_v = 4$.

Figures 5.15 and 5.16 show segregation plots for the same size ratio for the value $\Gamma = 2$. When compared with the corresponding plots for the vibrated hopper in figures 5.11 and 5.12, it is observed that the difference between the vibrated hopper with layering of the particles and without the layering of the particles does not vary widely with the vibrated hopper without layering showing slightly less segregation.

Design of hopper for mass flow rather than core flow is an accepted way to reduce segregation upon discharge. The use of vibration can result in funnel flow hoppers operating like a mass flow hopper. Figure 5.17 below shows plots for a rectangular with and without vibration. From the plots, it can clearly be noticed that the when vibration was applied to the hopper the level of segregation was reduced. The fluctuation in the segregation with without vibration would be due to the funnel type flow behavior from

the rectangular hopper. Figure 5.17 shows plots for a rectangular with and without vibration. From the plots, it can clearly be noticed that the when vibration was applied to the hopper the level of segregation was reduced. The fluctuation in the segregation with

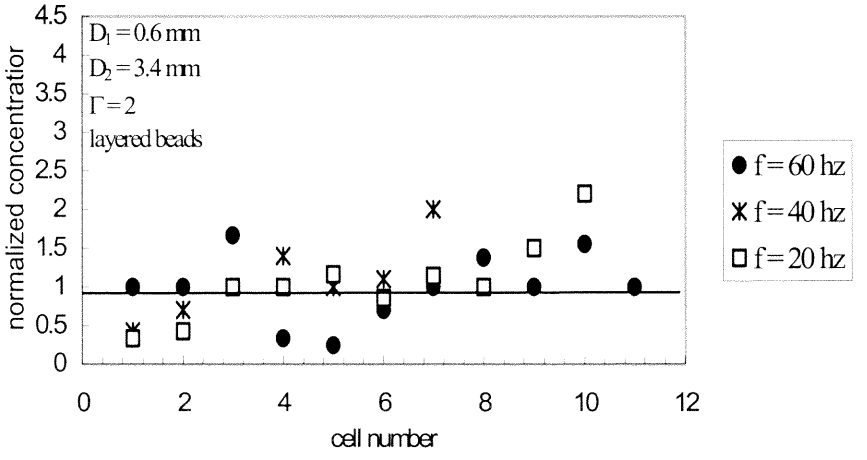

Figure 5.15 Plot of discharge segregation for layered particles size ratio $\Phi = 5.7$, $\Gamma_v = 2$

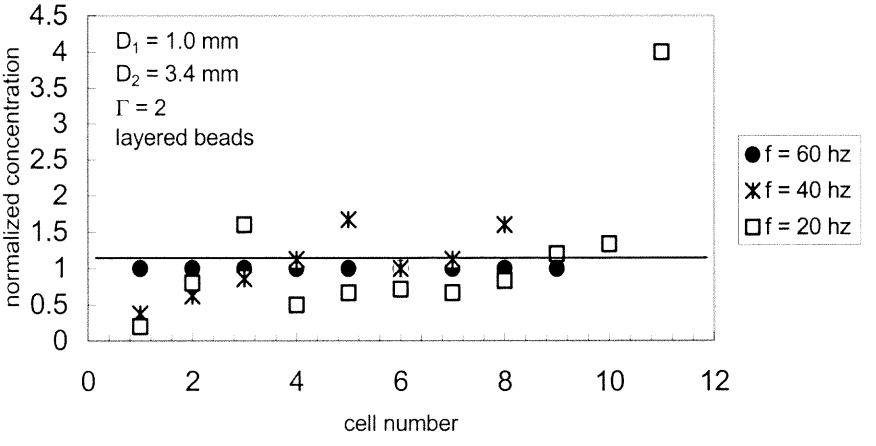

Figure 5.16 Plot of discharge segregation for layered particles size ratio $\Phi = 3.4$, $\Gamma_v = 2$

without vibration would be due to the funnel type flow behavior from the rectangular hopper. Examining the snapshots shown figure 5.18 shown highlights the behavior of the material with and without vibration.

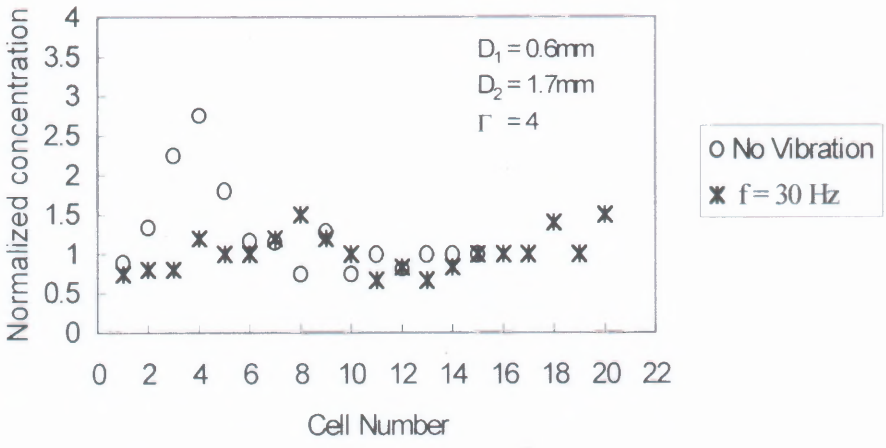

Figure 5.17 Plot of discharge segregation for particles size ratio $\Phi = 2.83$, for a rectangular hopper with and without vibration

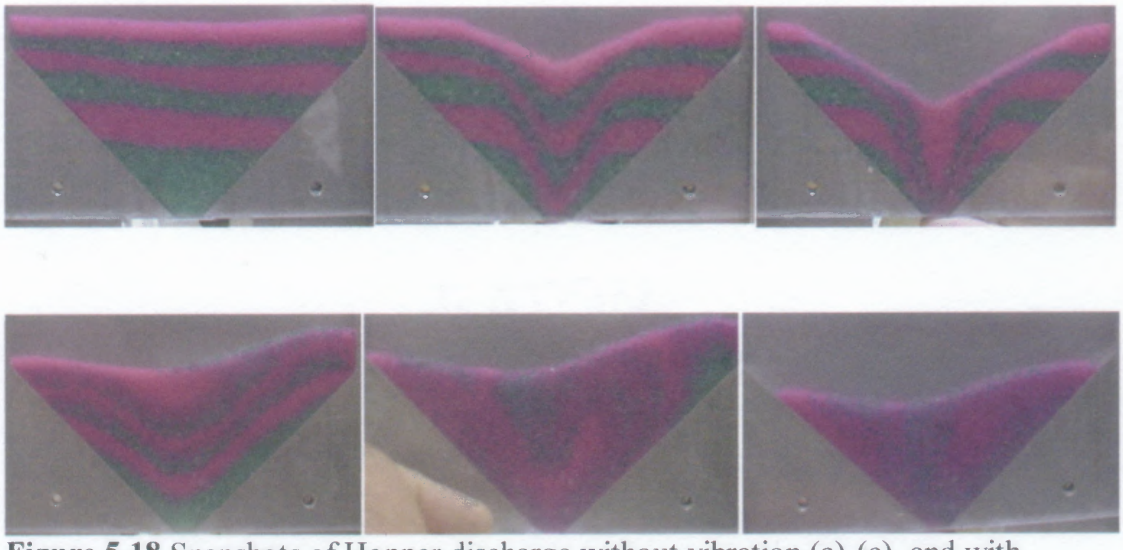

Figure 5.18 Snapshots of Hopper discharge without vibration (a)-(c), and with vertical vibration (d)-(f) showing mixing and mass flow characteristics

From figure 5.18, it can be seen that the hopper with 45 degree half-angle showed funnel flow characteristics without vibration. This resulted in the layered material being more segregated than for the case with vibration. With vibration, the material in the hopper

became quickly mixed and the flow pattern changed to that of a mass flow hopper. In the case of mass flow hoppers, the difference between the segregation upon discharge, for the vibrated and the non-vibrated hopper, is less than in funnel flow hoppers. Flow experiments were carried out for beads with diameter 1.7mm. The plots shown in figure 5.19 indicated that the difference in the segregation between the two cases of mass flow hopper, with vibration and without vibration is negligible.

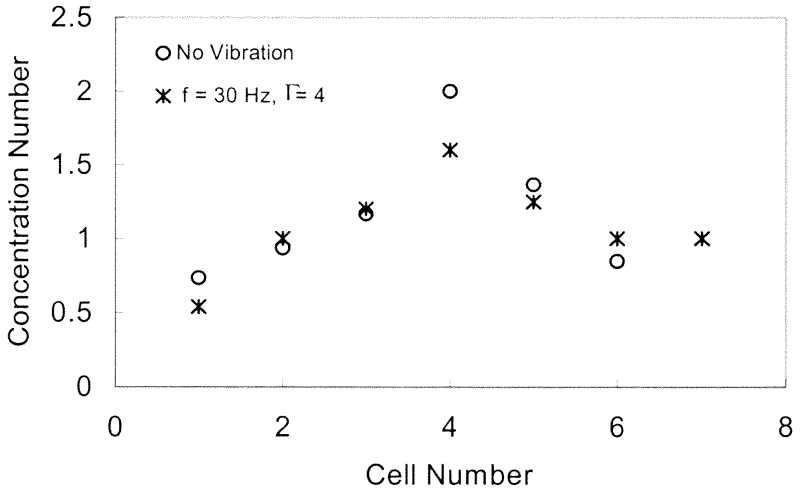

Figure 5.19 Plot of segregation upon discharge for a mass flow hopper with and without vibration.

5.7 Conclusion

Segregation studies indicate that depending on the operating parameters of the vibrated container the behavior of the materials in the hopper varies. The behavior of the materials may vary widely but seems to confirm defined regimes that can be predicted. For the selected range of particle diameters ratios in the system considered, the parameter that

affected the flow pattern behavior most significantly was the relative particle diameters and the vibration amplitude. As the diameter ratio of the particles increased, the level of segregation was larger due main to the larger particles finding it difficult to renter the bed once the circulated to the top. This confirms what was earlier work indicating that one of the most significant parameters for segregation is the diameter ratio of the particles. However, as summarized earlier, for the range of diameter ratios considered with the correct combination of vibration amplitude and operating frequency, a relatively uniformly mixed state may be achieved.

The behavior of the in-bed segregation is strongly influenced by the flow pattern instability and heaping which is probably due to the presence of unavoidable lateral vibrations due to the construction of the experimental apparatus. The influences of this inclination resulted in increase heaping with the larger particles running along the free surface in the form of avalanches to settle along the walls of the hopper at the lower end of the inclination. The effect of in-bed segregation on segregation upon discharge from hoppers is clearly demonstrated. The different initial conditions of the particles studied in the hopper clearly indicate that operating the hopper within the different mixing regimes defined influences the segregation pattern upon exit, with the least segregation occurring in the region of the best mixing or least segregation.

CHAPTER 6

CONCLUSIONS

1.1 Closing Remarks

This dissertation dealt with two important areas of material handling namely flow characterization measurement, and segregation of vibrated materials. A new method of measuring the Angle of Repose of Powders called the Magnetic Assisted Powder Flow Method (MAPF) has been used successfully to measure the angle of repose under a variety of operating conditions. The parameters affecting the angle of repose measurements using this method were analyzed experimentally using different types of powders having common properties with many of the powders used in industry. Comparisons were made using other popular existing methods of measuring angle of repose. One of the problems associated with the current methods of measuring angle of repose is inconsistent result due to the testing techniques being inadequate for carrying out test on cohesive materials. This method provided smooth slopes free of false heaps and gave constant values for the angle of repose. Test carried out on the MAPF method in this research, indicated that the method used to control flow, enhances the ability of the tester to control the momentum of the particles hitting the pile, which is the governing factor affecting the angle of repose measurement. The results obtained clearly indicate that the Magnetically Assisted Particle Flow device can be utilized both as a flow enhancement device and in the characterization of powders through measuring of the angle of repose.

The second part of this research examined the behavior of beads when subjected to vibration. A phase diagram outlining the behavior characteristics of glass beads was developed. Four distinct regimes defining the behavior of the beads subjected to vibrations were observed for the convection flow patterns, with some results similar to that found by previous researchers. A detailed description of the observed ranges is given in chapter 3 of this dissertation. The first regime was observed with the bed existing in a crystalline state where there is no relative movement between the particles. As the acceleration increased to higher value of approximately two, a second regime is observed where the horizontal free surface became unstable and inclined at an angle θ with the horizontal. Particles continuously rolled down this free surface forming one big continuous loop, and a smaller less active loop. This loop slopes to the left or right depending on the acceleration amplitude but is repeatable for the specific frequencies and acceleration applied. The slope of the free surface varied, depending on the amplitude of vibration but was not present for particles above 2.5mm. The third regime formed as the acceleration was increased, where the surface gradually approached a horizontal state, with the particles forming two almost symmetrical convective loops. Finally, increases in acceleration resulted in the gradual destruction of the uniform convective motion, with the formation of surface waved. In the fourth regime, the motion of the particles is somewhat random, although occasionally, clear convective cycles can be observed.

A possible explanation for surface heaping instability and inclination, which has eluded researchers for many years, is given. Measurements of the horizontal vibrations using carefully designed hoppers, and two different types of vibrating apparatus revealed that although horizontal vibration was not applied, horizontal vibration were always be

present. The sensitivity of the vibrating flow pattern to horizontal lateral vibrations was studied. Extensive work carried out in this dissertation both in the area of experimental analysis and computer simulations provides one possible answer of the sloping surface of granular materials when subjected to vibration. One distinct feature of this analysis is the close similarity between the experimental and the simulation parameters studied. This is a significant result as no prior literature was found where the same quantities of vibration amplitudes applied, (or measured) in experiments also applied in simulations, providing closely matching results.

The study of segregation upon discharge for a vibrating hopper, by first characterizing the segregation in the hopper, is introduced in chapter five of this research. After developing an understanding of the flow pattern of a monodisperse system, the segregation patterns in a binary systems of particles was characterized. Although further research needs to be done in this area, a clear relationship was found between the level of segregation in the hopper and the segregation upon discharge. Preliminary results have indicated that discharging the hopper within the regime of uniform mixing resulted in the least segregation upon discharge.

1.2 Extensions for Further Studies

In the first part of the research presented, the use of the Magnetically Assisted Flow Enhancement method as a powder characterization devise was supported by extensive tests. These tests were all carried out on laboratory type equipment. In order to further establish the use of this mechanism, further tests are necessary on a wider range of

materials, covering a wider range of material properties that affect flow. Such tests would identify the areas in which the mechanism can be improved.

The potential for a larger model of the MAPF should also be investigated through the scaling up of the current apparatus. Prior to doing this, the possibility of running the existing apparatus at higher voltages should be examined, since running the current apparatus at high voltages results in overheating. The current apparatus uses wire mesh at the base of the hopper to keep the beads in place. Efforts can be made to keep these particles in place without the use of mesh, through electromagnetic forces set up by the field. This feature may result in enhancing the operation of the MAPF, since the presence of the wire can restrict the smooth operation when using very cohesive powders.

The long-term usage of the magnetic particles used to create the fluidization of the powders need to be studied for wear. Such a study will establish the effects of the magnetic particle collision on the physical properties of these particles, and establish if there is any attrition. Alternative materials with suitable magnetic properties that would not contaminate any material used should also be identified.

The results presented for vibration flow patterns and segregation were obtained from a pseudo two-dimensional apparatus and a soft sphere two-dimensional simulation code. With the continuing development of faster and more efficient computers, similar research for larger two-dimensional systems and three-dimensional systems should be done. Due to computer limitations, the number of particles utilized is often many times less than that in real systems. Research should be done that establishes if the size of the system significantly affects the outcome of the results. Various researchers have done a limited amount of research examining three-dimensional systems, and found some

differences in the types of patterns observed. In the experimental study of flow pattern and segregation utilized in this work, the apparatus used was a pseudo two-dimensional hopper. As a result of this the behavior, patterns were not observed for a true three-dimensional system as utilized in industry. Efforts should be made to study the effects of the in-bed flow pattern and segregation in three- dimensional systems.

APPENDIX

SIMULATION FLOW CHART

This is a chart showing the procedure followed during the simulation.

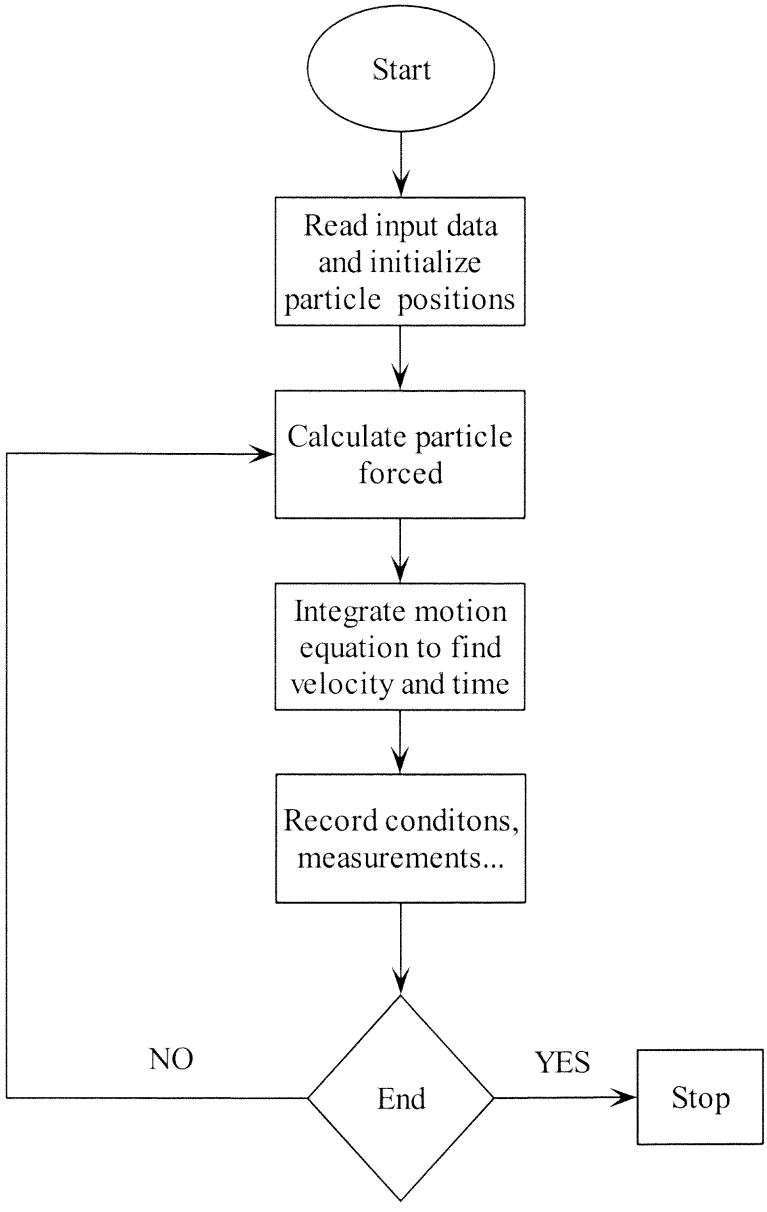

REFERENCES

1. Purutyan, H., Pittenger, B. H. and J. W. Carson. "Solve Solids Handling Problems by Retrofitting." *Chem. Eng. Prog.* April (1998): 27-39.

2. Merrow, E. W. "Estimating Startup Time for Solid Processing Plants." *Chem. Eng.* 24 (1998): 89-95.

3. Faraday, M. "On a peculiar class of acoustical figures and on certain forms assumed by groups of particles upon vibrating elastic surfaces." *Phil. Trans. R. Soc. London*, 52 (1831): 299-340.

4. Brown, R. L., and J. C. Richards. "Principles of Powder Mechanics." *Pergamon Press* (1970).

5. Nedderman, R. M. "Statics and Kinematics of Granular Materials." *Cambridge University Press* (1992).

6. Bagnold, R. A. "The Physics of Blown Sand and Desert Dunes." *Chapman and Hall* (1956).

7. Reynolds, O. "On the Dilatancy of Media Composed of Rigid Particles in Contact." *Philos. Mag. Fifth Series*, 20 (1885): 469-472.

8. Nedderman, R. M., and C. Laohakul. "The Thickness of Shear Zone in Flowing Granular Materials." *Powder Technol.* 25 (1980).

9. Hanes, D. M., and D. L. Inman. "Observations of Rapidly Flowing Granular-Fluid Materials." *J. Fluid Mech,* 150 (1985): 357-361.

10. Hanes, D. M., Jenkins, J. T., and M. W. Richman. "The Thickness of Steady Plane Shear Flows of Circular Discs Driven by Identical Boundaries." *J. Appl. Mech.* 55 (1988): 969.

11. Zhang, Y., and S. Campbell. "The Interface between Fluid-Like and Solid-Like Behavior in Two-Dimensional Granular Flows." *J. Fluid Mech.* 237 (1992): 541.

12. Savage, S. B. "The Mechanics of Rapid Granular Flows." *Adv. Appl. Mech.* 24 (1984): 289-294.

13. Bagnold, R. A. "Experiments on a Gravity-Free Dispersion of Large Solid Spheres in a Newtonian Fluid Under Shear." *Proc. Roy. Soc.* A 225 (1954): 49.

14. Carr R. L. "Evaluating the Flow Properties of Solids." *Chem. Eng.* (1965): 163-168.

15. American Society for Testing and Materials. D 6393-99 (1999).

16. Liffman, K., G. Metcalfe., and P. Clearly. "Convection due to Horizontal Shaking." in: *Powders and Grains 97*, R. P. Behringer and J. T. Jenkins (eds.), Rotterdam 1997.

17. Weathers, R. C., Hunt, M. L., Brennen, C. E., Lee, A. T., and C. R. Wassgren, "Effects of Horizontal Vibration on Hopper Flows of Granular Materials." in: *Mechanics of Deformation and Flow of Particulate Materials*, C. S. Chang., A. Misra., and M. Babic(eds), ASCE, (1997): 349-360.

18. Knight, J. B., Fandrich, C. G., Lau, C. N., Jaeger, H. M., and S. R. Nagel. "Density Relaxation in a Vibrated Granular Material." *Physical Review E.* 51 (1996): 3957-3963.

19. Evesque, P., and J. Rajchenbach. "Instability in a Sand Heap." *Physical Review Letters*. 62 (1989): 44-46.

20. Clement, E. Duran, J. and J. Rajchenbach. "Experimental Study of Heaping in a Two-Dimensional Sandpile." *Phys, Rev. Letter*. 69 (1992): 1189-1192.

21. Knight, J. B., Jaeger, H. M., and S. R. Nagel. "Vibration-Induced Size Segregation in Granular Media: The Convection Connection." *Phys. Rev. Letter*. 70 (1993): 3728-3731.

22. Pak, H. K., Doorn, V. E., and R. P. Behringer. "Surface Waves in Vertically Vibrated Granular Materials." *Phys Rev. Letter*. 71 (1991): 1832-1835.

23. Pak, H. K., Doorn, V. E., and R. P. Behringer. "Effect of Ambient Gas on Granular Materials Under Vertical Vibrations." *Phys Rev. Letter*. 74 (1995) 23.

24. Douady, S., Fauve, S., and C. Laroche."Subharmonic Instabilities and Defects in Granular Layer Under Vertical Vibrations." *Europhysics Letters*. 8 (1989): 621-627.

25. Evesque, P. "Comment on: Convective Flow of Granular Masses Under Vertical Vibration." *LeJournal De Physique* (J. PHYS. France). 51 (1990): 607-610.

26. Gallas, A. C., Herrmann, H. J., and S. Sokolowski. "Convection Cells in Vibrating Granular Media," *Physical Review Letters*. 69 (1992): 1371-1374.

27. Knight, J. B., Ehrichs, E. E., Kuperman, V. Y., Flint, J. K., Jaeger, H. M., and S. R. Nagel. "Experimental Study of Granular Convection." *Physical Review E.* 54 (1996): 5726-5738.

28. Akoi, K. M., Akiyama, T., Maki, Y., and T. Watanabe. "Convection Roll Patterns in Vertically Vibrated Bed of Granules." *Physical Review E.* 54 (1996): 874-883.

29. Ehrichs, E. E., Jaeger, H. M., Karczmar, G. S., Knight, J. B., Kuperman, V. Yu., and S. R. Nagel. "Granular Convection Observed by Magnetic Resonance Imaging." Science, 267 (1995): 1632.

30. Kuperman, V. Yu. "Nuclear Magnetic Resonance Measurements of Diffusion in Granular Media." *Physical Review Letter*. 77 (1996): 1178-1181.

31. De Gennes, P. G. "Reflection on the Mechanics of Granular Matter." *Physica A*. 261 (1998): 267-293.

32. Grossman, E. L. "Effects of Container Geometry on Granular Convection." *Physical Review E*, 56 (1997): 3290-3300.

33. Knight, J. B., "External Boundaries and Internal Shear Bands in Granular Convection." *Physical Review E*, 55 (1997) 6016-6023.

34. King, P. J., Swift, M. R., Benedict, K. A., and A. Routledge. "Surface Stability of Granular Systems Under Horizontal and Vertical Vibrations: The Applicability of a coefficient of friction." 62 (2000): 6982.

35. Tennakoon, S. G. K., and R. P. Bheringer. "Vertical and Horizontal Vibration of Granular Materials: Coulomb Friction and a Novel Switching State." Physical Review Letters 81 (1998) 794.

36. Arnold, P. C. "On the Influence of Segregation on the Flow Pattern in Silos." *Bulk Solids Handling*, 11(2) (1991): 447-449.

37. Ahmad, K., and I. J. Smalley. "Observation of Particle Segregation in Vibrated Granular Systems." *Powder Technol.* 8 (1973): 69-75.

38. Rosato, A., Strandburg, K. J., Prinz, F., and R. Swendsen, "Why the Brazil Nuts are on Top: Size Segregation of Particulate Matter by Shaking." *Phys. Rev. Lett.* 58 (1987): 1038-1040.

39. Rosato, A. Lan, Y., Wang, D. T. "Vibratory Particle size sorting in Multi-component Systems." *Powder Technol.*, 66 (1991): 149-160.

40. Jullien, R., Meakin, P., and A. Pavlovitch, "Three-Dimensional Model for Particle Size Segregation by Shaking." *Phys. Rev. Lett.*, 69 (1992): 640-643.

41. Duran, J., Rajchenbach, J., and E. Clement, "Arching Effect Model for Particle Size Segregation." *Phys. Rev. lett.,* Vol. 70 (1993): 2431-2434.

42. Dippel, S., and S. Luding. "Simulations on Size Segregation: Geometric Effects in the Absence of Convection." *J. Phys. I France,* 5 (1995): 1527-1537.

43. Cooke, S., Warr, S., Huntley., and R. C. Ball. "Particle Size Segregation in Two Dimensional Bed Undergoing Vertical Vibration." *Phys. Rev. E*, 53 (1996): 2812-2822.

44. Duran J., Mazozi, T., Rajchenbach, J., and E. Clement. "Size Segregation in a Two-Dimensional Sandpile: Convection and Arching Effects." *Phys. Rev. E*, 50 (1994): 5138-5141.

45. Poschel, H. "Size Segregation and Convection." *Europhys. Lett*, 29 (2) (1995):123-128.

46. Vanel, L., Rosato, A., and R. N. Dave. "Rise Regimes of a Large Sphere in Vibrated Bulk Solids." (1996).

47. Lan, Y., Rosato, A. D. "Convection Related Phenomenon in Granular Dynamics Simulations of Vibrated Beds." (1996).

48. Brone, D, Muzzio, F. J. Size-Segregation in Vibrated Granular Systems: A Reversible Process." submitted to *Phys. Rev. Lett.*, 56 (1997): 1059-1063.

49. Gallas, J. A. C., Herrmann, H. J., Poschel, and S. Sokolowski. "Molecular Dynamics Simulation of Size segregation in Three Dimensions." *Journal of Statical Physics*, 82 (1996): 443-450.

50. Half, P. K., and E. K. Werner. "Computer Simulation of the Mechanical Sorting of Grains." *Powder Technol.,* 48 (1986) 239-245.

51. Harwood, "Powder Segregation due to Vibaration." *Powder Technol.*, 16 (1976) 51-57.

52. Williams, J. C. "The Segregation of Particulate Materials. A Review." *Powder Technol.*, 15 (1976): 245-251.

53. Lan, Y. "Particle Dynamics Modeling of Vibrating Granular Beds." Ph.D Dissertation, New Jersey Institute of Technology, 1994.

54. Roberts, A. W., Ooms, M. and O. J. Scott. "Influence of Vibrations on the Strength and Boundary Friction Characteristics of Bulk Solids and the Effect on Bin Design and Performance." Bulk Solid Handling, 6 (1986): 161-169.

55. Allen M. P., and D. J. Tildesley. "Computer Simulation of Liquids." Oxford. 1987 (Clarendon Press).

56. Cundall, P. A., Strack O. D. L., "A Discrete Numerical Model for Granular Assemblies." *Geotechnique*, 29, (1979): 47-65.

57. Poschel, T., "Granular Material Flow Down an Inclined Chute: A Molecular Dynamics Simulation." *J. Physics. II* (France) 3, 27 (1993).

58. Taguchi, Y. H. "New Origin of a Convective Motion: Elastically Induced Convection Cells in Vibrating Granular Media." *Physical Review Letter* 69 (1992) 1367.

59. Luding, S., Clement, E., Blumen, A., Rajchenbach, J., and A. Blumen. "Onset of Convection in Molecular Dynamics Simulation of Grains." *Phys Rev.* E 50 R1762 (1994).

60. Walton O. R., "Particle-dynamics calculations of shear flow." in *Mechanics of Granular Media* Ed. by J. T. Jenkins and M. Strake. Amsterdam 1993 (Elsevier).

61. Lan, Y., and A. D. Rosato. "Convection Related Phenomenon in Granular Dynamics Simulations of Vibrated beds." *Physics of Fluids*, 7, (1996): 1818-1831.

62. Caram, H and D. C. Hong. "Random walk approach to granular Flows." *Phy. Revs. Lett.* 67 (1992): 828.

63. Brennen, C. E., Ghosh, S., and C. R. Wassgren. "Vertical Oscillation of a Bed of Granular Material." ASME Journal of Applied Mechanics, 63 (1993) 156-161.

64. Wassgren, C. R., 1997, Vibration of Granular Materials, Ph.D. Thesis, California Institute of Technology, Pasadena, CA.

65. Jenike, A. W. "Gravity Flow of Bulk Solids." Bulletin no. 108, Eng. Experiment Station, The University of Utah, Salt Lake City.1961

66. Jenike, A. W. "Storage and Flow of Solids." Bulletin no. 123, Eng. Experiment Station, The University of Utah, Salt Lake City.

67. Schwedes, J. "Measurement of flow properties of bulk solids." *Powder Technology,* 88 (1996) 285-290.

68. Fayed, M. E., and L. Otten. "Handbook of Powder Science and Technology." Van Nostrand Reinhold Company Inc., New York 1984.

69. Pipel, A., "Cohesive Pharmaceutical Powders," in H. S. Bean, A. H.Bekette, J. E. Carless (eds.): *Advances in Pharmaceutical Sciences 3*. Academic Press, New York. 1971.

70. Craik, D. J. "The Flow Properties of Starch Powders and Mixtures." *Journal of Pharmacy and Pharmocol.* 10 (1958): 73-79.

71. Train, D. "Some Aspects of the Angle of Repose of Powders." *Journal of Pharm. and Pharmocol.* 10 (1958): 127T –135T.

72. Carr, R. L. "Evaluating the Flow Properties of Solids." *Chem. Eng.*, (1965): 163-168.

73. Craik, J. D., and F. B. Miller. "The Flow Properties of Powder Under Humid Conditions." *J. Pharm. Pharmac.* (1958).

74. Pipel, A. "The flow properties of magnesia." *J. Pharm. Pharmac.* 16 (1964): 705-716.

75. Newman, S, B., "The flow properties of Powders." in H. S. Bean, A. H.

76. Jones, M. T., and A. Pipel. "Some Angular Properties of Magnesia and their relevance to Material Handling", *J. Pharm. Pharmac.* 18 (1966) 182S-189S.Bekette, J. E. Carless (eds.): Advances in Pharmaceutical Sciences 2. Academic Press, New York. 1967.

77. Wouters, M. I., and D. Geldart. "Characterizing Semi-Cohesive Powders Using Angle of Repose." *Part. Part. Syst. Charact.* 13 (1996): 254-259.

78. Teunou, E., Vasseur, J., and M. Krawczyk. "Measurement and Interpretation of Bulk Solids Angle of Repose for Industrial Process Design." *Powder Handling and Processing.* 7 (1995) 219-227.

79. Kaye, B. K. "Fractal Dimensions in Data Space; New Descriptors for Fineparticle Systems." *Part. Part. Syst. Charact.* 10 (1993) 191-200.

80. Wu, C. Y., Watano, S. and R. N. Dave. "Magnetically Enhanced Powder Discharge from Storage under High Consolidation." *Powder Handling & Processing Handling*, 10(4) (1998): 357-361.

81. Dave, R. N. Wu, C. Y., Bodhisattwa, and C., Watano. "Magnetically mediated Flow Enhancement for Controlled Powder of Cohesive Powders", *Powder Technology*, 112 (2000): 111-125.

82. Sadler, J. E. "Silo Problems." International Conference on Design of Silos for Strength and Flow, Lancaster, UK, September, 1980.

83. Melo, F., Ubanhovar, P., and H. L. and Swinney., "Transition to Parametric Wave Patterns in a Vertically Oscillated Granular Layer." *Physical Review Letters.* 72 (1994): 172-175.

84. Zhang, Y., and S. C. Campbell. "The Interface between Fluid-Like and Solid-Like Behavior in Two Dimensional Granular Flows" J. Fluid Mech. 237, 541 (1992).

85. Lee, J. "Density waves in the flows of Granular Media." *Phys. Rev. E* 49. 281 (1994).

86. Ristow, G. H., and H. J. Herrmann. "Density Patterns in two-dimensional hoppers." *Phys. Rev. E.* 50 R5 (1994).

87. Maw, N., J. R. Barber, and J. N. Fawcet. "The Oblique Impact of Elastic Spheres." Wear. 38, (1976).

88. Johnson K. L. "Contact Mechanics" Cambridge 1989 (Cambridge Univ. Press).

89. Goldsmith, W. "Impact: The Theory and Physical Behavior of Colliding Solids." Edward Arnold pub. (1960).

90. Bridges, F. G. Hatzes, A., and D. N. C. Lin. " Structure Stability and evolution of Saturn's rings." *Nature.* 303 (1987): 333-339.

91. Kwabara, G., Kono, K. "Restitution coefficient in a Collision between Two Spheres." *Jpn. . J. Appl. Phys.* 26 (1987): 1230-1236.

92. Sondergaard, R., Chanes. K., and C. E. Brennen. "Measurements of Solid Spheres Bouncing off Plates." *J. Appl. Mech.* 57 (1990).

93. Forrester, S. F., Longe, M. Y., Chang. H., and K. Allia. "Measurements of the Collision Properties of Small Spheres." *Phys. Fluids*, 6 (1994).

94. Mindlin, R. D., and H. Deresiewicz. "Elastic Spheres in Contact Under Varying Oblique Forces." *J. Appl. Mech.* 20 (1953): 327-333.

95. James, G., Malik, M., and R. N. Dave. "Experimentally –Observed and Numerically Simulated Characteristics of Granular Flow in Vibrated Wedge-Shaped Containers" AICHE Meeting, Los Angeles, CA Nov 12 – Nov 17, 2000.

96. Standish, N. "Size Segregation of Granular Materials in Storage and Discharge from a Hopper." *Bul Proc. Austras.* Inst. Min. Metall. 290

97. Arteza, P., and U. Tuzun. "Flow of Binary Mixtures of Equal Density Granules in Hoppers-Size Segregation, Flowing Density and Discharge Rates." *Chem. Eng. Sci.* 45 (1990): 205-222.

98. Grey, J. M. N. T., and K. Hutter. "Pattern Formation in Granular Avalanches." *Continuum Mech*, Thermodyn. 9 (1997): 341 – 346.